

Heavy Quark QCD at Finite Temperature and Density Using an Effective Theory

Dissertation
zur Erlangung des Doktorgrades
der Naturwissenschaften

vorgelegt beim Fachbereich Physik
der Johann Wolfgang Goethe-Universität
in Frankfurt am Main

von
Jonas Rylund Glesaaen
aus Oslo, Norwegen

Frankfurt am Main 2016
D30

vom Fachbereich Physik der
Johann Wolfgang Goethe-Universität als Dissertation angenommen.

Dekan: Prof. Dr. R. Reifarth

Gutachter: Prof. Dr. O. Philipsen
Prof. Dr. D. H. Rischke

Datum der Disputation:

The sun is a wondrous body. Like a magnificent father!
If only I could be so grossly incandescent!
Solaire of Astora –

Contents

ABSTRACT	v
DEUTSCHE ZUSAMMENFASSUNG	vii
ACKNOWLEDGEMENTS	xiii
I INTRODUCTION	1
1 INTRODUCTION	3
2 GAUGE THEORIES AND LATTICE GAUGE THEORIES	7
2.1 The free Dirac Lagrangian	7
2.1.1 The Dirac Lagrangian	8
2.2 A group theory perspective	9
2.2.1 Lie groups	9
2.2.2 Character and character expansion	10
2.2.3 Group integrals	10
2.3 Symmetries of the Lagrangian	11
2.3.1 Symmetries by construction	11
2.3.2 Gauge symmetries	12
2.4 Lattice discretisation	14
2.4.1 The lattice gauge theory Lagrangian	14
2.5 Fermion doubling and chiral symmetry	15
2.5.1 Wilson fermions	16
2.6 Scale setting and the continuum limit	17
2.7 Numerical evaluation of lattice gauge theories	18
2.7.1 Observables	19
3 STATISTICAL MECHANICS AND PHASE TRANSITIONS	21
3.1 Statistical mechanics	21
3.1.1 Phases and phase transitions	22
3.1.2 Yang Lee zeros	23
3.2 Thermal field theory	23
3.3 Thermal fields on the lattice	24
3.3.1 Thermodynamic quantities	24
3.4 Finite density simulations	25
3.4.1 Dense systems and lattice saturation	25

3.5	The sign problem	26
3.5.1	Reweighting	27
3.5.2	Imaginary chemical potentials	28
3.5.3	Taylor series	29
3.5.4	Stochastic quantisation	29
 II THE EFFECTIVE THEORY		33
 4 THE EFFECTIVE THEORY		35
4.1	The effective theory - <i>Introduction</i>	35
4.2	The character expansion	36
4.3	Pure gauge effective theory	36
4.4	The hopping parameter expansion	38
4.5	Pure fermion effective theory	39
4.5.1	Static determinant	39
4.5.2	Static propagator	40
4.5.3	Spatial hopping expansion	41
4.5.4	Multiple fermion flavours	44
4.6	Mixed contributions and gauge corrections	45
4.6.1	Fermionic corrections	45
4.6.2	Gauge corrections	45
4.7	Resummation	46
4.7.1	Method of moments and cumulants	47
4.7.2	Logarithmic resummation	49
4.8	The cold and dense regime	49
4.8.1	Combinatorics	50
4.8.2	Dirac indices	52
4.8.3	A comment on gauge corrections	53
4.8.4	The $\mathcal{O}(\kappa^8)$ effective action	54
4.8.5	Application region of the large- N_t approximation	57
4.9	Numerical evaluation	57
 5 ANALYTIC EVALUATION OF THE EFFECTIVE THEORY		61
5.1	Linked cluster expansion	61
5.1.1	Classical linked cluster expansion for nearest neighbour interactions	62
5.1.2	Graphical definitions	63
5.1.3	LCE for the effective theory at LO	65
5.2	Observables	67
5.2.1	Scale setting and the continuum limit	70
5.3	Linked cluster expansion for polymer interactions	71
5.3.1	Generalisation of the LCE to polymer interactions	72
5.3.2	Application to the effective theory, graph embeddings	75
5.3.3	Results	76
5.3.4	Padé approximants	78
5.4	Analytic resummation	79
5.4.1	Chain resummation	79

5.4.2	Cluster resummation	86
5.4.3	Ladder resummation	87
5.4.4	Results	89
5.5	Further applications	93
5.5.1	Large- N_c limit	93
5.5.2	Yang Lee zeros	94
III	DISCUSSION AND OUTLOOK	97
6	SUMMARY AND DISCUSSION	99
7	RESEARCH PERSPECTIVES	101
IV	APPENDIX	103
A	ANALYTICAL TOOLS FOR SU(N)	105
A.1	Computing the Haar measure	105
A.2	$\chi_r \chi_s$ integrals	107
A.2.1	Integrals over characters of SU(3)	107
A.2.2	Characters of plaquettes	108
A.3	$g^n (g^{-1})^m$ integrals	109
A.4	Static determinant	110
A.5	W_{nm} terms	111
B	ADDITIONAL ANALYTIC RESULTS	113
B.1	Non graphical $\mathcal{O}(\kappa^8)$ effective action	113
B.2	Integrated LCE n-point functions	115
B.3	Higher order z-functions	115
	BIBLIOGRAPHY	117

Abstract

In this thesis we explore the characteristics of strongly interacting matter, described by *Quantum Chromodynamics* (QCD). In particular, we investigate the properties of QCD at extreme densities, a region yet to be explored by first principle methods. We base the study on lattice gauge theory with Wilson fermions in the strong coupling, heavy quark regime. We expand the lattice action around this limit, and carry out analytic integrals over the gauge links to obtain an effective, dimensionally reduced, theory of Polyakov loop interactions.

The 3D effective theory suffers only from a mild sign problem, and we briefly outline how it can be simulated using either Monte Carlo techniques with reweighting, or the Complex Langevin flow. We then continue to the main topic of the thesis, namely the analytic treatment of the effective theory. We introduce the linked cluster expansion, a method ideal for studying thermodynamic expansions. The complex nature of the effective theory action requires the development of a generalisation of the linked cluster expansion. We find a mapping between generalised linked cluster expansion and our effective theory, and use this to compute the thermodynamic quantities.

Lastly, various resummation techniques are explored, and a chain resummation is implemented on the level of the effective theory itself. The resummed effective theory describes not only nearest neighbour, next to nearest neighbour, and so on, interactions, but couplings at all distances, making it well suited for describing macroscopic effects. We compute the equation of state for cold and dense heavy QCD, and find a correspondence with that of non-relativistic free fermions, indicating a shift of the dynamics in the continuum.

We conclude this thesis by presenting two possible extensions to new physics using the techniques outlined within. First is the application of the effective theory in the large- N_c limit, of particular interest to the study of conformal field theory. Second is the computation of analytic Yang Lee zeros, which can be applied in the search for real phase transitions.

Deutsche Zusammenfassung

In der vorliegenden Arbeit studieren wir die Eigenschaften der Quantenchromodynamik (QCD), welche die Dynamik der starken Wechselwirkung, eine der vier fundamentalen Kräfte des Universums, beschreibt. Die zugehörigen Quantenzahlen werden von den elementaren Bestandteilen der Nukleonen, den Quarks, getragen. Dabei ist die starke Wechselwirkung dafür verantwortlich, dass Quarks gebundene Zustände, sogenannten Hadronen, bilden. Die daraus resultierende Bindungsenergie entspricht 99% der Hadronen-Masse und somit ist die Stärke der starken Wechselwirkung der Ursprung des Großteils der sichtbaren Materie in unserem Universum.

Von großem Interesse ist insbesondere das Phasendiagramm der QCD für stark wechselwirkende Materie. Die QCD hat die Eigenschaft der asymptotischen Freiheit, was dazu führt, dass die Stärke der Wechselwirkung bei sehr hohen Energien (bzw. sehr kleinen Abständen) abnimmt. Die zugehörige Energieskala für dieses Phänomen ist $\Lambda_{\text{QCD}} \approx 200 \text{ MeV}$. Derartig hohe Energien können bei Kollisionen in Teilchenbeschleunigern entstehen, sind aber auch in thermodynamischen Systemen mit hinreichend hohen Temperaturen und/oder Dichten erreichbar.

Bei Temperaturen um $T_c \sim \Lambda_{\text{QCD}}$ tritt ein Crossover-Übergang auf, bei dem die charakteristischen Freiheitsgrade nicht mehr gebundene, hadronische Zustände bilden, sondern in einen Zustand quasi-freier Quarks und Gluonen, bekannt als das *Quark-Gluon-Plasma* (QGP), übergehen. Man geht davon aus, dass dieser Übergang in den anfänglichen Phasen unseres Universums vorzufinden war. Experimentell wird dieser Zustand in den verschiedenen Kollisionsexperimenten, die es weltweit gibt, untersucht. Dazu gehören beispielsweise der Relativistic Heavy Ion Collider (RHIC) am Brookhaven National Laboratory und der Large Hadron Collider (LHC) am CERN in Genf. Außerdem sind weitere Experimente an Einrichtungen, wie die Facility for Antiproton and Ion Research (FAIR) an der GSI in Darmstadt oder die Nuclotron-based Ion Collider Facility (NICA) am JINR in Dubna, in der Entstehung. In letzteren wird insbesondere der QGP-Übergang bei höheren Dichten und der sogenannte *critical endpoint* (CEP) untersucht.

Im Grenzwert niedriger Temperaturen und hoher Dichten findet man dagegen den Flüssigkeit-Gas-Phasenübergang bei chemischem Quark-Potential $\mu_c \sim M_p$ (Protonenmasse). Folgt man der Kurve des Phasendiagramms dieses Übergangs hin zu höheren

Dichten, so gelangt man ebenfalls an einen CEP, der jedoch nicht mit dem hypothetischen CEP des QGP zu verwechseln ist. Bei noch höheren Dichten wird erneut die asymptotische Freiheit deutlich. In diesem Grenzwert kalter und sehr dichter Materie befindet man sich zudem in der sogenannten supraleitenden Phase. Diese ist vergleichbar mit der supraleitenden Phase in der Elektrodynamik, wobei die zusätzliche Farbladung eine nicht triviale Rolle in der Konstruktion der Cooper-Paare einnimmt.

Das Hauptaugenmerk liegt in dieser Arbeit auf dem erwähnten Flüssigkeit-Gas-Phasenübergang. Dieser Übergang liegt im Bereich von Energien, die zu groß für effektive Theorien, jedoch zu klein zur Anwendung von Störungstheorie, sind. Deshalb wenden wir Gittereichtheorie im Rahmen der QCD an, in der die Raumzeit diskretisiert und durch ein endliches Gitter mit endlichem Gitterabstand beschrieben wird. Dadurch wird ein kleinster Abstand, der Gitterabstand a , genauso wie ein größter Abstand, aN , definiert. Mithilfe der Gitter-QCD lässt sich der Pfadintegralformalismus approximieren, in dem die unendliche Anzahl von möglichen Pfaden auf eine endliche, von der Gittergröße abhängige Anzahl reduziert wird. Diese Diskretisierung wurde erstmals von Wilson im Jahre 1974 formuliert. Sie ist so konstruiert, dass sie im Grenzwert $a \rightarrow 0$ (Kontinuumslimes) und $N \rightarrow \infty$ (sodass $aN \rightarrow \infty$) die volle QCD reproduziert. Abweichungen werden meist in zwei Kategorien unterteilt, einerseits *finite size* Effekte (aufgrund von $a \neq 0$) und andererseits *finite volume* Effekte (da $aN \neq \infty$).

Die Gitter-QCD hat zweifelsfrei ihre Wirkungskraft durch die Bestätigung einer Vielzahl experimenteller Ergebnisse von Vakuum-Observablen unter Beweis gestellt. Beispiele dafür sind die Massen leichter Hadronen, die bis auf wenige Prozent genau übereinstimmen. Dies dient nicht nur als eine Bestätigung der Gitter-QCD, sondern auch als eine Bestätigung der QCD und des Quark-Modells als eine Theorie zur Beschreibung der Natur.

Auch wenn die Gitter-QCD die mathematischen Herausforderungen der Berechnung von Observablen deutlich vereinfacht, muss man sich dennoch numerischer Methoden bedienen, um an die vollen nicht-perturbativen Ergebnisse zu gelangen. Gängige Methoden beruhen auf der stochastischen Integration, wie beispielsweise der Monte-Carlo-Integration oder der Langevin-Integration. Diese Methoden nutzen die Tatsache, dass man das Integrationsmaß selbst verwenden kann, um Informationen über die dominanten Beiträge zum vollen Integral zu erlangen.

Diese Methode lässt sich auch auf thermodynamische Systeme anwenden, in denen die Minkowski-Zeit durch die periodische euklidische Zeit ersetzt wird. Die euklidische Zeit steht dabei im Zusammenhang mit der Temperatur in thermodynamischen Feldtheorien. Der Versuch ein chemisches Potential hinzuzufügen bringt jedoch Probleme numerischer Natur mit sich. Auch wenn die Fermionen-Determinante (ein mathematisches

Objekt, das die volle fermionische Dynamik beinhaltet) bei verschwindendem chemischen Potential eine reelle Zahl ist, wird diese in die komplexe Ebene gerückt, sobald das chemische Potential von Null verschieden ist. Das stellt in der Kontinuumsphysik keine Probleme dar, da sich die imaginären Komponenten in der Betrachtung des vollen Satzes der Integrale gegenseitig eliminieren. Für die numerische Implementation ist das hingegen nicht der Fall, da man den komplexwertigen Integranden nicht mehr als Wahrscheinlichkeitsgewicht der stochastischen Variablen verwenden kann. Dieses Problem kann theoretisch umgangen werden, indem man eine leicht modifizierte, jedoch ähnliche Verteilung zur Berechnung der Observablen wählt. Dieses Verfahren ist bekannt als *reweighting*. Für $\mu/T > 1$ lassen sich jedoch häufig nur sehr schwer passende Verteilungen finden, wodurch eine stochastische Integration nicht mehr möglich ist. Dieser Sachverhalt wird im Allgemeinen als *sign problem* bezeichnet.

Eine weitere Schwierigkeit, die bei Gitterberechnungen mit endlichem chemischen Potential auftritt, hat ihren Ursprung im Pauli-Prinzip. Aufgrund der fermionischen Natur von Quarks kombiniert mit dem diskreten Gitter besitzt ein System in der Gitter-QCD eine obere Schranke für die Anzahl der zugelassenen Quarks. Dieses Gitter-Artefakt wird problematisch an dem Punkt, an dem das Gitter zur Hälfte gefüllt ist, also dem Punkt, an dem die Hälfte der möglichen Quantenzustände besetzt sind. Dieses Phänomen wird als *lattice saturation* bezeichnet und wird selten diskutiert, da das *sign problem* deutlich früher bei der Berechnung auftritt. Sobald wir letzteres überwunden haben, wird ersteres zu einer echten Herausforderung, die wir ebenfalls bewältigen müssen.

Um das *sign problem* abzuschwächen, verwenden wir eine effektive Gittertheorie, in der wir das auftretende Integral über einen Teil der Freiheitsgrade analytisch auswerten. Wir werden zeigen, dass diese Methode erfolgreich die Stärke des *sign problem* mildert und dass die daraus resultierende effektive Theorie leicht mithilfe von *reweighting*-Techniken simuliert werden kann. Um diese Rechnung durchführen zu können, muss der Integrand in bestimmten Grenzwerten entwickelt werden. Ein geeigneter Entwicklungspunkt ist die Theorie der stark gekoppelten statischen Quarks, in der die Integrale der Zustandssumme analytisch lösbar sind. Der zugehörige Grenzwert wird als *strong coupling limit* bezeichnet und entspricht dem Grenzwert $\alpha_s \rightarrow \infty$, was in der Gitter-QCD dem Verschwinden des Parameters $\beta \propto 1/\alpha_s$ der Wilson-Plakette entspricht. Des Weiteren bezeichnen statische Quarks jene mit Masse $m_q \rightarrow \infty$. Verwendet man Gitter-QCD mit Wilson-Fermionen, so taucht die Masse nur im sogenannten *hopping parameter* $\kappa = \frac{1}{2(4+am_q)}$ auf. Der Limes statischer Quarks ist somit eine Entwicklung um den Punkt $\kappa \rightarrow 0$, auch bekannt als *hopping expansion*.

Durch geeignete Reskalierung der Gittertheorie muss die zugehörige Kontinuumsphysik zugänglich sein. Aufgrund von Renormierungseffekten erhält die Kopplungskon-

stante eine Abhängigkeit von der Skala des Systems, das bedeutet $\beta \rightarrow \beta(\alpha)$, wodurch wir die α -Abhängigkeit der Observablen durch Variation von β bestimmen können. Das Verhalten des Kontinuumslikes in Abhängigkeit von β kann mithilfe von Störungstheorie studiert werden und den tatsächlichen Kontinuumslikes erlangt man durch $\beta(\alpha \rightarrow 0) \rightarrow \infty$, welches der entgegengesetzte Grenzwert zu unserer Entwicklung ist. Betrachtet man jedoch höhere Ordnungen dieses Parameters, kann man eine Aussage über die Skala der Gitter-QCD treffen, von der eine analytische Erweiterung zum Kontinuum möglich ist. Weitere Einzelheiten dazu folgen später im Text.

Die effektive Theorie gewährleistet die Bestimmung der korrekten Entwicklungskoeffizienten der vollen Gitter-QCD in den angesprochenen Grenzwerten. Damit ermöglicht sie es uns diese interessante Region des QCD-Phasenraumdiagrammes von fundamentaler Basis aus zu untersuchen. Der Hauptbestandteil der vorliegenden Arbeit ist die Herleitung dieser effektiven Theorie und beinhaltet ein volles Kapitel, das sich allein damit beschäftigt, die korrekten Entwicklungskoeffizienten Ordnung für Ordnung zu bestimmen. Es wird sich herausstellen, dass sich die Kombinatorik der Entwicklung bei niedrigen Temperaturen deutlich vereinfacht, was bezogen auf das Gitter einer großen zeitlichen Gitterausdehnung entspricht. Daraus resultiert ein dritter Entwicklungsparameter T (oder genauer $\alpha T = 1/N_t$). Schlussendlich profitieren wir auch noch von den Vereinfachungen, die bei sehr dichten Systemen auftreten. Wenn die chemischen Potentiale hoch genug sind, leisten die Antiquarks keinen großen Beitrag und können daher vernachlässigt werden. Die resultierenden Freiheitsgrade sind die sogenannten *Polyakov loops*, welche geschlossene Quarklinien in zeitlicher Richtung sind. Die effektive Wirkung setzt sich dann aus nächster-Nachbar-Wechselwirkungen, übernächster-Nachbar-Wechselwirkungen, etc. dieser Variablen zusammen. Man kann das System demnach als ein kompliziertes nicht-lokales System von kontinuierlichen Spins mit bestimmten Symmetrien betrachten. Wir werden am Ende der Arbeit ein $\mathcal{O}(\kappa^8 u^5 N_t^4)$ -Ergebnis dieser effektiven Theorie präsentieren.

Auch wenn die numerische Fähigkeit der effektiven Theorie diskutiert wird, ist sie nicht der Hauptreiz der gegenwärtigen Arbeit. Stattdessen präsentieren wir eine neue, rein analytische Behandlung der effektiven Theorie. Dabei basieren unsere Untersuchungen auf der klassischen *linked cluster* Entwicklung, welche die in der Praxis gängige Methode ist, um Ergebnisse für die Gleichgewichts-Thermodynamik von Spin-Systemen zu erhalten. Diese muss jedoch verallgemeinert werden, um den Anforderungen unserer nicht-lokalen Wirkung gerecht zu werden. Deshalb erarbeiten wir eine *polymer linked cluster* Entwicklung, welche sich Techniken der Graphentheorie bedient.

Wir verwenden eine Vielzahl analytischer Methoden, um die *resummation*-Verfahren, die mit numerischen Methoden unerreichbar sind, zu entwickeln. Dazu zählt die so-

genannte *chain resummation*, die alle Beiträge der effektiven Theorie zusammenzählt, die eine Kette bilden oder in eine solche eingeschlossen werden können. Eine weitere wäre die *ladder resummation*, die wir ebenfalls behandeln werden. Wir werden sehen, dass diese *resummation*-Methoden die Konvergenz der Theorie deutlich steigern, was den Anreiz schaffen sollte, zukünftige Arbeiten auf diese Art der Verbesserungen zu fokussieren.

Am Ende dieser Arbeit werden wir verschiedene thermodynamische Größen unter Verwendung unserer rein analytischen großkanonischen Zustandssumme berechnen. Dies wird im Temperaturbereich ~ 10 MeV und bei chemischen Potentialen nahe der Baryonenmasse geschehen. Dabei sehen wir einen Crossover-Übergang zu atomarer Materie, da sich der CEP des Flüssigkeit-Gas-Überganges in Richtung niedrigerer Temperaturen bewegt, wenn man die Quarkmasse erhöht. Eine Untersuchung der zuvor erwähnten *lattice saturation* wird ebenfalls gezeigt. Dieses Problem zeigt sich insbesondere in der Kontinuumsextrapolation und wir werden sehen, dass Gitter-Berechnungen bezüglich der Physik jenseits des Flüssigkeit-Gas-Phasenüberganges erschwert werden, obwohl Ergebnisse im Kontinuumslimit nicht von diesen Gitterartefakten beeinträchtigt werden.

Unser letztes und interessantestes Ergebnis bezieht sich auf die Zustandsgleichung für die QCD schwerer Quarks in kalter und dichter Materie. Es zeigt sich, dass die Kontinuumsphysik, die auf unseren Berechnungen mit schweren Quarks und starker Kopplung beruht, sehr ähnlich zur Physik schwach gekoppelter Fermionen ist. Der auftretende Wechsel der Freiheitsgrade des Systems ist ein dynamischer Prozess und demonstriert die Stärke unseres Ansatzes. Wir führen zwar Untersuchungen der beitragenden Freiheitsgrade durch, dennoch sind Fragen für weiterführende Arbeiten offen gelassen.

Die effektive Theorie kann zusätzlich erweitert werden, um Eichtheorien verschiedener lokaler Symmetriegruppen, wie zum Beispiel $SU(N_c)$ ($N_c = 3$ für QCD), zu beschreiben. Diese Tatsache macht sich in der gesamten Arbeit bemerkbar, da die Symmetriegruppe nur sehr selten explizit festgelegt wird. Eine Welt mit etwa $N_c = 4$ würde sich sehr von unserer unterscheiden, da beispielsweise jedes Hadron ein Boson wäre. Der Grundstock einer solchen Untersuchung ist in CHAPTER 5 zu finden und weiterführende Berechnungen sind aktuell im Gange. Es wird außerdem ein Appendix angeboten, in dem die zugehörigen mathematischen Werkzeuge detailliert beschrieben werden.

Acknowledgements

First and foremost I would like to thank my supervisor Owe Philipsen, for letting me come to Frankfurt, for giving me a very interesting project to work on, and for letting me approach it in my own whimsical way.

I would also like to extend a thank you to the entire working group, who has made my stay here a pleasant one. A special thanks to the interesting people I have had the pleasure of sharing an office with, and for enduring my presence.

I am forever grateful to my friends and family in Norway, without whom I would be a very different person than I am today.

Finally, a big thank you to my friends who helped proofread this thesis; Christopher Kolbjørnsen, Mathias Neuman, Jonas Scheunert, Inga Strümke and Savvas Zafeiropoulos. As well as additional thanks to Björn Wagenbach for translating the German summary.

PART I

INTRODUCTION

INTRODUCTION

The current state of human knowledge suggests that the majority of visible matter in the universe is made up of hadrons which in turn consist of the more fundamental *quarks*. We have so far discovered six species, or flavours, of quarks, namely the up, down, strange, charm, top and bottom. These fundamental particles carry three sets of charges: electric charge, flavour charge and colour charge. The latter manifests itself through the confinement process that binds the quarks together into inseparable hadrons, and the resulting binding energy is responsible for almost 99 % of the mass of these bound particles. For example the proton has a mass of 938.27 MeV, while its constituents, two up quarks and a single down quark, have a total rest mass of no more than 9.8 (1.9) MeV [Olive et al., 2014]. It is therefore of great importance to understand the dynamics governing interactions between particles carrying colour charges and the force's mediators, the *gluons*.

Throughout the various stages of discoveries in the world of particle physics, the theories we use to describe nature have evolved. The current reigning model of the universe is called the Standard Model of particle physics, and categorises the known world consisting of 6 leptons, 18 quarks, 13 mediators, and their antiparticles into symmetry groups. This theory describes three of the four established fundamental forces as a quantum theory of fields, electromagnetism, the strong- and weak nuclear forces, and it is the most successful theory to date, predicting experimental values with astonishing accuracy.

The subset of the Standard Model that describes the interaction between quarks and gluons is called *Quantum Chromodynamics* (QCD). The advent of QCD came in the 1960's, in a period where a great number of "fundamental" particles were discovered. Both Gell-Mann [1962] and Ne'eman [1961] found structure and symmetry in this zoo of new particles, and to explain this phenomenon, the existence of quarks was suggested [Gell-Mann, 1964]. Due to the fermionic nature of the quarks, an additional quantum number was needed to allow for the quarks inside baryons to occupy the required spin and flavour quantum states. This new quantum number was named *colour*, hence *chromodynamics*, from ancient Greek $\chi\rho\acute{\omega}\mu\alpha$ [Greenberg, 1964].

QCD has an extremely rich structure, being confining at low energies, while also possessing *asymptotic freedom*. It has an internal energy scale, $\Lambda_{\text{QCD}} \approx 200$ MeV, which arise from dimensional transmutation, and gives the defining length scales of the theory. It also has a non-trivial topological structure, resulting in instanton configurations in

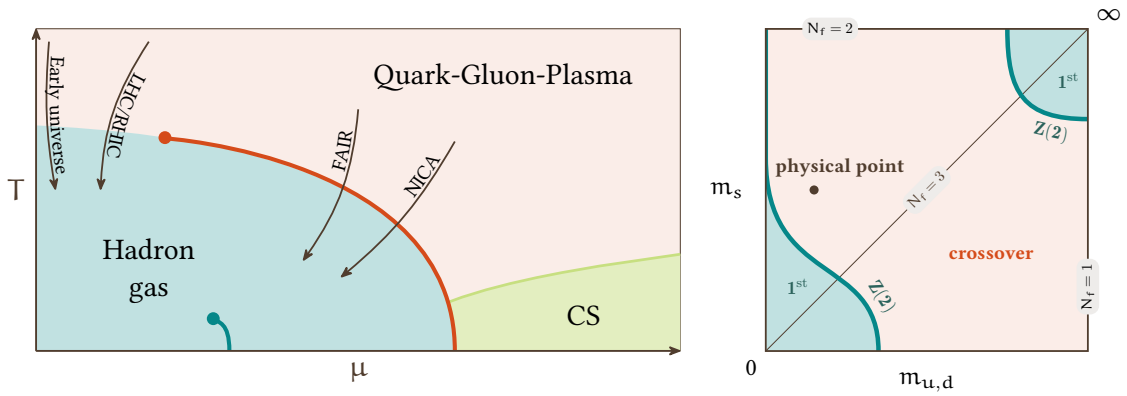


Figure 1.1.: Left: A simplified, conjectured phase diagram of QCD with path symbolising the scan lines of various current and future experiments. Right: The Columbia plot, showing the deconfinement transition order for various quark masses.

the vacuum [’t Hooft, 1976].

Of particular interest is the phase diagram of QCD in the temperature-chemical potential plane, sketched in FIGURE 1.1 (left). At low temperatures and densities, QCD is confining, and thus the effective degrees of freedom are the bound states, baryons and mesons. Moving along the temperature axis, one eventually passes into the quark-gluon-plasma phase, a phase in which the thermodynamic energies are high enough that the quarks and gluons deconfine. In this phase the quarks and gluons move around semi-freely, weakly interacting with each other within the bulk of the plasma. This *deconfinement transition* is in fact not a phase transition at all, but has been shown to be a crossover transition, with a pseudo-critical temperature $T_c \approx 150 - 170$ MeV [Aoki et al., 2006]. It is still an open question whether moving along this line of crossover transitions eventually will result in a phase transition and an accompanying critical endpoint. The nature of the crossover transition depends on the constituent quark masses and the number of quark flavours, degenerate or otherwise. This dependence is often represented in a *Columbia* plot, FIGURE 1.1 (right). Although the physical point clearly sits in the crossover area, the existence of a critical endpoint depends on whether the lower $Z(2)$ critical line shrinks or expands at increasing chemical potential. It is also an open question whether this critical line actually touch the chiral axis in the left or not [Philipsen and Pinke, 2016].

Back to the T - μ phase diagram, moving along the chemical potential axis at zero temperature, one finds a first order liquid-gas phase transition at baryon chemical potentials around the proton mass. Following this transition curve to higher temperature, it will eventually end in a critical endpoint. On the other hand, continuing to even higher chemical potentials, Cooper’s theorem tells us that we should find various colour superconducting phases. This has been shown for asymptotically large densities. However, no first principle proof for intermediate values exists. Due to the nature of QCD, and the enlarged number of quantum numbers, there are multiple superconducting phases. These phases differ in which quantum numbers are fixed to create Cooper pairs. One has the 2-flavour superconducting phase and the colour-flavour-locked superconducting

phase, where the colour indices play different roles in the two cases. For a discussion on the phase structure of QCD see e.g. [Rajagopal and Wilczek, 2000; Rischke, 2004].

The goal of this thesis is to attempt a study of QCD at low temperatures and high densities, close to the liquid-gas phase transition. Due to the confining nature of QCD, such a study cannot be carried out with the use of perturbation theory. A common approach to this is using low energy effective models for QCD, such as hadron gas resonant models, and meson models. We will be more ambitious, and will undertake a first principle study through the medium of lattice gauge theories. As we will see in the introductory chapters, the lattice formalism is ill-suited for carrying out simulations in the cold and dense regime of QCD due to the sign problem, which we will surmount by the use of an effective lattice theory that has matching series coefficients to full QCD in a specific parameter region.

The outline of the thesis is as follows. We introduce the necessary formalism in CHAPTER 2. This will include the quantum field theoretical description of a special type of quantified local symmetries, and a short introduction to the group theory of continuous groups. We then introduce lattice gauge theory through the discretisation of space-time, and finally an overview of important lattice concepts is given.

In CHAPTER 3 we proceed to introducing the necessary formalism for transitioning our quantum field theory, and with it lattice gauge theory, into the realm of thermodynamics and statistical mechanics. In this section we take great care to properly define difficulties that arise in high density lattice simulations, namely the sign problem. We also present a handful of "remedies", and discuss their applicability.

This is followed by CHAPTER 4 in which we introduce our method of choice for dealing with the sign problem. This is a systematic series expansion approach around the dynamics of heavy quarks ($m_q \rightarrow \infty$) and strong coupling ($\alpha_s \rightarrow \infty$). The derivation of the effective theory is carried out in great detail, and various important steps for convergence is discussed. We round off the chapter with a discussion on the numerical evaluation of this simplified lattice theory.

The thesis culminates in the purely analytical treatment of this effective lattice theory. CHAPTER 5 begins with the introduction of the linked cluster expansion, which enter as a bedrock on which we build the remainder of the analysis, and is the de factor method for studies of thermodynamics through series expansions. We then develop a generalisation to the cluster expansion for more intricate theories, and name it the *polymer linked cluster expansion*. We then introduce powerful resummation schemes to extend the region of relevance of our theory further. Finally, the equation of state for cold and dense, heavy QCD is studied and discussed.

GAUGE THEORIES AND LATTICE GAUGE THEORIES

In this chapter we formally introduce the quantum field theory describing fermions invariant under local group transformations, and introduce the Dirac Lagrangian in SECTION 2.1. SECTION 2.2 gives a brief overview of basic group theory, introducing the concepts and tools necessary for the thesis. In SECTION 2.3 we investigate the defining symmetry properties of our quantum field theory, and how these can be extended. After this introduction to continuum physics, SECTION 2.4 discretises space-time and puts our theory on a lattice. In SECTIONS 2.5, and 2.6, we review the similarities and differences between the lattice and the continuum, and stress where additional care has to be taken. Finally, we give a very quick introduction to numerical evaluation of lattice theories in SECTION 2.7.

For the introduction, standard texts on the subject matter have been consulted. Among these are introductory volumes on quantum field theory [e.g. Peskin and Schroeder, 1995; Maggiore, 2004], lattice gauge theory [e.g. Montvay and Münster, 1997; Gattringer and Lang, 2009] and group theory [e.g. Georgi, 1999; Fulton and Harris, 2013].

2.1 THE FREE DIRAC LAGRANGIAN

The undoubtedly most important quantity in Quantum Field Theory (*QFT*) and Statistical Mechanics (*SM*) are the generating functional, named \mathcal{Z} , and the partition function, for the two theories respectively. In *SM*, it is defined as

$$\mathcal{Z}_E = \text{tr} e^{-H/T} = \int \prod_i d\phi_i e^{-S_E[\phi_i]}, \quad (2.1)$$

where we have chosen to represent the trace over the Hamiltonian matrix by an integral over a continuous system, described by a set of field parameters, ϕ_i . There is an analogue between the two theories and one can convert from one to the other by Wick rotating the time coordinate $x_E^0 = -ix_M^0$. Whenever the possibility for confusion exists we use an *M* to symbolise Minkowski space, the world of *QFT*, and an *E* to symbolise Euclidean space, the world of *SM*.

The action, \mathcal{S} , is in turn defined by the Lagrangian density

$$\mathcal{S}[\phi_i] = \int d^4x \mathcal{L}[\phi_i(x)], \quad (2.2)$$

and our theories are uniquely defined by \mathcal{L} and the properties of the fields ϕ_i .

Of physical interest are expectation values of Hermitian operators \widehat{O} , which in the path integral formalism can be computed using the partition function

$$\langle \widehat{O}[\phi_i] \rangle = \frac{1}{\mathcal{Z}_E} \int \prod_i d\phi_i O[\phi_i] e^{-S_E[\phi_i]}, \quad (2.3)$$

It is the set of Hermitian operators that represents physical observables. These can for example be accessed by the introduction of source terms to the action

$$\mathcal{Z}_E[J_i] = \int \prod_i d\phi_i e^{-S_E[\phi_i] - \int J_i \phi_i} \quad (2.4)$$

with which we can rewrite the expectation value in terms of functional derivatives

$$\langle O[\phi_i] \rangle = O \left[\frac{\delta}{\delta J_i} \right] \log \mathcal{Z}_E \Big|_{J=0}, \quad (2.5)$$

hence the name generating functional.

2.1.1 The Dirac Lagrangian

Our starting point will be the Dirac Lagrangian, which reads

$$\mathcal{L} = \bar{\psi}_i (i\gamma^\mu \partial_\mu - m_i) \psi_i. \quad (2.6)$$

Here we have introduced the fermionic fields ψ_i . To get the right statistics, these fields have to obey the anti-commutation relations, and therefore they have to comply with the *Grassmann algebra*

$$\{\psi_i, \psi_j\} \equiv \psi_i \psi_j + \psi_j \psi_i = 0, \quad (2.7)$$

$$\{\bar{\psi}_i, \bar{\psi}_j\} \equiv \bar{\psi}_i \bar{\psi}_j + \bar{\psi}_j \bar{\psi}_i = 0, \quad (2.8)$$

$$\{\bar{\psi}_i, \psi_j\} \equiv \bar{\psi}_i \psi_j + \psi_j \bar{\psi}_i = \delta_{ij}. \quad (2.9)$$

This Lagrangian describes the dynamics of a set of free, massive fermions, which by itself is not very exciting. There are however different ways to add interactions while still maintaining the desired symmetry properties (which we will discuss later). Depending on the physics one is interested in describing, one such extension is given by the addition of a self interacting coupling of the fermions, e.g. a four point term, $g(\bar{\psi}\psi)^2$, which is named the NJL model [Nambu and Jona-Lasinio, 1961]. Another option is to introduce new fields and corresponding couplings to these fields. One such model is the linear sigma model [Gell-Mann and Lévy, 1960], describing effective low energy couplings between quarks and mesons. Finally, by localising certain symmetries of the system one can organically induce new fields and coupling to the theory, which we examine closer. For such a study we need a short overview of group theory, which we will present next.

2.2 A GROUP THEORY PERSPECTIVE

A group G is a set and a rule for assigning to every (ordered) pair in the set a new element also in the set

$$\text{For every } f, g \in G, \text{ then } h = fg \in G, \quad (2.10)$$

this assignment is called the group product. The group product is associative, and in every group a unit element (e) exists. Every element also has an inverse so that

$$\forall f \in G, \exists f^{-1} : f^{-1}f = ff^{-1} = e. \quad (2.11)$$

A representation of a group G on a complex vector space V is a homomorphism

$$D_R : G \rightarrow GL(V) \quad (2.12)$$

of the group G on the group of automorphisms of V . Therefore representations have to maintain the group structure, meaning

$$D_R(e) = \mathbb{1}_R, \quad (2.13)$$

$$D_R(f)D_R(g) = D_R(fg). \quad (2.14)$$

In physics we are normally content with a coordinate basis, in which the representations map to n by n invertible matrices, i.e. $V := \mathbb{C}$, $GL(V) := M_{\mathbb{C}}(n, n)$.

2.2.1 Lie groups

If the elements of a group G depends smoothly on some set of parameters, $g(\alpha_i) \in G$, we call that group a Lie group. Lie groups make up the theory of continuous transformations, and are therefore of special interest to physics. The continuous nature of the Lie groups creates a sense of closeness where two elements that are close to each other can be represented through differentials, e.g.

$$D_R(g(\delta\alpha_i)) = \mathbb{1}_R + i \delta\alpha_i T_{Ri} + \mathcal{O}(\delta\alpha^2). \quad (2.15)$$

One commonly refers to T_{Ri} as the generators of the group G . Applying the smoothness condition to the group product, EQ (2.14), we find that the commutator of the generators follow a special relation

$$[T_{Ri}, T_{Rj}] = i f_{ijk} T_{Rk}. \quad (2.16)$$

The structure constants, f_{ijk} , are in fact independent of the representation R . They are tremendously important as they summarise the entire group multiplication law. They are also referred to as the *algebra* of the group, \mathfrak{g} . The generators and the group algebra will come into play when we later introduce continuous symmetries of our quantum theory of fields. Using the Jacobi identity, it is possible to see that the structure constants themselves comply with the multiplication law. We can therefore use the structure constants as a representation of the algebra \mathfrak{g} called the *adjoint representation*

$$[T_{\text{adj}i}]_{jk} \equiv -i f_{ijk}, \quad (2.17)$$

which fulfils EQ (2.16).

2.2.2 Character and character expansion

The character of a representation is defined as

$$\chi_R(g) = \text{tr } D_R(g). \quad (2.18)$$

The characters appear frequently in field theory due to the cyclic properties of the trace and its ability to facilitate the creation of invariant objects. On top of this, the characters span a basis of functions that share this cyclic property, i.e. any function $\rho(fgf^{-1}) = \rho(g)$. Hence

$$\rho(g) = \sum_r \rho_r \chi_r(g), \quad (2.19)$$

with

$$\rho_r = \int_{g \in G} dg \chi_r^*(g) \rho(g). \quad (2.20)$$

It is common to factor out both the trivial representation ($D_0(g) = 1$), as well as the dimension of the representation, $d_R = \text{tr } D_R(e)$, and write

$$\rho(g) = \rho_0 \left(1 + \sum_{r \neq 0} d_r \bar{\rho}_r \chi_r(g) \right), \quad (2.21)$$

which we will refer to as the character expansion. We will make use of this in SECTION 4.2.

2.2.3 Group integrals

Lastly we need to define integrals over continuous groups. We introduce the Haar integration measure, which has the following properties

$$\int dg \rho(g) = \int dg \rho(fg) = \int dg \rho(gf) \quad \forall f \in G \quad (2.22)$$

and the normalisation

$$\int dg = 1. \quad (2.23)$$

Throughout the derivation of the effective theory, we will encounter polynomial integrals on the form

$$I = \int dg g^n (g^{-1})^m \quad (2.24)$$

or more commonly, with a representation

$$I_{i_1, j_1, \dots, i_n, j_n}^{k_1, l_1, \dots, k_m, l_m} = \int dg D_R(g)_{i_1 j_1} \cdots D_R(g)_{i_n j_n} D_R(g^{-1})_{k_1 l_1} \cdots D_R(g^{-1})_{k_m l_m}. \quad (2.25)$$

There are multiple ways of handling these integrals, depending on the Lie group one is interested in. For $SU(N)$ one can for instance decompose the integral into generalised Euler angles [as described in Tilma and Sudarshan, 2004], construct generating functionals for the integrals $I_{i_1, j_1, \dots, i_n, j_n}^{k_1, l_1, \dots, k_m, l_m}$ [details in Creutz, 1978b], or one can use tensor product decompositions to write the integrals in terms of Young projectors [Christensen et al., 2015]. In the present work, a combination of the first two approaches is used, and extensive details are provided in APPENDICES A.1, A.2, and A.3.

2.3 SYMMETRIES OF THE LAGRANGIAN

With the necessary formalism in place, we can now discuss the symmetries of the Lagrangian we introduced in EQ (2.6). We first look at the symmetries that come by construction before delving into possible ways of extending the theory to be both globally and locally symmetric under additional transformations.

2.3.1 Symmetries by construction

Every quantum field theory is constructed to be symmetric under the full Poincaré group, namely the group of space-time translations plus Lorentz transformations.

To see the other symmetries of the Dirac Lagrangian we have to decompose the fields into its spinorial components. Every element of ψ_i in EQ (2.6) is a four-component spinor, and the γ^i 's, 4×4 matrices. In the standard representation they take the form

$$\psi = \frac{1}{\sqrt{2}} \begin{pmatrix} \psi_R + \psi_L \\ \psi_R - \psi_L \end{pmatrix}, \quad \gamma^0 = \begin{pmatrix} 1 & 0 \\ 0 & -1 \end{pmatrix}, \quad \gamma^i = \begin{pmatrix} 0 & \sigma^i \\ -\sigma^i & 0 \end{pmatrix}. \quad (2.26)$$

The fields $\psi_{R,L}$ are two component fields that transform under two distinct representations of the Lorentz group, $(\frac{1}{2}, 0)$ and $(0, \frac{1}{2})$ respectively. With this choice of basis the Dirac Lagrangian reads

$$\mathcal{L} = i\bar{\psi}_R \gamma^\mu \partial_\mu \psi_R + i\bar{\psi}_L \gamma^\mu \partial_\mu \psi_L - m(\bar{\psi}_R \psi_L + \bar{\psi}_L \psi_R). \quad (2.27)$$

It is apparent that this Lagrangian is symmetric under the $U(1) \otimes U(1)$ transformation

$$\psi_{R,L} \rightarrow e^{i\alpha_{R,L}} \psi_{R,L} \quad (2.28)$$

if and only if the mass term is set to zero. Invariance of the independent transformations of the left- and right-handed fields is called *chiral* symmetry, and signals the existence of helicity eigenstates. The presence of the mass term explicitly breaks the symmetry into a single $U(1)$ symmetry, where $\alpha_R = \alpha_L$, commonly referred to as the vector- $U(1)$.

The global symmetry group of ψ can be trivially extended to admit any Lie group by making the field live in the vector space the representation of choice acts on, and carry out transformations in the following way

$$\psi \rightarrow D_R(g)\psi, \quad \bar{\psi} \rightarrow \bar{\psi} D_R^\dagger(g), \quad g \in G. \quad (2.29)$$

This symmetry has an associated conserved Noether current for every generator of the group G

$$j_i^\mu = \bar{\psi} \gamma^\mu T_i \psi, \quad \text{where} \quad \partial_\mu j_i^\mu = 0, \quad (2.30)$$

which gives the associated charge

$$Q_i = \int d^3x \bar{\psi} \gamma^0 T_i \psi. \quad (2.31)$$

2.3.2 Gauge symmetries

We just saw that the Lagrangian can be trivially extended to be invariant under global symmetry transformations. Next, we want to promote them to local symmetries. This is motivated post facto by QED, which exhibits a local $U(1)$ symmetry.

The idea was first explored by Weyl, who tried introducing local scale transformations to the metric

$$g_{\mu\nu}(x) \rightarrow e^{\sigma(x)} g_{\mu\nu}(x) \quad (2.32)$$

which prompted the need for an additional vector field to gauge how much one needs to adjust scales to compare two separate points. Weyl then showed that these vector fields need to follow Maxwell's equations, and postulated that the vector fields were in fact nothing else than Maxwell's electromagnetic potentials [Weyl, 1918]. It was later discovered that classically scale invariant theories lose this symmetry due to a quantum effect sometimes referred to as the *Weyl anomaly*. In fact, it is this very effect that is responsible for the bulk contribution to the hadron masses in QCD. So, although Weyl's ideas do not describe how the world actually works, it served as a cornerstone on which the theories connecting the geometry of space to local symmetries was built. Instead of adjusting local length scales, we will apply group transformations to vector spaces that live on top of space-time.

We define a local group element by a Lie group whose parameters are space-time dependent $g(\alpha_i(x))$. We will use the short hand notation $U(x) = D_R(g(\alpha_i(x)))$ for representations of such group elements. We suppress the representation R -subscript wherever it is not needed. The transformations of the fields at a single coordinate follow trivially from EQ (2.29)

$$\psi(x) \rightarrow U(x)\psi(x), \quad \bar{\psi}(x) \rightarrow \bar{\psi}(x)U^\dagger(x). \quad (2.33)$$

There is however no way to make derivative terms invariant under these symmetries. This becomes obvious when writing the derivative in terms of limits

$$\eta^\mu \partial_\mu \psi(x) = \lim_{\delta \rightarrow 0} \frac{1}{\delta} (\psi(x + \delta\eta) - \psi(x)) \quad (2.34)$$

where η^μ is some unit vector. We have to take the difference between fields at two different points in space-time, which transform independently under EQ (2.33). Naively calculating this difference is nonsensical as one is allowed to choose the basis of the representation of the different points independently, meaning that $\psi(x)$ and $\psi(y)$ can be members of different vector spaces. We therefore introduce the parallel transporters, $\Lambda(y, x)$, which transforms between the vector spaces of the fields at the points x and y in a smooth way [Wu and Yang, 1975]. We define the *covariant derivative* as

$$\eta^\mu D_\mu \psi(x) = \lim_{\delta \rightarrow 0} \frac{1}{\delta} (\psi(x + \delta\eta) - \Lambda(x + \delta\eta, x)\psi(x)). \quad (2.35)$$

where the transporter Λ makes sure we subtract quantities which are defined on the same vector space. These transformations are nothing but coordinate transformations of the vector spaces, and must therefore itself be a member of the representations on G . From this it follows that Λ transforms as

$$\Lambda(y, x) \rightarrow U(y)\Lambda(y, x)U^\dagger(x). \quad (2.36)$$

This in turn gives rise to the subsequent transformation rule for the covariant derivative

$$D_\mu \psi(x) \rightarrow U(x) D_\mu \psi(x), \quad (2.37)$$

ensuring that terms of the form $\bar{\psi} D_\mu \psi$ remain invariant under local symmetry transformations. As Λ is a representation of G , we can express it in terms of the generators of the group. On infinitesimal form, this is

$$\Lambda(x + \delta\eta, x) = 1 + ig\delta\eta^\mu A_\mu^i(x) T_i + \mathcal{O}(\delta^2) \quad (2.38)$$

where the A_μ^i have to transform as

$$A_\mu^i \rightarrow A_\mu^i + \partial_\mu \alpha^i - gf^{ijk} \alpha^j A_\mu^k + \mathcal{O}(\alpha^2), \quad (2.39)$$

which is independent of the representation. The locally symmetric Dirac Lagrangian thus reads

$$\mathcal{L} = \bar{\psi}(i\gamma^\mu D_\mu - m)\psi. \quad (2.40)$$

Unfortunately, without a kinetic term for the newly introduced fields A_μ^i , the theory would permit violently oscillating fields with no cost in energy [’t Hooft, 2002]. This would make our theory non-renormalisable, which we obviously want to avoid. We therefore need to find a kinetic term for the fields that admits all of our restrictions. When constructing such a term, it is natural to once more turn to the parallel transporters, it being the main ingredient in adjusting the kinetic term of the fermions. Using the gauge transformation of Λ , it is easy to see that the geometric plaquette could create such a term

$$\begin{aligned} U_{\mu\nu}(x) = & \Lambda(x, x + \hat{\nu}\delta) \Lambda(x + \hat{\nu}\delta, x + \hat{\mu}\delta + \hat{\nu}\delta) \\ & \times \Lambda(x + \hat{\mu}\delta + \hat{\nu}\delta, x + \hat{\mu}\delta) \Lambda(x + \hat{\mu}\delta, x) \end{aligned} \quad (2.41)$$

which transforms as

$$U_{\mu\nu}(x) \rightarrow U(x) U_{\mu\nu}(x) U^\dagger(x), \quad (2.42)$$

and hence $\text{tr } U_{\mu\nu}(x)$ is invariant under local group transformations. Expanding $U_{\mu\nu}$ in the fields A_μ^i , we get

$$U_{\mu\nu} = 1 + ig\delta^2 T_i (\partial_\mu A_\nu^i - \partial_\nu A_\mu^i + gf^{ijk} A_\mu^j A_\nu^k) + \mathcal{O}(\delta^3) \quad (2.43)$$

from which we extract the term

$$F_{\mu\nu}^i = \partial_\mu A_\nu^i - \partial_\nu A_\mu^i + gf^{ijk} A_\mu^j A_\nu^k, \quad (2.44)$$

which is both invariant under the gauge transformations as well as being the kinetic term we were looking for. The full gauge extended Lagrangian thus reads

$$\mathcal{L} = \bar{\psi}(i\gamma^\mu D_\mu - m)\psi - \frac{1}{4} F_{\mu\nu}^i F^{i\mu\nu}. \quad (2.45)$$

There are higher order combinations of these ingredients which are invariant under the symmetries discussed so far, such as the dual field strength

$$\mathcal{L}_D = g_D \varepsilon^{\alpha\beta\mu\nu} F_{\alpha\beta}^i F_{\mu\nu}^i, \quad (2.46)$$

and magnetic dipole interactions

$$\mathcal{L}_{MD} = g_{MD} \bar{\psi} \sigma^{\mu\nu} F_{\mu\nu}^i \psi. \quad (2.47)$$

We ignore these in the present study as they contribute to the breaking of other symmetries and/or systematics, some of which we are interested in conserving at the scope of this thesis, such as CP symmetry and renormalisability,

2.4 LATTICE DISCRETISATION

With the Lagrangian at hand we want to actually evaluate the partition function integral from EQ (2.1). The integral is however infinite dimensional, and has no known closed analytical form unless the theory is trivial (non-interacting). If the theory is close to being trivial, one can apply perturbation theory and systematically solve the integral order by order. This is however not the case for the theories we plan to study, and we must resort to other means.

In the lattice approach one discretises space-time into a grid, or lattice, restricting the fields and variables to exist only at these points. We thus introduce a shortest distance, namely the spacing between these grid points, commonly named a . The coordinates are thus restricted to

$$(\mathbf{x}_0, \mathbf{x}_1, \mathbf{x}_2, \mathbf{x}_3) \in \mathbb{R}^4 \rightarrow (\mathbf{n}_0, \mathbf{n}_1, \mathbf{n}_2, \mathbf{n}_3) \in \{0, 1, \dots, N-1\}^4. \quad (2.48)$$

In addition to having a shortest distance, which works as a natural regulariser for this approach, we also have a finite volume $\Omega = a^4 N^4$ ⁽¹⁾. Therefore, to recover physical results, we need to take the continuum limit, $a \rightarrow 0$, and the infinite volume limit, $N \rightarrow \infty$, in such a way that Ω is large enough in physical units to encompass the scales we are interested in studying.

Having introduced the lattice, we see that the partition function of the discretised theory is simplified compared to the continuum. The simplification is not obvious as it quietly changes the number of integrals from being infinite to being an albeit still large, but finite number.

In the following sections we will first construct a Lagrangian to put on the lattice and analyse its new symmetry properties. We will then briefly discuss how to determine the lattice scale and compare lattice results with continuum physics. Finally a brief overview of the real world computations and applications of lattice gauge theories will be given.

2.4.1 The lattice gauge theory Lagrangian

Constructing a *good* discretised Lagrangian is both a subject and an art in of itself. Naively one would think that any Lagrangian that reduces to the continuum Lagrangian of EQ (2.45) when we send $a \rightarrow 0$ would suffice. Or broader, Lagrangians that at most introduce total derivatives with vanishing borders when $a \rightarrow 0$. Though this is to some extent true, we will see that as always, the devil are in the details, and if one does not take great care, the continuum theory will not be as it first appears.

In the previous section we introduced the parallel transporters to define how to associate two different points in space that can belong to different vector spaces. This procedure complies nicely with the lattice approach, as the only modification we have to make to the definition of the covariant derivative is to replace δ by a , and abolish the limit. We will exclusively use the transporter between nearest neighbour lattice sites, and therefore make the abbreviation $U(\mathbf{x} + a\boldsymbol{\eta}_\mu, \mathbf{x}) = U_\mu(\mathbf{x}) = U_{-\mu}^\dagger(\mathbf{x} + a\boldsymbol{\eta}_\mu)$. Hence,

⁽¹⁾We later distinguish between spatial and temporal lattice directions, and denote the total number of lattice points in one such direction by N_s and N_t .

the fermion contribution to the lattice action with a symmetrised derivative reads

$$\mathcal{S}_f = a^4 \sum_x \left(m \bar{\psi}(x) \psi(x) - \frac{1}{2a} \sum_{\mu=\pm 0}^{\pm 3} \bar{\psi}(x + \hat{\mu}) \gamma^\mu U_\mu(x) \psi(x) \right), \quad (2.49)$$

where the sum is over the discrete points on the lattice, and we have used the shorthand definition $\gamma^{-\mu} \equiv -\gamma^\mu$. We have also switched to Euclidean space, which is a conscious choice that will benefit us later in the stochastic evaluation of the path integral. It is common to factor the fields out of the definition and write the action in terms of a vector-matrix product

$$\mathcal{S}_f = a^4 \bar{\psi}_y Q_{yx} \psi_x, \quad Q_{yx}[U_\mu] = m \delta_{y,x} - \frac{1}{2a} \sum_{\mu=\pm 0}^{\pm 3} \gamma^\mu U_\mu(x) \delta_{y-\mu,x}, \quad (2.50)$$

where the spin and gauge indices are hidden. This is to simplify the expression for the integral over the fermion fields, which can be evaluated exactly

$$\int \prod_{i,j} d\bar{\psi}_i \psi_j e^{\bar{\psi}_i Q_{ij} \psi_j} = \det Q, \quad (2.51)$$

with Q commonly referred to as the *Dirac operator* or the *fermion matrix*, and $\det Q$ the *fermion determinant*. The matrix can either be represented as a higher dimensional tensor, or using a super index describing all degrees of freedom.

Having introduced the *plaquette* transporter in EQ (2.41), constructing a lattice gauge action is straightforward

$$\mathcal{S}_g = \beta_R a^4 \sum_x \sum_{\mu < \nu} \left(1 - \frac{1}{d_R} \text{Re tr } U_{R\mu\nu}(x) \right), \quad (2.52)$$

where d_R is the dimension of the representation. β_R is the coupling constant, and by comparison with the continuum field strength tensor (EQ (2.44)), we find

$$\beta_R = \frac{2d_R}{g^2}. \quad (2.53)$$

2.5 FERMION DOUBLING AND CHIRAL SYMMETRY

Although the Lagrangian in EQ (2.49) has the desired transformation properties, and reproduces the Dirac Lagrangian in the continuum, it suffers from a degeneracy in its energy eigenvalues. The easiest way to see this is by choosing the trivial representation of the gauge fields and writing down the fermion Hamiltonian

$$\mathcal{H}_f = \sum_{\vec{x}} \left(m \bar{\psi}(\vec{x}) \psi(\vec{x}) + \frac{i}{2a} \sum_{k=1}^3 \left(\bar{\psi}(\vec{x} + \hat{k}) \gamma^k \psi(\vec{x}) - \bar{\psi}(\vec{x} - \hat{k}) \gamma^k \psi(\vec{x}) \right) \right). \quad (2.54)$$

From experience we know that the free Hamiltonian is diagonal in momentum space, so we introduce a Fourier transform

$$\tilde{\psi}(\vec{p}) = a^3 \sum_{\vec{x}} e^{-i\vec{p}\cdot\vec{x}} \psi(\vec{x}) \quad (2.55)$$

where the possible values of \vec{p} are restricted to the Brillouin zones

$$p_i = \frac{2\pi}{aN} v_i, \quad v_i \in \left\{ -\left(\frac{1}{2}-1\right), \dots, \frac{1}{2} \right\} \Rightarrow p_i \in (-\pi, \pi]. \quad (2.56)$$

After a Fourier transformation the Hamiltonian is

$$\mathcal{H}_f = \frac{1}{(aN)^3} \sum_{\vec{p}} \tilde{\psi}(\vec{p}) \left(m + \frac{1}{a} \gamma^k \sin(ap_k) \right) \tilde{\psi}(\vec{p}). \quad (2.57)$$

It can easily be seen that it has eigenvalues

$$H_{\vec{p}} = \pm \sqrt{m^2 + \frac{1}{a^2} \sum_{k=1}^3 \sin^2(ap_k)} \quad (2.58)$$

which for every momentum \vec{p} is 8-fold degenerate, owing to the periodicity of the sine function. This implies that we have 7 additional, unwanted fermions in the theory whenever we put one in. These *doublers* come from the corners of the Brillouin zone, and therefore disappear as we take the continuum limit. This is however of little comfort, as they would give incalculable effects to loop diagrams at finite volumes which cannot easily be factored out. In four dimensional space-time an additional set of 8 energy eigenstates appear from doublings in the additional temporal Brillouin corners.

2.5.1 Wilson fermions

In an attempt to resolve this issue, Wilson introduced an additional term to the Lagrangian in the form of a second order derivative. This new term, appropriately named the *Wilson term*, is one order higher in a , and therefore disappears in the continuum limit. After reordering the terms, adding the Wilson term to the Lagrangian gives us

$$\mathcal{S}_{f,w} = a^4 \sum_x \left(\left(m + \frac{4r}{a} \right) \bar{\psi}(x) \psi(x) - \frac{1}{2a} \sum_{\mu=\pm 0}^{\pm 3} \bar{\psi}(x + \hat{\mu}) (r + \gamma^\mu) U_\mu(x) \psi(x) \right). \quad (2.59)$$

We have introduced the *Wilson parameter* r , which has to be in the interval $(0, 1]$, and is commonly chosen to be 1. Using the Wilson action, one can calculate the Hamiltonian's eigenvalues, and show that they are modified to

$$H_{\vec{p}} = \pm \sqrt{\left(m + \frac{r}{a} \sum_{k=1}^3 (1 - \cos(ap_k)) \right)^2 + \frac{1}{a^2} \sum_{k=1}^3 \sin^2(ap_k)}. \quad (2.60)$$

The addition of the Wilson term has given an additional mass of nr/a to the unwanted doublers, meaning that they properly decouple from the theory in the continuum where their masses diverge.

However, including the Wilson term does not come without a cost. By introducing the Wilson term, we explicitly break chiral symmetry. As a result, regardless of whether we choose $m = 0$ for the bare mass parameter, the transformation of EQ (2.28) is no longer a symmetry of the system.

There is in fact a theorem by Nielsen and Ninomiya [1981a; 1981b] which states that one cannot have a lattice theory both chirally symmetric and free of doublers at the same time with a Dirac Lagrangian that is also local and possesses the correct continuum limit properties.

Yet all hope is not lost as Ginsparg and Wilson shortly after stated a modified equation the fermion propagator has to fulfil to give a chiral theory in the continuum [Ginsparg and Wilson, 1982]. Although Wilson fermions do not meet these requirements, solutions to the equations have since been found. Two notable discretisation schemes are *overlap fermions* [Neuberger, 1998a,b], and *domain wall fermions* [Kaplan, 1992] (which heed the equation in a special limit of its internals).

2.6 SCALE SETTING AND THE CONTINUUM LIMIT

We previously mentioned that the lattice spacing a works as a non-perturbative regulariser of the theory, and thus sets the internal scale. Any parameter in the lattice theory appears as dimensionless combinations, such as \vec{x}/a , $a\vec{p}$, am , $a^{3/2}\psi(x)$; the scale is therefore to some extent hidden, and the only way to access it is by computing observables and comparing them to experimental values

$$\lim_{a \rightarrow 0} O(m, g; a) = O_{\text{phys}}. \quad (2.61)$$

Simply sending a to 0 is considered to be the *naive* continuum limit, as it fails to take into account the parameters' dependence on the scale. The parameters that enter our theory are called *bare*, as they vary together with the scale

$$m_{\text{phys}} = \lim_{a \rightarrow 0} m_{\text{bare}}(a), \quad g_{\text{phys}} = \lim_{a \rightarrow 0} g_{\text{bare}}(a). \quad (2.62)$$

The scale dependence of the theory's parameters is summarised by the Callan-Symanzik equations, which can be computed for any physical observable O_{phys}

$$a \frac{d}{da} O_{\text{phys}} = \left(a \frac{\partial}{\partial a} - \beta \frac{\partial}{\partial g} - \gamma \frac{\partial}{\partial m} \right) O_{\text{phys}} = 0. \quad (2.63)$$

The β -function describes how much the coupling changes as a function of the lattice spacing, while the anomalous dimension γ gives the field strength scaling. To lowest order in perturbation theory, the β -function is

$$\begin{aligned} \beta(g) &= -a \frac{\partial g}{\partial a} = -\frac{g^3}{(4\pi)^2} \left(\frac{11}{3} C_{\text{adj}2} - \frac{4}{3} n_f C_R \right) + \mathcal{O}(g^5), \\ &\equiv -\beta_0 g^3 + \mathcal{O}(g^5) \end{aligned} \quad (2.64)$$

Here we encounter the group's Casimir operators, C_R and $C_{\text{adj}2}$. They are defined as

$$C_{R2} = \|\text{Tr}_i f^{iab} f^{jba} \text{Tr}_j\|, \quad C_R = \frac{d_R}{d_{\text{adj}}} C_{R2}, \quad (2.65)$$

and take the following values for the fundamental representation of $SU(N)$

$$C_F = \frac{1}{2}, \quad C_{\text{adj}2} = N. \quad (2.66)$$

One can solve the differential equation in EQ (2.64) and get

$$g = \frac{1}{\sqrt{1 - 2\beta_0 \log(\alpha/\alpha_0)}} \Leftrightarrow \alpha = \frac{1}{\Lambda} \exp \left\{ \frac{-1}{2\beta_0 g^2} \right\}. \quad (2.67)$$

We see that although g was initially dimensionless, we have generated an energy scale Λ through the renormalisation group, a phenomenon known as *dimensional transmutation*. We also see that the lattice spacing α goes to zero as g goes to zero (and the lattice coupling β goes to infinity). This is the *true* continuum limit, where one, as opposed to the naive limit, takes the change of the parameters into account.

2.7 NUMERICAL EVALUATION OF LATTICE GAUGE THEORIES

Although the lattice discretisation has decreased the number of integrals in the definition of \mathcal{Z} from infinity to something finite, the number of free variables is still too large for it to be evaluated, even numerically. The fermion fields have $2N_f d_R$ independent degrees of freedom at every position; the gauge field is a four vector at every space-time point with d_{adj} degrees of freedom. Even though the fermion fields can be integrated out exactly, as seen in EQ (2.51), this still leaves a highly dimensional integral if one wants to look at anything but miniscule volumes.

The only feasible way to handle these types of integrals is by using approximate integration schemes, many of which are stochastic in nature. One such algorithm is *Monte Carlo integration*, which instead of summing over all values the degrees of freedom can take, as one does in standard numerical integration, only samples a small number of these configurations. The value of the integral is then reconstructed using this (small) number of configurations.

For this to work well one has to sample the configuration space in an optimal way as the integrand is usually sharply peaked around a small set of very specific, although unknown, configurations. A first step is to do importance sampling, where one uses the integrand as a probability distribution for the configuration space, in the case of the partition function

$$P([\psi, \bar{\psi}, \mathbf{U}_\mu]) \propto e^{-S[\psi, \bar{\psi}, \mathbf{U}_\mu]}. \quad (2.68)$$

This is only a viable interpretation as long as the right hand side is real and positive. We evaluate the fermion integrals according to EQ (2.51), giving us

$$P([\mathbf{U}_\mu]) \propto \det Q[\mathbf{U}_\mu] e^{-S_g[\mathbf{U}_\mu]}. \quad (2.69)$$

The exponent of the gauge action is clearly both real and positive. The fermion determinant can be shown for Wilson fermions to be real by using the fact that it is γ^5 -hermitian

$$\gamma^5 Q \gamma^5 = Q^\dagger. \quad (2.70)$$

It is however not guaranteed to be positive. We can fix this by studying systems with an even number of pairwise degenerate quarks. The QCD action does not mix the different quark species, and we therefore get a separate fermion matrix for every quark flavour

$$\det Q = \prod_f \det Q_f. \quad (2.71)$$

Since direct sampling from the distribution is not possible in practice, one usually constructs a chain of samples, each being related to the previous through a Markov chain

$$\left\{ [\psi, \bar{\psi}, \mathbf{U}_\mu]_1, [\psi, \bar{\psi}, \mathbf{U}_\mu]_2, \dots, [\psi, \bar{\psi}, \mathbf{U}_\mu]_N \right\} \quad (2.72)$$

where the probability of choosing one configuration given another follows the detailed balance equation

$$\frac{P([\mathbb{1}]_n | [\mathbb{1}]_{n-1})}{P([\mathbb{1}]_{n-1} | [\mathbb{1}]_n)} = e^{\mathcal{S}[\mathbb{1}]_{n-1} - \mathcal{S}[\mathbb{1}]_n}, \quad (2.73)$$

which will converge to the correct distribution as long as the chain is *ergodic*, i.e. will reach any field configuration in finite (albeit arbitrarily long) time.

2.7.1 Observables

Using this process to select a finite set of configurations, one can obtain an estimate for the expectation value of observables. Commonly named the *ensemble average*, it is given by

$$\bar{O}[\psi, \bar{\psi}, \mathbf{U}_\mu] = \frac{1}{N} \sum_{n=1}^N O([\mathbb{1}]_n). \quad (2.74)$$

If the set of configurations behaves as described in the previous section, it converges to the true average, EQ (2.3), when $N \rightarrow \infty$.

We want an estimate of the error for any realisable number of configurations. This information is encoded in the *autocorrelation function*

$$C_O(m) = \langle O([\mathbb{1}]_n) O([\mathbb{1}]_{n+m}) \rangle_n - \langle O([\mathbb{1}]_n) \rangle_n^2, \quad (2.75)$$

which quantizes how correlated consecutive measurements are. Since the $n + 1$ 'th configuration depends on the n 'th configuration through the Markov chain, $C_O(m) \neq 0$ for $m > 0$. However, it is how quickly this function decreases that determine how good the estimate for the average is. An important quantity for this is the *integrated autocorrelation time*

$$\tau_O = \frac{1}{2} \sum_{m=-\infty}^{+\infty} \frac{C_O(m)}{C_O(0)}. \quad (2.76)$$

One can show that approximately $2\tau_O$ of the consecutive measurements will be correlated, meaning that it is advantageous to sample only the observable at this interval instead of for every new configuration [Montvay and Münster, 1997, sect. 7.1.3].

STATISTICAL MECHANICS AND PHASE TRANSITIONS

This chapter give a short overview of some aspects of statistical mechanics that are important in the present work. This is done in SECTION 3.1. Then the field theoretical equivalent is given in SECTION 3.2, before we once more study the discretised theory in SECTION 3.3. We tie up the chapter in SECTIONS 3.4, and 3.5 with a thorough discussion of simulations of finite density systems, and the hurdles that need to be overcome.

Several volumes of the standard literature have been consulted with respect to the contents of this chapter. These include, but are not limited to, Landau and Lifshitz [2013]; Pathria and Beale [2011] for introductions to statistical mechanics, Kapusta and Gale [2006] with an introduction to Thermal Field Theory (*TFT*), and Montvay and Münster [1997]; Philipsen [2010] for the lattice formulation of finite temperature theory.

3.1 STATISTICAL MECHANICS

Every quantity of interest in the study of equilibrium thermodynamics is contained in the previously mentioned partition function

$$\mathcal{Z} = \sum_i \mathcal{Z}_i = \sum_i e^{-\beta E_i}. \quad (3.1)$$

The sum is over all states of the degrees of freedom of the system, E_i being the energy cost of the configuration, and $\beta = 1/T$ the reciprocal temperature⁽¹⁾. How one chooses to define the scope of these *states* depends on the physics one is interested in, as different physical quantities are more accessible to certain descriptions compared to others. Three common descriptions are the *microcanonical*, *canonical* and *grand canonical* ensembles. They differ in their scope as the microcanonical ensemble includes systems at a fixed energy shell, the canonical ensemble a system of fixed temperature and particle number while the grand canonical ensemble also allows for fluctuations in particle number.

Both the canonical and grand canonical ensembles have associated partition functions,

⁽¹⁾This should not be confused with the lattice gauge coupling, which was introduced in the previous chapter. β will be used to indicate $1/T$ in this chapter only.

and the two are related through

$$\mathcal{Z}_{\text{GC}}(z, V, T) = \sum_{N=0}^{\infty} z^N \mathcal{Z}_{\text{C}}(N, V, T), \quad (3.2)$$

where $z = e^{\beta\mu}$ is the fugacity and μ the chemical potential. The partition function can in turn be used to calculate a multitude of thermodynamic quantities

$$\mathcal{P} = \frac{1}{\beta} \left(\frac{\partial}{\partial V} \log \mathcal{Z} \right)_{\beta, z}, \quad (3.3)$$

$$\mathcal{E} = - \left(\frac{\partial}{\partial \beta} \log \mathcal{Z} \right)_{z, V}, \quad (3.4)$$

$$\mathcal{N} = z \left(\frac{\partial}{\partial z} \log \mathcal{Z} \right)_{\beta, V}, \quad (3.5)$$

pressure, average energy and average particle number respectively.

3.1.1 Phases and phase transitions

The phase of a system is linked to the characteristic behaviour of one or more of its physical quantities, such as the magnetisation of spin glasses, the average positions of atoms in a crystal and the molecular composition of solutions. We refer to these defining physical quantities as the *order parameters* of the phases. The transitions between two or more phases is known as a *phase transition*, and due to the very nature of phases, happens through the induction of mathematical singularities.

The order of a phase transition is exactly described by which derivative of the free energy with respect to the order parameter of choice diverges. First order transitions have discontinuous first derivatives, while only higher order derivatives diverge for second order transitions.

However, if the order parameter approaches zero, without ever reaching it, one can define a pseudo-phase transition, known as a *crossover*, to be the point of the most rapid change of the order parameter (the inflection point). While this is not a real phase transition, following its trajectory in a phase diagram will result in one, if a transition exists, and thus linking the two concepts.

Phase transitions are an inherently macroscopic concept, and do not know about the microscopic details of the theory. Theories with different microscopic properties might therefore still behave alike on the macroscopic level. These categorise into *universality classes*, catalogued by the singular behaviour of their physical quantities close to the transition. If we denote the order parameter by m , and the ordering field by $h^{(2)}$, we can define some of the critical exponents by

$$m \sim (T - T_c)^\beta, \quad (3.6)$$

$$\left(\frac{\partial m}{\partial h} \right)_T \sim (T - T_c)^{-\gamma}, \quad (3.7)$$

$$C_V = -\beta^2 \left(\frac{\partial^2 \mathcal{F}}{\partial \beta^2} \right)_V \sim (T - T_c)^{-\alpha}. \quad (3.8)$$

Systems which have the same critical exponents fall into the same universality class.

⁽²⁾a characteristic variable which define the transition, $m \rightarrow 0$ as $h \rightarrow 0$

3.1.2 Yang Lee zeros

An alternative approach to a rigorous study of the phase transitions was proposed by Yang and Lee [1952b; 1952a]. They suggested that one can analyse the properties of the thermodynamic functions around a transition by studying the zeros of the grand canonical partition function in the complex fugacity plane.

Seeing as the partition function is per definition the normalisation factor of a statistical system, it can never be zero for real and positive values of z . The Yang Lee zeros thus lie in the complex plane. However, as one increases the volume of the system, the number of zeros increases, and tends to a continuous curve in the thermodynamic limit, $V \rightarrow \infty$. As this curve forms, zeros on the positive and negative imaginary axis could coincide at the real axis, signalling the onset of a phase transition.

3.2 THERMAL FIELD THEORY

The quantum partition function is defined similarly to the classical one, but with the energy and particle numbers promoted to operators

$$\mathcal{Z}_{\text{GC}} = \sum_{[\phi_i, \pi_i]} \langle [\phi_i, \pi_i] | z^{\hat{N}} e^{-\beta \hat{H}} | [\phi_i, \pi_i] \rangle. \quad (3.9)$$

This sum reduces to a form similar to EQ (2.1) after introducing the second quantisation and evaluating the integrals over the conjugate momentum fields π_i .

Focussing on the canonical ensemble, there are two amendments which need to be made to the Euclidean action in EQ (2.2). First the Euclidean time τ_E has to be integrated over the half open interval $[0, \beta)$

$$\mathcal{S}_E[\phi_i] = \int_0^\beta d\tau_E \int d^3x \mathcal{L}_E[\phi_i(x)]. \quad (3.10)$$

The second rectification is a bit more subtle and concerns the periodic boundary conditions of the fields. For the fields to respect their statistical properties (Bose- vs Fermi statistics) they need to obey the boundary conditions

$$\phi(\tau_E + \beta) = \begin{cases} \phi(\tau_E), & \text{for bosonic fields,} \\ -\phi(\tau_E), & \text{for fermionic fields.} \end{cases} \quad (3.11)$$

We can now return to the grand canonical ensemble and the particle number operator \hat{N} . A suitable operator can be created from the conserved Noether charges, such as the one from EQ (2.31). For every distinct conserved charge one wishes to study the dynamics of, there should be a separate chemical potential. Two common systems of interest are those of quark- and isospin chemical potential. Quark chemical potential is connected to the global U(1) symmetry of the fermion fields. The associated Noether charge is that of total fermion number

$$N_f = \int d^3x \bar{\psi}_f(x) \gamma^0 \psi_f(x), \quad (3.12)$$

with either separate or degenerate μ_f for each of the fermion species. The isospin charge is related to the Cartan generator of the flavour mixing $SU(2)$ symmetry of a two flavour system (the third Pauli matrix)

$$N_I = \int d^3x \bar{\psi}_i(x) \gamma^0 (\sigma^3)_{ij} \psi_j(x), \quad (3.13)$$

which for QCD gives the up and down quarks chemical potentials that only differ in sign. By tuning the value of μ_I , one can study the effects of a u/d asymmetry, while adjusting μ_f induces a particle/antiparticle imbalance.

3.3 THERMAL FIELDS ON THE LATTICE

Following the same path as in SECTION 2.4, discretising the expression for the partition function \mathcal{Z} is straightforward. We see that lattice theory naturally describe systems at non-zero temperature, as the temporal extent is always finite. The temperature is given in terms of the number of temporal lattice sites, N_t ,

$$T = \frac{1}{a N_t}. \quad (3.14)$$

Therefore, when analysing continuum physics it is important to take a proper infinite volume limit for spatial coordinates, while for the Euclidean temporal extent one sends $a \rightarrow 0$ and $N_t \rightarrow \infty$ in such a way that $a N_t$ remains finite.

At a first glance it might seem as if when integrating lattice theories we can only vary the temperature in finite increments, seeing as N_t has to be an integer. It is however much more common to keep N_t fixed while varying a , which one does by tuning the gauge coupling g , as in SECTION 2.6.

Other than imposing the proper boundary conditions for the variables, no other amendments need to be made for the finite temperature simulations. These follow directly from EQ (3.11)

$$\psi(\mathbf{n}_t + N_t) = -\psi(\mathbf{n}_t), \quad (3.15)$$

$$U_\mu(\mathbf{n}_t + N_t) = U_\mu(\mathbf{n}_t). \quad (3.16)$$

3.3.1 Thermodynamic quantities

In SECTION 3.1 we stated the thermodynamic quantities \mathcal{P} , \mathcal{E} and \mathcal{N} in terms of derivatives of the partition function. However, one cannot sample the partition function through Monte Carlo simulations, and we therefore have to devise a different scheme to calculate these quantities. By interchanging the order of the derivatives and the integrals we get

$$\mathcal{E} = -\frac{\partial}{\partial \beta} \log \mathcal{Z} = \frac{1}{\mathcal{Z}} \int \prod_i d\phi_i \left(\frac{\partial \mathcal{S}}{\partial \beta} \right) e^{-\mathcal{S}} \equiv \left\langle \frac{\partial \mathcal{S}}{\partial \beta} \right\rangle. \quad (3.17)$$

However, there is still a problem in defining the derivative with respect to β . As we wish to keep N_t fixed, we have to vary β by varying a , but we only want to vary the lattice spacing in the temporal direction, not the spatial ones. By naively varying a , we

would not only change the temperature, but also the volume, which must stay fixed in the definition of \mathcal{E} .

To rectify this we have to introduce an anisotropic lattice, one in which the spatial and temporal lattice spacings are different. The magnitude of this difference is encoded in the anisotropy parameter $\xi = a_s/a_t$. By varying a_s and a_t separately we can compute derivatives with respect to temperature and volume independently, and calculate the thermodynamic quantities

$$\mathcal{P} = -\frac{a_s}{3\beta V} \left\langle \frac{\partial \mathcal{S}}{\partial a_s} \right\rangle, \quad (3.18)$$

$$\mathcal{E} = \frac{a_t}{\beta} \left\langle \frac{\partial \mathcal{S}}{\partial a_t} \right\rangle, \quad (3.19)$$

$$\mathcal{N} = -z \left\langle \frac{\partial \mathcal{S}}{\partial z} \right\rangle. \quad (3.20)$$

Now that they are expressed in terms of ensemble averages we can use the previously introduced Monte Carlo methods to estimate their values.

3.4 FINITE DENSITY SIMULATIONS

In order to carry out simulations of systems with non-zero quark number density we saw that we have to introduce a quark chemical potential. Unfortunately, a naive discretisation of the quark number operator from EQ (3.12) leads to divergences in the thermodynamic quantities in the continuum limit [Hasenfratz and Karsch, 1983; Kogut et al., 1983]. This is due to the lack of an implicit gauge invariance of the lattice action needed for the right continuum cancellations to take place.

The correct way to introduce a quark chemical potential to the lattice action is by weighing the appropriate gauge links with the correct single step fugacity

$$U_0(x) \rightarrow e^{a\mu} U_0(x), \quad U_0^\dagger(x) \rightarrow e^{-a\mu} U_0^\dagger(x). \quad (3.21)$$

Adding this change to the Wilson fermion matrix from EQ (2.59) yields

$$\begin{aligned} Q_{yx} &= \left(m + \frac{4r}{a}\right) \delta_{y,x} - \frac{1}{2a} \sum_{\mu=\pm 1}^{\pm 3} (r + \gamma^\mu) U_\mu(x) \delta_{y-\hat{\mu},x} \\ &\quad - \frac{1}{2a} \left(e^{a\mu} (r + \gamma^0) U_0(x) \delta_{y-\hat{0},x} + e^{-a\mu} (r - \gamma^0) U_0^\dagger(x - \hat{0}) \delta_{y+\hat{0},x} \right), \end{aligned} \quad (3.22)$$

which is also the final form of the lattice action we will study in this thesis.

3.4.1 Dense systems and lattice saturation

Lattice studies of systems at finite chemical potential is limited in the very dense regime by lattice saturation. This is a mere lattice artefact arising from the Pauli exclusion principle, which tells us that two fermion degrees of freedom cannot occupy the same quantum state. Due to the discretised nature of it, a lattice cannot accommodate more than $2N_f N_c N_t N_s^3$ fermions.

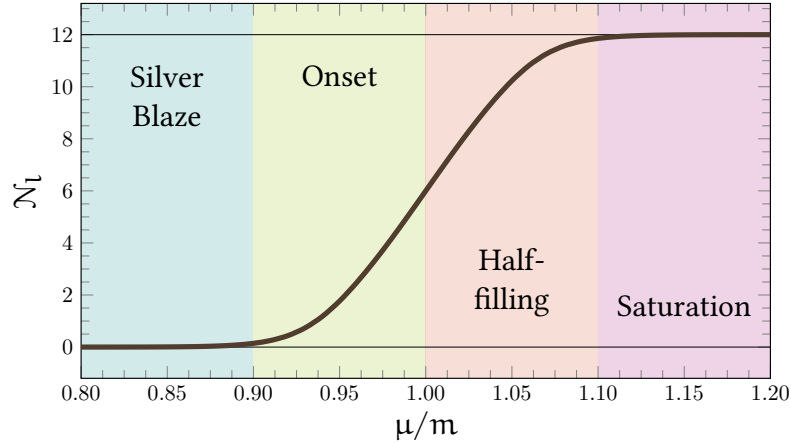


Figure 3.1.: Sketch of the average number of quarks per lattice site as a function of baryon chemical potential on the lattice, $N_f = 2$, $N_c = 3$. Starts in the silver blaze state, moves into onset, reaches half filling then saturates at $2N_f N_c$.

This limitation is sketched in FIGURE 3.1 where a stereotypical lattice curve has been plotted. At small and intermediate values of the chemical potential, we see the *Silver Blaze* property. Coined by Cohen [2003], is the phenomenon that at any chemical potentials smaller than the smallest mass of the theory, the eigenvalues of the Dirac operator are μ independent. Slightly before $\mu = m$ we have onset, which signals the beginning of the nuclear condensation phase change, after which the system will eventually reach half-filling, where half of the states on the lattice are occupied. One should generally ignore results beyond this point, as lattice artefacts become dominant. This was the study of [Rindlisbacher and de Forcrand, 2016], in which the authors discovered a particle-hole symmetry around half-filling, similar to electron-hole symmetries in solid state systems. As the lattice continues to fill up we eventually reach saturation, at which point the lattice states are all occupied, dynamics stop, and no more quarks can be added to the system. As we see in the sketch, this happens when every lattice site is populated by $2N_f N_c$ fermions.

3.5 THE SIGN PROBLEM

An issue arises when trying to numerically evaluate the partition function integrals of finite chemical potential systems through Monte Carlo methods. We saw that we can use the probability density

$$P([\mathbf{U}_\mu]) \propto \det Q[\mathbf{U}_\mu] e^{-S_g[\mathbf{U}_\mu]} \quad (3.23)$$

to evaluate the integrals numerically. This requires that the fermion determinant be positive definite, something we can guarantee from the fact that the matrix is γ^5 -hermitian. Unfortunately, this property is lost when a chemical potential is introduced. When digging deeper we find that this conceptual issue is just the tip of the iceberg, and that there is a more fundamental issue at play.

The partition function has to be a real positive quantity, and so we know that if we carry out the integral properly, all the imaginary contributions have to cancel out in the

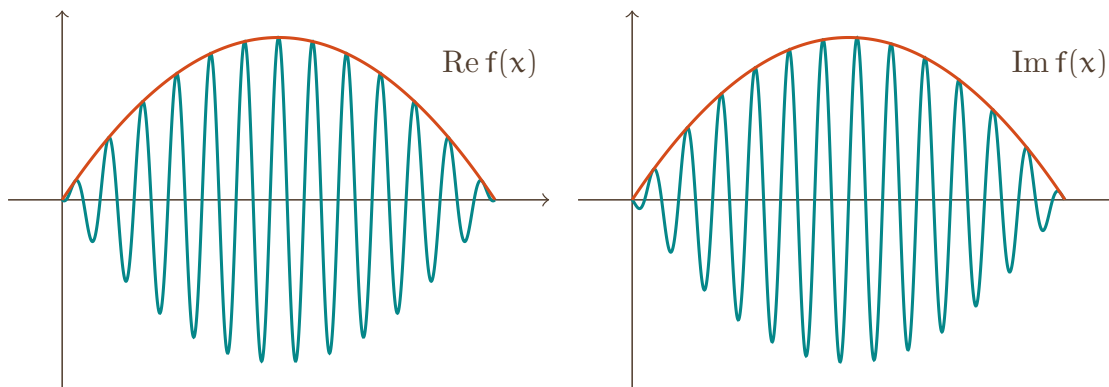


Figure 3.2.: The essence of the sign problem. Real and imaginary part of a function with a phase, $f(x)e^{i\theta(x)}$.

end. It is getting these exact cancellations out of inexact numerical methods that is the underlying complication. This is what is referred to as the *sign problem*, and the issue is not exclusive to lattice studies of fermionic systems at finite density. Being categorised as an NP-hard problem [Troyer and Wiese, 2005], it is unlikely that we will ever find a generic solution to it, and it needs to be tackled through deep understanding of the source of the issue itself.

The problem is most easily illustrated using a sketch. In FIGURE 3.2 we have plotted the real and imaginary part of a symmetric function with a complex phase, $f(x)e^{i\theta(x)}$. The real part integrates to something finite that is exponentially suppressed by the phase, while the imaginary part integrates to zero. However, this subtlety is hard to reproduce numerically, just as it is hard to see with the bare eye that one of the two plots integrate to zero, while the other something finite. The number of operations needed to keep the errors down grow exponentially with the system size, making continuum studies impossible.

There are multiple workarounds devised to allow for evaluating finite density systems using Monte Carlo methods. Such methods include reweighting, Taylor expansions, and analytic continuation from imaginary chemical potential; there is also stochastic quantisation, which is not a Monte Carlo method. Although none of these procedures actually tackle the essence of the sign problem, with sufficiently powerful computers results with reasonable accuracy can be obtained. However, one should take great care to sample correctly if one wants sensible results, as was demonstrated in [Osborn et al., 2008].

The remainder of this chapter is dedicated to covering the basic ideas of these methods, and refer to [de Forcrand, 2009] for a more thorough review.

3.5.1 Reweighting

Reweighting is a highly effective refactoring scheme, where one takes the phase of the fermion determinant as part of the observation rather than the probability weight. Factoring out the phase

$$\det Q = |\det Q| e^{i\theta} \quad (3.24)$$

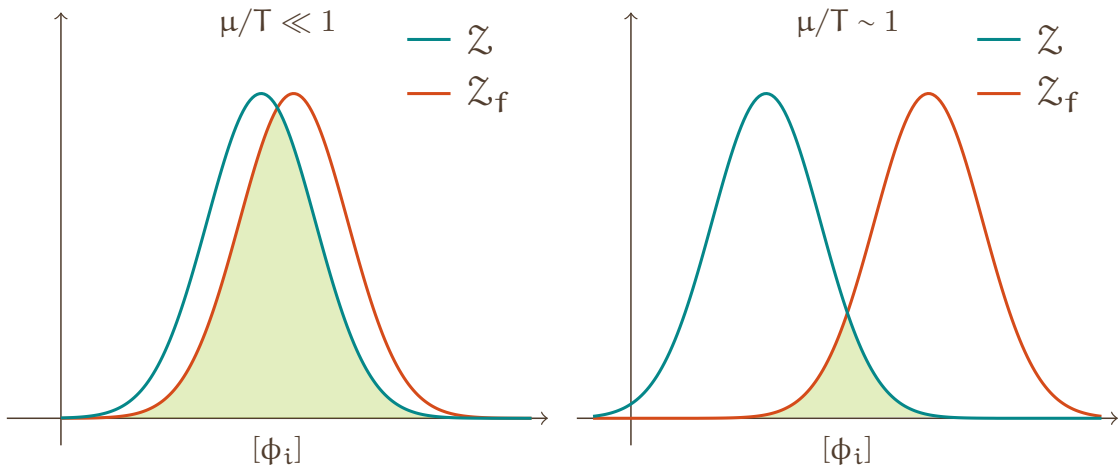


Figure 3.3.: Overlap of the full ensemble to the reweighted ensemble at low and high chemical potential.

one can rewrite the expectation value of an observable as

$$\begin{aligned} \langle O \rangle &= \frac{1}{Z} \int \prod_i d\phi_i O |\det Q| e^{i\theta} e^{-S_g} \\ &= \frac{Z_{pq} \int \prod_i d\phi_i O |\det Q| e^{i\theta} e^{-S_g}}{Z_{pq} \int \prod_i d\phi_i |\det Q| e^{i\theta} e^{-S_g}} = \frac{\langle O e^{i\theta} \rangle_{pq}}{\langle e^{i\theta} \rangle_{pq}}. \end{aligned} \quad (3.25)$$

The *phase quenched* ensembles, where the phase is kept constant, only have real weights, and one can therefore use Monte Carlo techniques. It is possible to introduce a positive function of the phase, $f(\theta)$, to lessen the difference between the true ensemble and the phase quenched one

$$\langle O \rangle = \frac{\langle O e^{i\theta} / f(\theta) \rangle_f}{\langle e^{i\theta} / f(\theta) \rangle_f}. \quad (3.26)$$

This was explored in [de Forcrand et al., 2003], and an optimal choice for f was determined to be $f(\theta) = |\cos \theta|$.

The sign problem comes into play when the average phase drastically deviates from 1, in which case the ensemble we sample is far from the ensemble we want to measure, drastically increasing the required statistics. The issue is sketched in FIGURE 3.3 where we see the overlap between the full and reweighted ensembles. Because the reweighted ensemble deviates significantly from the full ensemble at high chemical potentials, most of the sampled configurations will be discarded, often referred to as the *overlap problem*.

3.5.2 Imaginary chemical potentials

Another method that has been given much attention recently is simulating at purely imaginary chemical potentials, and then using analytic continuation from the negative μ^2 parameter region to the positive. At purely imaginary μ the measure becomes a real, positive quantity, which can be seen from

$$\det Q^\dagger(\mu) = \det Q(-\mu^*). \quad (3.27)$$

This has been used to study the critical surfaces of the Columbia plot (FIGURE 1.1, right), where one can compute the curvature of this surface upon crossing into the region of real chemical potential [de Forcrand and Philipsen, 2002; D’Elia and Lombardo, 2003].

In addition to being a useful method of extrapolating to real chemical potentials, the interesting phase structure in the region of imaginary chemical potentials can be studied. Because the imaginary chemical potentials introduce a pure phase, the partition function is periodic under centre transformations of the group. This is known as the Roberge-Weiss symmetry, and the periodicity leads to a phase transition of the same name [Roberge and Weiss, 1986]. Never developments in the field can be found in e.g. [Wu and Meng, 2013; Cuteri et al., 2016; Philipsen and Pinke, 2016].

3.5.3 Taylor series

A similar approach to analytic extrapolation is to calculate the Taylor series of an observable and then change the order of integration and derivation, leading to the expansion

$$\langle O \rangle_\mu = \langle O \rangle_0 + \left\langle \frac{dO}{d\mu} \right\rangle_0 \mu + \frac{1}{2} \left\langle \frac{d^2 O}{d\mu^2} \right\rangle_0 \mu^2 + \mathcal{O}(\mu^3). \quad (3.28)$$

This has been used to try and follow the trajectory of the phase transition into the region of finite μ [Allton et al., 2003]. The convergence region is however governed by the partition function’s behaviour at imaginary chemical potential, and the Roberge-Weiss transition is to our knowledge the bound for any extrapolation from zero chemical potential. There is therefore a strict limit on how far this expansion is valid, which was the study of [Osborn et al., 2008].

3.5.4 Stochastic quantisation

The final method we will cover is the use of stochastic quantisation. This approach is different from the others as it doesn’t use Monte Carlo methods at all. Instead, one uses a different stochastic process to estimate the partition function integral, the Langevin equations [Parisi and Wu, 1981]. One introduces an additional continuous parameter of the fields, α , and then evolves the system in this new parameter following the stochastic differential equation

$$\frac{\partial \phi_i(x, \alpha)}{\partial \alpha} = -\frac{\delta \mathcal{S}}{\delta \phi} + \eta(x, \alpha) \quad (3.29)$$

where η is Gaussian white noise. The method then relies on the fact that in the $\alpha \rightarrow \infty$ limit, the expectation value of observables with respect to the η distribution is identical to the true expectation value evaluated via the path integral

$$\lim_{\alpha_i \rightarrow \infty} \langle O[\phi(x, \alpha)]_i \rangle_\eta = \langle O[\phi(x)]_i \rangle, \quad (3.30)$$

where the noise average is defined as

$$\langle O \rangle_\eta = \frac{\int \prod_i d\eta_i O e^{-\frac{1}{4} \int d^4x \eta(x)^2}}{\int \prod_i d\eta_i e^{-\frac{1}{4} \int d^4x \eta(x)^2}}. \quad (3.31)$$

This equality can be rigorously proven for real actions [Damgaard and Huffel, 1987; Huffel and Kelnhofer, 2004]. One can nevertheless apply the method to complex actions.

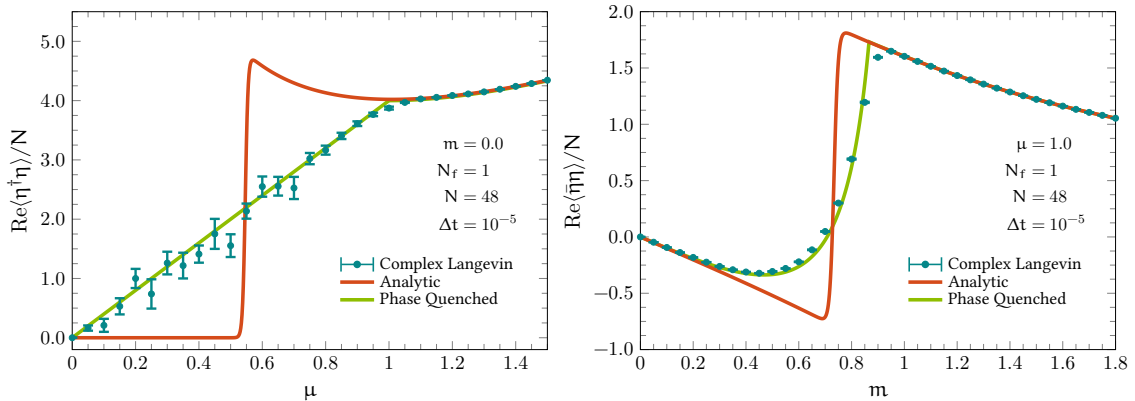


Figure 3.4.: Left: Baryon number density of the Stephanov model measured by complex Langevin compared to full and phase quenched analytical results at fixed $m = 0.0$. Phase quenched computed using a mean field approach. Right: Same comparison for the chiral condensate at fixed $\mu = 1.0$.

Although using a complex action induces imaginary contributions to the noise average, these are expected to average out in the limit for physical observables. This is not always the case, as the complex Langevin sometimes diverges towards unphysical solutions [Ambjorn and Yang, 1985], the reason for which is still an open question.

The sign problem manifests itself in the complex flow of the fields. For large values of the chemical potential, the field configurations will spend a considerable amount of time in the complex phase, resulting in the need for longer flow times before the imaginary contributions average out. This can to some extent be remedied by the introduction of gauge cooling [Seiler et al., 2013], which is the application of invariant transformations on the variables that push them closer to non-complex field values. For QCD it has been shown that this places a restriction on the coupling strengths for which the method is applicable. A recent comparison made between the reach of reweighting to that of stochastic quantisation shows that they are comparable [Fodor et al., 2015]. The newest developments can be found in [Aarts et al., 2016].

To demonstrate a case in which we can clearly see the Langevin flow converging to the wrong theory, we study a *Random Matrix Theory* (RMT), which is a simple model also suffering from a strong sign problem. One such RMT is the Stephanov model [Stephanov, 1996], whose partition function is

$$\mathcal{Z}_S = \int [dW] e^{-N \Sigma^2 \text{tr} W^\dagger W} \det^{N_f} \begin{pmatrix} M & iW + \mu \\ iW^\dagger + \mu & M \end{pmatrix}, \quad (3.32)$$

where the degrees of freedom are random matrices $W \in M_{\mathbb{C}}(N, N)$. The mass matrix M , chemical potential matrix μ , and flavour number N_f , are introduced to mimic the parameters of QCD. This model has the advantage that it is analytically solvable both at finite μ , as well as in the phase quenched limit [Stephanov, 1996; Halasz et al., 1997b]. The results from simulating this theory using the unimproved complex Langevin algorithm is shown in FIGURE 3.4. In the same plots the full analytic result is plotted in red, and the phase quenched result in green. It should be noted that the phase quenched is only accessible in the thermodynamic limit, $N \rightarrow \infty$, though 48 is close enough to this limit

to expect only few discrepancies from finite volume effects. We see that the complex Langevin results clearly converge to the phase quenched theory even though the full theory is used as input. Further analysis is yet to be made regarding improvement of this case. This includes the aforementioned gauge cooling method, which was studied in [Nagata et al., 2016a,b] for a different RMT, namely the Osborn model, and proved to be effective with the right choice for the required *cooling norm*. Another alternative comes from the theory of Lefschetz thimbles, where one can use the thimbles to weigh the probability distributions at the stochastic step [Di Renzo and Eruzzi, 2015].

PART II

**THE EFFECTIVE
THEORY**

THE EFFECTIVE THEORY

Having presented the challenges and difficulties in simulating strongly interacting fermions, especially in the dense regime, we will introduce an effective theory that handles some of these problems, while reproducing the full theory in a certain parameter region. We will see that although simulations of the effective theory still suffer from the side effects of the sign problem (e.g. complex actions), the sign problem is in essence weak enough that reweighting can be readily applied.

The work in this thesis builds on previous work with the effective theory while pushing the derivation further and introducing analytic tools, which we will cover in the next chapter.

In the present chapter we will first introduce the effective theory before introducing two expansion schemes that facilitate the computation of the theory. These are namely the *character expansion*, mentioned in SECTION 2.2, and the *hopping parameter expansion* for heavy fermions. We round off the chapter with a discussion on the numerical evaluation of the effective theory.

4.1 THE EFFECTIVE THEORY - INTRODUCTION

The essence of the derivation of the effective theory is to integrate out some of the degrees of freedom analytically. This will ease the burden of the numerical evaluation, having fewer degrees of freedom left to vary, which in turn lessens the sign problem. The sign problem will be milder due to the fact that many, or as we will see, most, of the fluctuations cancel exactly, as they should. Integrating out the spatial gauge links in the partition function

$$\mathcal{Z} = \int \prod_{x,\mu} d\mathbf{U}_\mu(x) \det Q[\mathbf{U}_\mu] e^{-S_g[\mathbf{U}_\mu]} \equiv \int \prod_x d\mathbf{U}_0(x) e^{-S_{\text{eff}}[\mathbf{U}_0]}, \quad (4.1)$$

defines the effective action

$$S_{\text{eff}} = -\log \int \prod_{x,i} d\mathbf{U}_i(x) \det Q[\mathbf{U}_\mu] e^{-S_g[\mathbf{U}_\mu]}. \quad (4.2)$$

The integrals over the spatial gauge links $\mathbf{U}_i(x)$ is unfortunately not something we can evaluate analytically without the aid of approximations. We will therefore introduce

two expansion schemes and work towards deriving the effective theory such that it reproduces the exact expansion coefficients of the full lattice gauge theory in the end.

4.2 THE CHARACTER EXPANSION

The first expansion we will apply is the character expansion introduced in SECTION 2.2. In the form of an exact equality, it is not of much help. Nevertheless, from the character expansion of the single plaquette gauge contribution ⁽¹⁾

$$e^{-\beta(1-\frac{1}{N_c}\text{Re tr } U_p)} = u_0(\beta) \left(1 + \sum_{r \neq 0} d_r u_r(\beta) \chi_r(U_p) \right), \quad (4.3)$$

we see that the character expansion coefficients are dependent on the lattice gauge coupling β . It can be easily seen that the higher dimensional representations come with a higher power of this coupling. A natural ordering therefore arises if one expands around the infinite coupling limit, $g \rightarrow \infty$, $\beta \rightarrow 0$. This expansion scheme is aptly named the *strong coupling expansion*, and has been the focus of numerous studies for the past decades, also having been picked up in recent years by groups studying conformal field theories. Introductions to the field can be found in [Drouffe and Zuber, 1983] and [Montvay and Münster, 1997].

The lowest order character expansion coefficient, namely that of the fundamental representation, has for SU(3) been calculated to high orders

$$\begin{aligned} u_F(\beta) &= \frac{1}{N_c} \frac{\int dg \text{tr } g e^{-\frac{\beta}{2N_c}(\text{tr } g + \text{tr } g^\dagger)}}{\int dg e^{-\frac{\beta}{2N_c}(\text{tr } g + \text{tr } g^\dagger)}} \\ &= \frac{x + \frac{1}{2}x^2 + x^3 + \frac{5}{8}x^4 + \frac{13}{24}x^5 + \mathcal{O}(x^6)}{1 + x^2 + \frac{1}{3}x^3 + \frac{1}{2}x^4 + \frac{1}{4}x^5 + \mathcal{O}(x^6)}, \quad x = \frac{\beta}{2N_c}. \end{aligned} \quad (4.4)$$

To leading order $u_F(\beta) \approx \frac{\beta}{2N_c^2}$, and we therefore use u_F as our expansion parameter rather than β . The character coefficients are in fact always smaller than or equal to 1, and therefore do an excellent job as expansion parameters. The character expansion only permits a single plaquette from any representation to be placed at each position, making order counting easier than a standard Taylor expansion of the gauge action.

4.3 PURE GAUGE EFFECTIVE THEORY

With the character expansion at hand we can evaluate the pure gauge contributions to the effective action. Ignoring the quark contribution, the effective action is

$$e^{-S_{\text{eff}}} = \int [dU]_i \prod_p \left(1 + \sum_{r \neq 0} d_r u_r(\beta) \chi_r(U_p) \right), \quad (4.5)$$

where we have introduced the shorthand $[dU]_i = \prod_{x,i} dU_i(x)$ for the integration measure. Expanding the product over the plaquettes gives a sum of terms which are of the form

$$d_{r_1} u_{r_1}(\beta) \chi_{r_1}(U_{p_1}) d_{r_2} u_{r_2}(\beta) \chi_{r_2}(U_{p_2}) \cdots \quad (4.6)$$

⁽¹⁾We will from this point onward assume that the gauge group is SU(N_c) and that the fermions transform under the fundamental representation, unless stated otherwise.

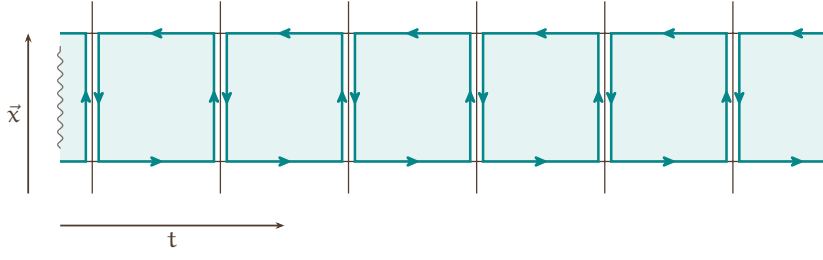


Figure 4.1.: Lowest order pure gauge contribution to the effective action

If one or more of the plaquettes in a term have a link that falls on (χ, μ) , this gives the integral

$$\int d\mathbf{U}_\mu(\chi) \chi_{r_1}(\mathbf{U}_{s_1} \mathbf{U}_\mu(\chi)) \chi_{r_2}(\mathbf{U}_{s_2} \mathbf{U}_\mu(\chi)) \cdots, \quad (4.7)$$

where \mathbf{U}_{s_i} is the remaining *staple* after the link $\mathbf{U}_\mu(\chi)$ has been factored out of the plaquette. One approach to solving these integrals is to compute the Kronecker product of the representation matrices and decompose them to their irreducible representations using the Clebsch-Gordan coefficients. We see that only products of characters whose Clebsch-Gordan series contains the trivial representation do not vanish due to the identity

$$\int dg \chi_r(g) = \delta_{r,0}. \quad (4.8)$$

On top of restricting the valid plaquette combinations sharing a link, it also restricts the graphs created from plaquette combinations to ones that have no boundaries. On an infinite lattice the lowest order contribution would therefore come from combining six fundamental plaquettes into a cube.

For finite lattices, the periodic boundary can be utilised to create closed surfaces. In fact, only graphs periodic in the temporal direction contribute to the finite temperature observables as the non-periodic ones can be normalised out. Since we only integrate spatial links, the contributing graphs need only have closed surfaces in the spatial directions. The lowest order contribution to the effective action comes from a strip of plaquettes spanning the temporal direction as shown in FIGURE 4.1. Since only two links meet at all the spatial sites we need only the integral

$$\int d\mathbf{U} \chi_r(\mathbf{V}\mathbf{U}) \chi_s(\mathbf{W}\mathbf{U}^{-1}) = \delta_{r,s} \frac{1}{d_r} \chi_r(\mathbf{V}\mathbf{W}), \quad (4.9)$$

which can be represented graphically as

$$\int d\mathbf{U} \mathbf{v} \left[\begin{array}{c} \square \\ \uparrow \mathbf{u} \\ \square \end{array} \right] \mathbf{w} = \frac{1}{d_r} \mathbf{v} \left[\begin{array}{c} \square \\ \square \end{array} \right] \mathbf{w}. \quad (4.10)$$

Integrating out the spatial links of the strip of plaquettes leaves two disconnected loops at the neighbouring spatial lattice sites

$$e^{-S_{\text{eff}}} = 1 + \sum_{\langle \bar{x}, \bar{y} \rangle} \mathbf{u}_F^{N_t} (\mathbf{L}_{\bar{x}} \mathbf{L}_{\bar{y}}^* + \mathbf{L}_{\bar{x}}^* \mathbf{L}_{\bar{y}}) + \mathcal{O}(\mathbf{u}_F^{N_t+4}) \quad (4.11)$$

where L is the so-called *Polyakov loop*

$$L_{\vec{x}} = \text{tr} \prod_{t=0}^{N_t-1} U_0(\vec{x}, t). \quad (4.12)$$

We see that the explicit time dependence of the links has disappeared, as the only degrees of freedom left are full windings. The integral over the effective action thus simplifies to

$$\mathcal{Z}_{\text{eff}} = \int [dU]_0 e^{-S_{\text{eff}}[L]} = \int \prod_{\vec{x}} dL_{\vec{x}} \sqrt{\det U_0} e^{-S_{\text{eff}}[L]}, \quad (4.13)$$

where $\sqrt{\det U_0}$ is the reduced Haar measure of the group, the calculation of which is covered in APPENDIX A.1. As one can see, the effective theory is a three dimensional theory of Polyakov loop interactions. To first order we have a nearest neighbour spin system with an effective coupling $u_F^{N_t}$.

At higher orders in β , new effects are introduced through interactions between loops at higher order representations, next to nearest neighbour interactions as well as corrections to the nearest neighbour coupling between fundamental Polyakov loops. The effects of higher order representations in Polyakov loop effective theories were studied in [Wozar et al., 2007]. The corrections to the fundamental nearest neighbour coupling was calculated to $\mathcal{O}(u_F^{N_t+10})$ in [Langelage et al., 2011] while the effects of long range interactions was examined in [Bergner et al., 2015].

We will leave the topic of pure gauge effective theories for now as the work in this thesis is mostly concerned with the cold and dense regime. At low temperatures the pure gauge contribution is exponentially suppressed as $\lambda_i \sim u^{nN_t}$, with $n \leq 1$. The pure gauge sector plays no role in the cold regime, and will be subsequently neglected.

4.4 THE HOPPING PARAMETER EXPANSION

Even for lattice simulations at zero chemical potential, evaluating the fermion determinant is by far the most expensive operation. For heavy quarks it takes a close to block diagonal form, while for light quarks the dynamics delocalise, and no such simplifications appear. It is therefore clear that the analysis of heavy quarks is of reduced complexity, and an expansion around this limit can be used to derive an effective theory for heavy quarks. By rescaling the fields, we see from EQ (2.50) that the single flavour quark matrix can be refactored to be

$$Q_{yx} = \delta_{yx} - \kappa H_{yx}, \quad \kappa = \frac{1}{2(4 + am)} \quad (4.14)$$

where we have introduced the *hopping parameter* κ and the *hopping matrix* H . The hopping matrix for Wilson fermions with $r = 1$ is

$$H_{yx} = (1 \pm \gamma^0) e^{\pm a\mu} U_{\pm 0}(x) \delta_{y \mp \hat{0}, x} + \sum_{\mu=\pm 1}^{\pm 3} (1 + \gamma^\mu) U_\mu(x) \delta_{y - \hat{\mu}, x}. \quad (4.15)$$

We then expand the fermion propagator in powers of κ resulting in

$$Q_{yx}^{-1} = \sum_{n=0}^{\infty} \kappa^n (H^n)_{yx}. \quad (4.16)$$

Since every factor of H comes with a $\delta_{y+\hat{\mu},x}$, they symbolise a single discrete hop on the lattice. The full fermion propagator is therefore the sum of all fermion lines starting at x and ending at y . Due to the fact that every hop carries a spin factor $(1 \pm \gamma^\mu)$, and the identity $(1 - \gamma^\mu)(1 + \gamma^\mu) = 0$, the path is restricted to lines with no backtracking. If the series is truncated, it is approximated by lines with a specific upper bound for their length. The fermion matrix can likewise be rewritten using the trace-log identity

$$\det Q = \exp(\text{tr} \log(1 - \kappa H)) = \exp\left(-\sum_{n=1}^{\infty} \frac{1}{n} \kappa^n \text{tr} H^n\right). \quad (4.17)$$

The trace over H^n gives all closed fermion loops of length n with no backtracking. In lieu of the hopping expansion we see that the fermion propagator is the sum of all fermion lines while the determinant is the exponential of all fermion loops.

4.5 PURE FERMION EFFECTIVE THEORY

The first step towards deriving an effective three dimensional theory for heavy quarks and strong coupling is to separate the temporal and spatial hops

$$H_{yx} = T_{yx} + \sum_{i=1}^3 S_{i,yx}, \quad (4.18)$$

where the temporal and spatial hopping matrices are divided into positive and negative components: $T = T^+ + T^-$, $S_i = S_i^+ + S_i^-$, and

$$T_{yx}^\pm = (1 \pm \gamma^0) e^{\pm a\mu} U_{\pm 0}(x) \delta_{\vec{y},\vec{x}} \delta_{t_y,t_x \pm 1}, \quad (4.19)$$

$$S_{i,yx}^\pm = (1 \pm \gamma^i) U_{\pm i}(x) \delta_{\vec{y},\vec{x} \pm \hat{i}} \delta_{t_y,t_x}. \quad (4.20)$$

The fermion determinant can then be refactored into static and kinematic factors by factoring out the temporal hopping matrix

$$\det(Q) = \det(1 - \kappa T - \kappa S) = \underbrace{\det(1 - \kappa T)}_{Q_{\text{stat}}} \underbrace{\det\left(1 - \frac{\kappa S}{1 - \kappa T}\right)}_{Q_{\text{kin}}}. \quad (4.21)$$

4.5.1 Static determinant

For the derivation of the effective theory we need the full static propagator and static determinant. Since every hop in the temporal direction comes with a fugacity factor, the true temporal hopping expansion parameter is $e^{\pm a\mu} \kappa$, which is not a small parameter for sufficiently dense systems.

We rewrite the static determinant through the trace-log identity

$$\det Q_{\text{stat}} \equiv \det(1 - \kappa T) = \exp\left(-\sum_{n=1}^{\infty} \frac{1}{n} \kappa^n \text{tr}(T^+ + T^-)^n\right). \quad (4.22)$$

Due to the no backtracking restriction we get no mixed T^+T^- terms, and the static determinant factorises into fermion and anti-fermion static determinants

$$\det(1 - \kappa T) = \det(1 - \kappa T^+) \det(1 - \kappa T^-). \quad (4.23)$$

The trace in the determinant restricts us to closed loops, which for the static hopping matrix exclusively results in full windings in the temporal direction. A term that winds the lattice n times in the positive direction has the mathematical form

$$\begin{aligned} & (-1)^n \kappa^{nN_t} (1 + \gamma^0)^{nN_t} e^{nN_t a \mu} \sum_{i=0}^{N_t-1} \prod_{t_i=0}^{nN_t-1} \mathcal{U}_0(\vec{x}, t_i) \\ &= \frac{1}{2} N_t (-1)^n (2e^{a\mu} \kappa)^{nN_t} (1 + \gamma^0) W^n(\vec{x}), \end{aligned} \quad (4.24)$$

where $W(\vec{x})$ denotes an untraced Polyakov loop, the minus sign originates from fermion anti-periodicity, and we have used the fact that $(1 \pm \gamma^\mu)^2 = 2(1 \pm \gamma^\mu)$. The positive static determinant therefore simplifies to

$$\exp\left(-\frac{1}{2} \text{tr}(1 + \gamma^0) \sum_{n=1}^{\infty} \frac{1}{n} (-h_1)^n \text{tr} W^n(\vec{x})\right) = \prod_{\vec{x}} \det(1 + h_1 W(\vec{x}))^2, \quad (4.25)$$

in which $h_1(\mu) = (2e^{a\mu} \kappa)^{N_t} = z e^{N_t \log(2\kappa)} (= \bar{h}_1(-\mu))$ is the static loop (anti loop) weight. Since W is simply a product of \mathcal{U}_0 matrices, it has to belong to the same symmetry group as \mathcal{U}_0 . We can therefore use trace decomposition of the determinant together with the Cayley-Hamilton theorem to express it in terms of the traces of W , namely the Polyakov loops. We state the result for $SU(3)$

$$\det(1 + h_1 W) = 1 + h_1 L + h_1^2 L^* + h_1^3 \quad (4.26)$$

and refer to APPENDIX A.4 for the more general approach. The full static determinant is

$$\det(1 - \kappa T) = \prod_{\vec{x}} (1 + h_1 L_{\vec{x}} + h_1^2 L_{\vec{x}}^* + h_1^3)^2 (1 + \bar{h}_1 L_{\vec{x}}^* + \bar{h}_1^2 L_{\vec{x}} + \bar{h}_1^3)^2. \quad (4.27)$$

4.5.2 Static propagator

The static propagator can be calculated in several ways. One option is to apply the Cayley-Hamilton theorem to calculate the matrix inverse. Alternatively, one can expand in κ and then resum the resulting expression to all orders. Since the latter approach is limited in convergence, we will choose a third method, a straightforward calculation of the matrix inverse. Once more, due to the fact that backtracking is disallowed, the propagator separates into two pieces

$$Q_{\text{stat}}^{-1} \equiv \frac{1}{1 - \kappa T} = \frac{1}{1 - \kappa T^+} + \frac{1}{1 - \kappa T^-} - 1, \quad (4.28)$$

and we are content calculating one of these. The matrix in temporal indices has a simple pseudo upper triangular shape, except for one term from the periodic boundary conditions

$$(1 - \kappa T^+)_{t_y t_x} = \begin{pmatrix} 1 & -\eta \mathcal{U}_0(1) & 0 & 0 & \cdots & 0 \\ 0 & 1 & -\eta \mathcal{U}_0(2) & 0 & \cdots & 0 \\ 0 & 0 & 1 & -\eta \mathcal{U}_0(3) & \cdots & 0 \\ \vdots & \vdots & \vdots & \vdots & \ddots & \vdots \\ \eta \mathcal{U}_0(N_t) & 0 & 0 & 0 & \cdots & 1 \end{pmatrix}, \quad (4.29)$$

where $\eta = (1 + \gamma^0)\kappa e^{\alpha\mu}$ is the time independent factor in Γ^+ . This matrix can be easily inverted by standard row reduction, giving

$$\frac{1}{1 + \prod_{t=1}^{N_t} \eta U_0(t)} \begin{pmatrix} 1 & \eta U_0(1) & \eta^2 U_0(1)U_0(2) & \cdots & \prod_{t=1}^{N_t-1} \eta U_0(t) \\ -\eta^{N_t-1} U_0^\dagger(2) & 1 & \eta U_0(2) & \cdots & \prod_{t=2}^{N_t-1} \eta U_0(t) \\ -\eta^{N_t-2} U_0^\dagger(2)U_0^\dagger(3) & -\eta^{N_t-1} U_0^\dagger(3) & 1 & \cdots & \prod_{t=3}^{N_t-1} \eta U_0(t) \\ \vdots & \vdots & \vdots & \ddots & \vdots \\ -\eta \prod_{t=2}^{N_t} U_0^\dagger(t) & -\eta^2 \prod_{t=3}^{N_t} U_0^\dagger(t) & -\eta^3 \prod_{t=4}^{N_t} U_0^\dagger(t) & \cdots & 1 \end{pmatrix} \quad (4.30)$$

which in component form simplifies to

$$(1 - \kappa \Gamma^\pm)^{-1}_{t_y t_x} = \delta_{t_y, t_x} + \frac{1 \pm \gamma^0}{2} B_{t_y t_x}^\pm, \quad (4.31)$$

$$B_{t_y t_x}^+ = \frac{h_1 W}{1 + h_1 W} \delta_{t_y t_x} + (2e^{\alpha\mu} \kappa)^{t_y - t_x} \frac{U_0(t_x \rightarrow t_y)}{1 + h_1 W} (\theta_{t_y, t_x} - h_1 W \theta_{t_x, t_y}), \quad (4.32)$$

$$B_{t_y t_x}^- = \frac{\bar{h}_1 W^\dagger}{1 + \bar{h}_1 W^\dagger} \delta_{t_y t_x} + (2e^{-\alpha\mu} \kappa)^{t_x - t_y} \frac{U_0(t_x \rightarrow t_y)}{1 + \bar{h}_1 W^\dagger} (\theta_{t_x, t_y} - \bar{h}_1 W^\dagger \theta_{t_y, t_x}). \quad (4.33)$$

where θ is the Heaviside step function. We have introduced the gauge transporter $U_0(t_x \rightarrow t_y)$, which is

$$U_0(t_x \rightarrow t_y) = \begin{cases} \prod_{t=t_x}^{t_y-1} U_0(t) & \text{if } t_x < t_y, \\ \prod_{t=t_y}^{t_x-1} U_0^\dagger(t) & \text{if } t_x > t_y. \end{cases} \quad (4.34)$$

The full static propagator reads

$$(Q_{\text{stat}}^{-1})_{t_y, t_x} = \delta_{t_y, t_x} + \frac{1 + \gamma^0}{2} B_{t_y, t_x}^+ + \frac{1 - \gamma^0}{2} B_{t_y, t_x}^- \quad (4.35)$$

4.5.3 Spatial hopping expansion

We now have all the necessary ingredients to start a systematic expansion of the kinetic quark determinant. First, we introduce the fundamental building blocks of the spatial hopping expansion

$$P = \sum_{i=1}^3 P_i = \frac{1}{1 - \kappa \bar{\Gamma}} \sum_{i=1}^3 \kappa S_i^+, \quad (4.36)$$

$$M = \sum_{i=1}^3 M_i = \frac{1}{1 - \kappa \bar{\Gamma}} \sum_{i=1}^3 \kappa S_i^-. \quad (4.37)$$

The P and M symbolise a single lattice hop in positive or negative spatial directions, combined with arbitrary movement in the temporal direction, including all windings. The kinetic determinant, the object of our expansion, is simply

$$\det Q_{\text{kin}} = \det(1 - P - M) = \exp \left(- \sum_{n=1}^{\infty} \frac{1}{n} \text{tr}(P + M)^n \right), \quad (4.38)$$

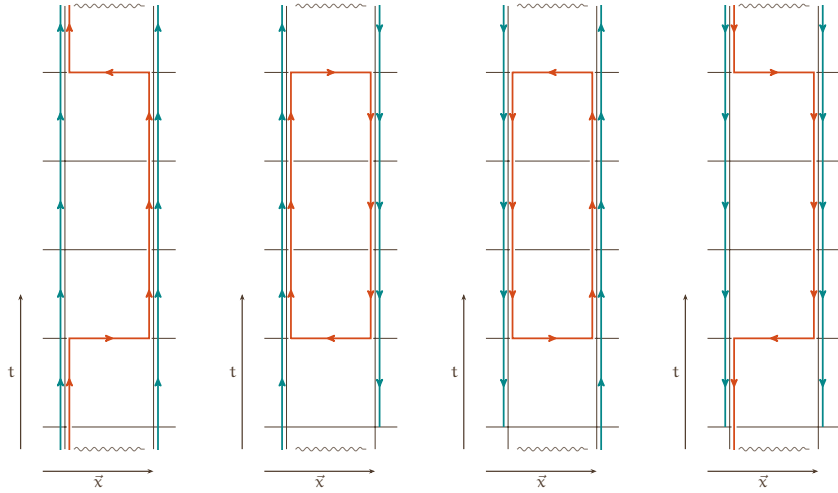


Figure 4.2.: The four contributions from the lowest order spatial hopping expansion. The principal path is indicated in red and the additional windings in blue.

and since P and M both come with a single power of κ , we can expand around these two being 0. The determinant is described by all closed fermion lines, and thus we need an equal number of positive and negative hops (ignoring finite size boundaries). The next to leading order contribution is

$$\det Q_{\text{kin}} = \exp \left(-\text{tr}(PM) - \text{tr}(PPMM) - \frac{1}{2} \text{tr}(PMPM) + \mathcal{O}(\kappa^6) \right). \quad (4.39)$$

For every P and M we get a multitude of different combinations of terms depending on whether we have fermions coupled to fermions, or fermions to anti-fermions. The four combinations of the lowest order $\text{tr}(PM)$ term is shown in FIGURE 4.2.

To be able to calculate the spatial gauge integrals, it is necessary to expand the exponential. The lowest non-trivial order contribution to the partition function is

$$\mathcal{Z}_2 = \int [d\mathbf{U}]_{\mu} \det Q_{\text{stat}} e^{-\text{tr}(PM)} = \int [d\mathbf{U}]_{\mu} \det Q_{\text{stat}} (1 - \text{tr}(PM) + \mathcal{O}(\kappa^4)). \quad (4.40)$$

The only non-trivial integral is the one over the PM factor. Focussing on the spatial links only, the integral to be solved is

$$\begin{aligned} I[PM] &= \int [d\mathbf{U}]_i \text{tr}(PM) \\ &= \kappa^2 \int [d\mathbf{U}]_i \sum_{\vec{x}, j} \text{tr}_{\text{sct}} \left(Q_{\text{stat}}^{-1}(\vec{x})(1 + \gamma_j) \mathbf{U}_j(\vec{x}, t_1) Q_{\text{stat}}^{-1}(\vec{x} + \hat{j})(1 - \gamma_j) \mathbf{U}_j^{\dagger}(\vec{x}, t_2) \right). \end{aligned} \quad (4.41)$$

Using one of the simplest gauge integral selection rules EQ (A.35), we see that this integral is non-zero only if the two links overlap, i.e. if $t_1 = t_2$, the implication of which place restrictions on the temporal indices only. We therefore divide the evaluation of the trace into its three remaining indices; spin, colour and temporal.

The spin indices are unrelated to the group integral and can be evaluated immediately. Inserting the expression for Q_{stat}^{-1} , EQ (4.35), we get

$$\begin{aligned} \text{tr}_s \left(\left(1 + \frac{1+\gamma^0}{2} B_{\vec{x}}^+ + \frac{1-\gamma^0}{2} B_{\vec{x}}^- \right) (1 + \gamma_j) \left(1 + \frac{1+\gamma^0}{2} B_{\vec{x}+\hat{j}}^+ + \frac{1-\gamma^0}{2} B_{\vec{x}+\hat{j}}^- \right) (1 - \gamma_j) \right) \\ = 2(B_{\vec{x}}^+ - B_{\vec{x}}^-)(B_{\vec{x}+\hat{j}}^+ - B_{\vec{x}+\hat{j}}^-). \end{aligned} \quad (4.42)$$

Inserted back into EQ (4.41) we have reduced its complexity

$$\begin{aligned} I[\text{PM}] &= 2\kappa^2 \int [dU]_i \sum_{\vec{x}, j} \text{tr}_{ct} \left((B_{\vec{x}}^+ - B_{\vec{x}}^-) U_j(\vec{x}, t_1) (B_{\vec{x}+\hat{j}}^+ - B_{\vec{x}+\hat{j}}^-) U_j^\dagger(\vec{x}, t_2) \right), \\ &= 2\kappa^2 \text{tr}_t \sum_{\vec{x}, j} (B_{\vec{x}}^+ - B_{\vec{x}}^-)_{ab} (B_{\vec{x}+\hat{j}}^+ - B_{\vec{x}+\hat{j}}^-)_{cd} \delta_{t_1, t_2} \int dU U_{bc} U_{da}^\dagger. \end{aligned} \quad (4.43)$$

In the second line we reintroduced the colour indices, carried out the unoccupied link integrals and renamed the spatial links to U . Making use of the group integral EQ (A.36), we get

$$\begin{aligned} I[\text{PM}] &= \frac{2\kappa^2}{N_c} \text{tr}_t \sum_{\vec{x}, j} (B_{\vec{x}}^+ - B_{\vec{x}}^-)_{ab} (B_{\vec{x}+\hat{j}}^+ - B_{\vec{x}+\hat{j}}^-)_{cd} \delta_{t_1, t_2} \delta_{ab} \delta_{cd}, \\ &= \frac{2\kappa^2}{N_c} \text{tr}_t \sum_{\vec{x}, j} \text{tr}_c (B_{\vec{x}}^+ - B_{\vec{x}}^-) \text{tr}_c (B_{\vec{x}+\hat{j}}^+ - B_{\vec{x}+\hat{j}}^-) \delta_{t_1, t_2}. \end{aligned} \quad (4.44)$$

The final step missing is evaluating the temporal trace, which is easily done by summing over the delta and picking out only the diagonal pieces of B^\pm

$$\begin{aligned} I[\text{PM}] &= \frac{2\kappa^2}{N_c} \sum_{t_1, t_2} \sum_{\vec{x}, j} \text{tr}_c (B_{\vec{x}}^+ - B_{\vec{x}}^-)_{t_1 t_2} \text{tr}_c (B_{\vec{x}+\hat{j}}^+ - B_{\vec{x}+\hat{j}}^-)_{t_2 t_1} \delta_{t_1, t_2}, \\ &= \frac{\kappa^2 N_t}{N_c} \sum_{\langle \vec{x}, \vec{y} \rangle} \text{tr}_c \left(\frac{h_1 W_{\vec{x}}}{1 + h_1 W_{\vec{x}}} - \frac{\bar{h}_1 W_{\vec{x}}^\dagger}{1 + \bar{h}_1 W_{\vec{x}}^\dagger} \right) \\ &\quad \times \text{tr}_c \left(\frac{h_1 W_{\vec{y}}}{1 + h_1 W_{\vec{y}}} - \frac{\bar{h}_1 W_{\vec{y}}^\dagger}{1 + \bar{h}_1 W_{\vec{y}}^\dagger} \right). \end{aligned} \quad (4.45)$$

The final sum over the time-slice resulted in a factor N_t . Analysing this expression we see that due to the fact that there is no colour mixing between sites, the lowest order contribution to the spatial hopping expansion of the kinetic determinant is simply a nearest neighbour interaction between Polyakov loop dependent objects. We will see later that it is useful to introduce the short hand notation

$$W_{nm}(\vec{x}) = \text{tr}_c \frac{(h_1 W_{\vec{x}})^m}{(1 + h_1 W_{\vec{x}})^n}, \quad \text{and} \quad \bar{W}_{nm}(\vec{x}) = \text{tr}_c \frac{(\bar{h}_1 W_{\vec{x}}^\dagger)^m}{(1 + \bar{h}_1 W_{\vec{x}}^\dagger)^n}, \quad (4.46)$$

and thus the lowest order spatial hopping contribution to the effective action can be written as

$$e^{-S_{\text{eff}}} = 1 - \frac{\kappa^2 N_t}{N_c} \sum_{\langle \vec{x}, \vec{y} \rangle} (W_{11}(\vec{x}) - \bar{W}_{11}(\vec{x})) (W_{11}(\vec{y}) - \bar{W}_{11}(\vec{y})) + \mathcal{O}(u, \kappa^4). \quad (4.47)$$

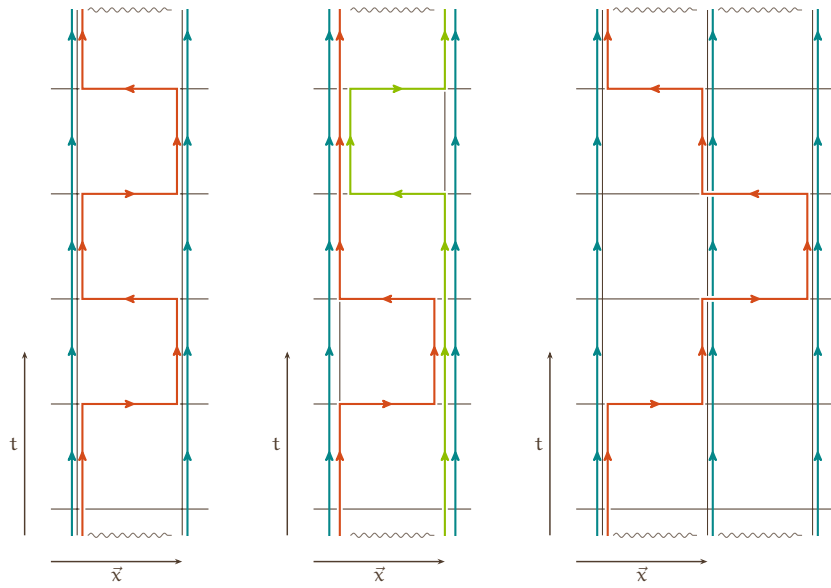


Figure 4.3.: Examples of next to leading order contributions to the kinematic determinant. Left: Single fermion hopping twice between nearest neighbouring sites. Middle: Two separate fermions hopping between the same nearest neighbouring sites. Right: Single fermion visiting a next to nearest neighbour.

At next to leading order in κ we get new terms both in the nearest neighbour contribution as well as non-local terms spanning further on the lattice. Examples of these contributions are sketched in FIGURE 4.3.

4.5.4 Multiple fermion flavours

The introduction of multiple fermion flavours is in principle trivial. As we have no flavour changing processes, the different flavours decouple, and the effective theory at N_f different fermion flavours is simply

$$\mathcal{Z} = \int [d\mathbf{U}]_{\mu} \prod_{f=1}^{N_f} \det Q_{f,\text{stat}} \exp \left(- \sum_{f=1}^{N_f} \sum_{n=1}^{\infty} \frac{1}{n} \text{tr}(\mathbf{P}_f + \mathbf{M}_f)^n \right). \quad (4.48)$$

The only distinction between different fermionic flavours in QCD is their masses, and chemical potentials; the flavour dependence enter simply through the parameters κ_f and μ_f . For degenerate flavours the situation is even simpler, in that case N_f enters as a simple number in the equations

$$\mathcal{Z} = \int [d\mathbf{U}]_{\mu} \det Q_{\text{stat}}^{N_f} \exp \left(- N_f \sum_{n=1}^{\infty} \frac{1}{n} \text{tr}(\mathbf{P} + \mathbf{M})^n \right). \quad (4.49)$$

This factor easily carries through in the computation, and the correct prefactors are determined simply by the number of fermion traces from which the term originates.

4.6 MIXED CONTRIBUTIONS AND GAUGE CORRECTIONS

So far we have only considered either pure gluonic contributions or pure fermionic contributions, and no mix between the two. In SECTION 4.3 we considered an expansion in β , ignoring corrections from κ , while in SECTION 4.5 we carried out an expansion in κ only. In this section we will see how these two expansions affect each other, and how the effects can mostly be absorbed into shifts in the effective coupling constants.

4.6.1 Fermionic corrections

The simplest fermionic correction imaginable is one where any gauge plaquette is replaced by a fermionic loop, given that they have the same group structure⁽²⁾

$$\begin{array}{c} \square \\ \text{with arrows} \end{array} \longrightarrow \begin{array}{c} \square \\ \text{with arrows} \end{array} + \begin{array}{c} \square \\ \text{with arrows} \end{array}. \quad (4.50)$$

We get a contribution from every fermionic flavour, which results in a shift in β

$$\beta_R \rightarrow \beta_R + 16d_R \sum_f \kappa_f^4. \quad (4.51)$$

The next order contribution comes from replacing a pair of plaquettes by six fermion hops

$$\begin{array}{c} \square \square \\ \text{with arrows} \end{array} \longrightarrow \begin{array}{c} \square \square \\ \text{with arrows} \end{array} + \begin{array}{c} \square \square \\ \text{with arrows} \end{array}, \quad (4.52)$$

which only gives the same result after link integration due to EQ (4.10). Higher order corrections can be constructed in a similar manner. We will see that this means that most of the finite β corrections to the effective theory can also be implemented in terms of κ corrections by simply replacing the plaquettes by a sufficiently long fermion loop with the same geometric border.

4.6.2 Gauge corrections

As many of the gluonic correction to our theory can be reproduced by fermionic loops, we turn our attention to these gauge corrections. We will focus on amendments to the pure fermionic effective theory, ignoring the pure gauge theory as it is subdominant in the cold and dense regime.

The first corrections to consider are modifications to the static determinant. They consist of making detours in the spatial directions, filling the surface with plaquettes

$$Q_{\text{stat}}^{N_t} e^{-S_g} = \begin{array}{c} \longrightarrow \\ \text{with arrows} \end{array} + \begin{array}{c} \square \\ \text{with arrows} \\ \longrightarrow \\ \text{with arrows} \end{array} + \begin{array}{c} \square \square \\ \text{with arrows} \\ \longrightarrow \\ \text{with arrows} \end{array} + \dots \quad (4.53)$$

These types of diagrams also result in Polyakov loops after spatial gauge integration⁽³⁾, and can therefore be absorbed into a redefinition of the invariant parameters of the static determinant, namely the loop weight $h_1(z, \kappa)$. The shift in h_1 has been calculated to

⁽²⁾Plaquettes depicted as filled squares, fermion loops are empty.

⁽³⁾As long as their extended boundary is not in contact with other links or Polyakov loops at the point of integration.

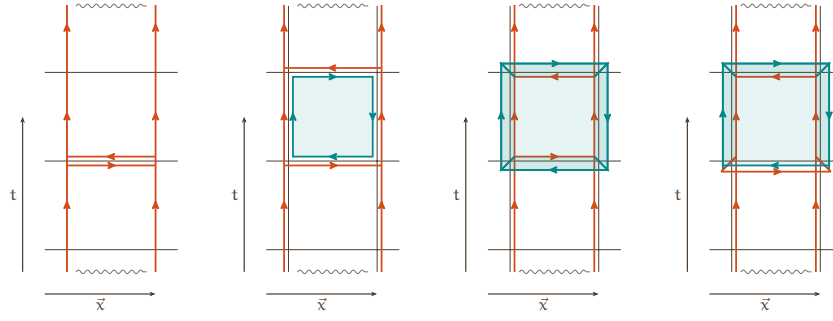


Figure 4.4.: Diagrams contributing to the corrections to the nearest neighbour coupling constant of the effective theory. From left to right $\mathcal{O}(1)$, $\mathcal{O}(u)$, $\mathcal{O}(u^5)$ and $\mathcal{O}(\kappa^2 u^4)$ respectively.

higher orders in the expansion parameters, κ, u [Fromm et al., 2012; Christensen et al., 2014]

$$h_1(z, \kappa, \beta) = h_1(z, \kappa) \exp \left(6N_t \kappa^2 u \left(\frac{1 - u^{N_t - 1}}{1 - u} + 4u^4 - 12\kappa^2 + 9\kappa^2 u + \mathcal{O}(\kappa^4, u^4) \right) \right). \quad (4.54)$$

Analogously, the nearest neighbour coupling strength has a similar correction scheme where we shift spatial hops and fill it with plaquettes. The diagrams are shown in FIGURE 4.4 and they give the following corrections to nearest neighbour interactions [Langelage et al., 2014]

$$I[\text{PM}] \rightarrow \frac{\kappa^2 N_t}{N_c} \left(1 + 2 \frac{u - u^{N_t}}{1 - u} + 8u^5 + 16\kappa^2 u^4 \right) \times \sum_{\langle \vec{x}, \vec{y} \rangle} (W_{11}(\vec{x}) - \bar{W}_{11}(\vec{x})) (W_{11}(\vec{y}) - \bar{W}_{11}(\vec{y})). \quad (4.55)$$

It is useful to introduce the nearest neighbour coupling constant

$$h_2(\kappa, \beta) = \frac{\kappa^2 N_t}{N_c} \left(1 + 2 \frac{u - u^{N_t}}{1 - u} + 8u^5 + 16\kappa^2 u^4 + \mathcal{O}(\kappa^4 u^3) \right), \quad (4.56)$$

which will appear frequently in later calculations.

4.7 RESUMMATION

One of the more powerful tools available to improve convergence is the process of resumming an infinite series of terms into a closed analytic expression. This has already been done in the expression for h_1 , EQ (4.54). We will however go through the exponentiation of the effective action in great detail as it is an integral part of the linked cluster expansion which will be introduced in CHAPTER 5.

Expanding the single hop partition function, EQ (4.40), to all powers gives

$$\mathcal{Z}_2 = \int [dU]_{\mu} \det Q_{\text{stat}} \sum_{n=0}^{\infty} \frac{(-1)^n}{n!} (\text{tr}_{\text{xsc}}(\text{PM}))^n, \quad (4.57)$$

where every power carries an independent sum over the spatial degrees of freedom. These traces will contain both terms in which the PM matrices have overlapping spatial links as well as terms where they are separate. In the latter case the integrals themselves separate, and to lowest order we have

$$\begin{aligned} \mathcal{Z}_2 &= \int [d\mathbf{U}]_0 \det Q_{\text{stat}} \sum_{n=0}^{\infty} \frac{(-1)^n}{n!} \left(\int [d\mathbf{U}]_i \text{tr}_{\text{xsc}}(\text{PM}) \right)^n + \mathcal{O}(\kappa^4), \\ &= \int [d\mathbf{U}]_0 \det Q_{\text{stat}} \exp \left(- \int [d\mathbf{U}]_i \text{tr}_{\text{xsc}}(\text{PM}) \right) + \mathcal{O}(\kappa^4). \end{aligned} \quad (4.58)$$

We see that, since the effective action stems from an exponential, it naturally also resums to one. Corrections due to overlapping terms can be taken into account order by order in a systematic way. This resummation gives a more satisfactory expression for S_{eff} which we gave to first order in EQ (4.47)

$$S_{\text{eff}} = \frac{\kappa^2 N_t}{N_c} \sum_{\langle \vec{x}, \vec{y} \rangle} (W_{11}(\vec{x}) - \bar{W}_{11}(\vec{x})) (W_{11}(\vec{y}) - \bar{W}_{11}(\vec{y})) + \mathcal{O}(\mathbf{u}, \kappa^4). \quad (4.59)$$

Since the effective action is given by the logarithm of the partial partition function, it is more advantageous to expand this quantity directly. To facilitate this we introduce the method of moments and cumulants.

4.7.1 Method of moments and cumulants

The method of moments and cumulants is an elegant mathematical formalism which can be used to extract the correct infinite volume limit for thermodynamic physics [Rushbrooke et al., 1974; Münster, 1981], and will be an integral part in the linked cluster expansion of CHAPTER 5.

The *moment*, $\langle \rangle$, is a symmetric function operating on symbols where the moment product

$$\langle \rangle_1 \otimes \langle \rangle_2 = \langle \rangle_3 \quad (4.60)$$

is defined by

$$\langle \alpha, \dots, \beta \rangle_3 = \sum_{p_2} \langle \alpha, \dots, \delta \rangle_1 \langle \gamma, \dots, \epsilon \rangle_2 \quad (4.61)$$

where the sum is over all partitions of the symbols α, \dots, β in two sets. The *cumulant*, $[]$, of the moment $\langle \rangle$ is defined through the \otimes exponential

$$\exp_{\otimes} [] = 1 + \sum_{n=1}^{\infty} \frac{1}{n!} []^{\otimes n} \equiv 1 + \langle \rangle. \quad (4.62)$$

The moments and the cumulants can then be defined in terms of each other using partition sums

$$\langle \alpha_1, \dots, \alpha_n \rangle = \sum_{k=1}^n \sum_{p_k} [\alpha_1, \dots, \alpha_m]_1 \dots [\alpha_i, \dots, \alpha_j]_k \quad (4.63)$$

$$[\alpha_1, \dots, \alpha_n] = \sum_{k=1}^n (-1)^{k-1} (k-1)! \sum_{p_k} \langle \alpha_1, \dots, \alpha_m \rangle_1 \dots \langle \alpha_i, \dots, \alpha_j \rangle_k \quad (4.64)$$

We define the generating functional $f_{\langle \rangle}$ through indexed variables, x_α for α in the set of symbols

$$f_{\langle \rangle}(\{x_\alpha\}) = \sum_{n=1}^{\infty} \sum_{\alpha_1, \dots, \alpha_n} \frac{1}{n!} \langle \alpha_1, \dots, \alpha_n \rangle x_{\alpha_1} \cdots x_{\alpha_n} \quad (4.65)$$

with an analogous definition for $f_{[\]}(\{x_\alpha\})$. The main theorem of the method of moments and cumulants then tells us

$$\exp f_{[\]}(\{x_\alpha\}) = 1 + f_{\langle \rangle}(\{x_\alpha\}), \quad (4.66)$$

which can be easily proven through induction.

Next, we want to apply this method to the so far computed effective theory so that we can generalise the exponentiation procedure. We want to compute the effective action which is defined by EQ (4.2). Let us for now consider the strong coupling limit of this expression

$$e^{-S_{\text{eff}}} = \int [d\mathbf{U}]_i \exp \left(- \sum_{n=1}^{\infty} \frac{1}{n} \text{tr}(\mathbf{P} + \mathbf{M})^n \right). \quad (4.67)$$

We define the general polymer variables X_i to represent a combination of $\text{tr}(\mathbf{P} + \mathbf{M})^n$ factors with a connected set of overlapping links and a given spatial extent on the lattice. The function $I(X_i)$ gives the value after integration over the spatial links of the polymer X_i . We introduce a cluster moment such that

$$\langle X_1, \dots, X_n \rangle = \begin{cases} 1, & \text{if every } X_i, X_j \text{ is disconnected,} \\ 0, & \text{otherwise,} \end{cases} \quad (4.68)$$

with which we can easily express the effective action

$$e^{-S_{\text{eff}}} = 1 + \sum_{n=1}^{\infty} \sum_{X_1, \dots, X_n} \frac{1}{n!} \langle X_1, \dots, X_n \rangle I(X_1) \cdots I(X_n) \quad (4.69)$$

because we know that the integrals factorise if the polymers share no spatial links. We can then compute the logarithm of the above expression using EQ (4.66)

$$S_{\text{eff}} = - \sum_{n=1}^{\infty} \sum_{X_1, \dots, X_n} \frac{1}{n!} [X_1, \dots, X_n] I(X_1) \cdots I(X_n). \quad (4.70)$$

The crucial observation is that due to the alternating sign in the formula for the cumulant in terms of the moments, the cumulants possess the opposite property of the moments

$$[X_1, \dots, X_n] \neq 0 \iff X_1 \cup \cdots \cup X_n \text{ is connected.} \quad (4.71)$$

We can thus conclude that the effective action properly exponentiates if one considers connected polymers only, and their combinatorial prefactors are given by the cumulants. It should be noted that this is only true in the infinite volume limit, but corrections can easily be calculated on an order by order basis. Later, in the analytical chapter we will work in the actual limit where the exponentiation is exact.

4.7.2 Logarithmic resummation

One final resummation scheme will be discussed in this section. It is based on a resummation of the exponentiated action into a logarithm, as was carried out for the pure gauge action in [Langelage et al., 2011]. Although it does not provide as much numerical benefit to the heavy quark effective theory as it does for the pure gauge theory, we will see that it will prove to be a useful tool when we turn to analytic evaluation.

We will focus on the lowest order term in the effective action before integration, the previously mentioned \mathcal{Z}_2 . We want to study the expression one obtains when all the nearest neighbour interactions lie on the same spatial link

$$S_{\text{eff}} = - \sum_{n=1}^{\infty} \sum_{\mathcal{X}} \frac{1}{n!} [\mathcal{X}, \dots, \mathcal{X}] I(\mathcal{X})^n + \mathcal{O}(\kappa^4), \quad (4.72)$$

where $\mathcal{X} = \text{tr}_{\text{sc}}(\text{PM})$. Combining the results of SECTION 4.5.3, $\sum_{\mathcal{X}} = N_t \sum_{\langle x, y \rangle}$, with the expression for the single link cumulant, $[\mathcal{X}, \dots, \mathcal{X}] = (-1)^{n-1} (n-1)!$, the \mathcal{Z}_2 effective action yields

$$\begin{aligned} S_{\text{eff}} &= -N_t \sum_{\langle x, y \rangle} \sum_{n=1}^{\infty} \frac{(-1)^{n-1}}{n} I(\mathcal{X})^n + \mathcal{O}(\kappa^4), \\ &= N_t \sum_{\langle x, y \rangle} \log(-I(\mathcal{X})) + \mathcal{O}(\kappa^4) \end{aligned} \quad (4.73)$$

and the full \mathcal{Z}_2 is

$$\mathcal{Z}_2 \approx \int [d\mathbf{U}]_0 \det Q_{\text{stat}} \prod_{\langle \vec{x}, \vec{y} \rangle} \left(1 - \frac{\kappa^2}{N_c} (W_{11}(\vec{x}) - \bar{W}_{11}(\vec{x})) (W_{11}(\vec{y}) - \bar{W}_{11}(\vec{y})) \right)^{N_t}, \quad (4.74)$$

with higher order corrections at $\mathcal{O}(\kappa^4)$. This formulation is particularly useful for studying e.g. the finite volume dependence of the Yang Lee zeros, which we will analyse in SECTION 5.5.2.

4.8 THE COLD AND DENSE REGIME

Although we have built the foundations for calculating the effective 3D theory, we have still not presented any results beyond leading order in the hopping expansion apart from the discussions on resummation. In [Langelage et al., 2014] the effective theory was computed to $\mathcal{O}(\kappa^4)$, and a detailed computation of the appearing terms, as well as gauge corrections can be found in [Neuman, 2015]. In the same publication an observation was made that the effective action greatly simplifies in the cold and dense limit, an area of QCD which is of great interest. The two limits aid our computations in two ways: In the dense limit the thermodynamics is dominated by quarks, not anti-quarks, and we can therefore neglect any terms involving anti-quarks. Mathematically, this would be an expansion to zeroth order in \bar{h}_1 . The simplifications coming from the cold limit, the limit in which $N_t \rightarrow \infty$, are more subtle and easier understood through an example.

Consider the term $\text{tr}(\text{PMPM})$ appearing at NLO of the hopping parameter expansion. The term has four spatial hops which have to pair up for the gauge integral to give

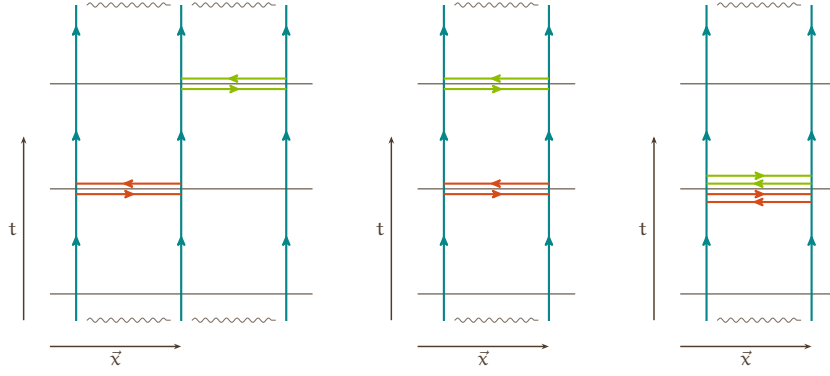


Figure 4.5.: The different spatial and temporal occupation of the $\text{tr}(\text{PMPM})$ term appearing at the NLO of the hopping parameter expansion. The last figure shows all spatial hops occupying the same spatial link, meaning that they will vanish in the large- N_t limit.

something non-zero. There are three fundamental scenarios which fulfil this criterion, and they are depicted in FIGURE 4.5. In the leftmost graph the two pairs of hops occupy different spatial positions and can therefore never overlap. The temporal sum in this case gives a factor N_t^2 as the two hops can independently choose a temporal slice. When the two hops occupy the same nearest neighbour pair, we have two situations. There are $N_t(N_t - 1)$ copies in which they occupy different time slices and N_t copies in which they overlap. Since

$$\int dU UU^\dagger UU^\dagger \neq \left(\int dU UU^\dagger \right)^2 \quad (4.75)$$

they naturally give different results, all of which are accounted for by the method of moments and cumulants. However, the integrals and spin traces are independent of the number of temporal lattice sites, and there therefore has to exist an N_t for which

$$N_t(N_t - 1) \left(\int dU UU^\dagger \right)^2 \gg N_t \int dU UU^\dagger UU^\dagger \quad (4.76)$$

and the more complicated overlapping diagrams can be neglected. This is equivalent to a leading order expansion in $1/N_t$.

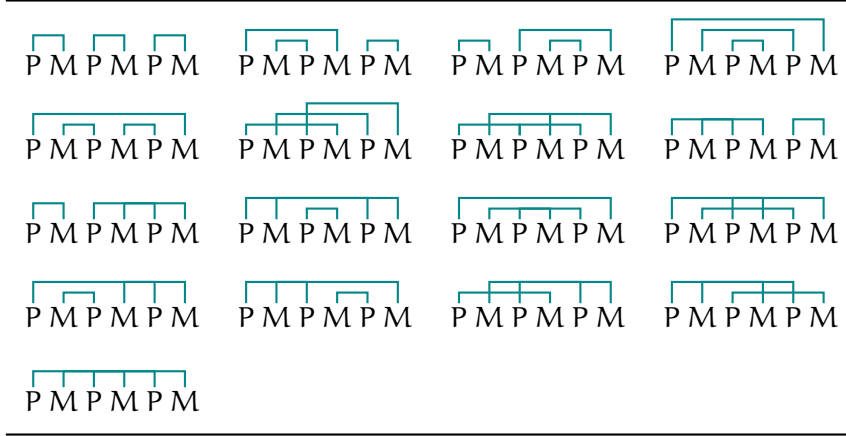
4.8.1 Combinatorics

Before we present the $N^3\text{LO}$ result for the effective action in the cold and dense limit, we review some of the combinatorics that went into the computation.

Because of the selection criterion for non-vanishing gauge integrals, EQ (A.35), we see that one must restrict the coordinate sums in the matrix multiplications of the P and M matrices in such a way that spatial links overlap and give contributing results. We therefore define a contraction

$$\overbrace{P_{xy} M_{zw}} = P_{xy} M_{zw} \delta_{\bar{y}\bar{z}} \delta_{\bar{x}\bar{w}} \delta_{t_y t_w}, \quad (4.77a)$$

$$\overbrace{P_{xy} P_{zw}} = P_{xy} P_{zw} \delta_{\bar{x}\bar{z}} \delta_{\bar{y}\bar{w}} \delta_{t_y t_w}, \quad (4.77b)$$

Table 4.1.: All contractions contributing to the $\mathcal{O}(\kappa^6)$ term $\text{tr}(\text{PMPMPM})$.

which can trivially be extended to the contraction of more elements. We see that the contraction fixes a single temporal index as well as fully fixes the spatial position and orientation of every matrix but one. One can also contract more than one matrix, as shown in TABLE 4.1 which contains all non-vanishing contractions of the NNLO term $\text{tr}(\text{PMPMPM})$. Due to the fact that every contraction fixes a temporal index in all matrices involved we see that the degrees of freedom naturally decrease. The various contractions of TABLE 4.1 can be categorised into three distinct groups

$$\sum_{t_1, t_2, t_3} \overbrace{P M} \overbrace{P M} \overbrace{P M} \propto N_t^3, \quad (4.78a)$$

$$\sum_{t_1, t_2} \overbrace{P M P M P M} \propto N_t^2, \quad (4.78b)$$

$$\sum_{t_1, t_2} \overbrace{P M P M P M} \propto N_t^2, \quad (4.78c)$$

$$\sum_{t_1} \overbrace{P M P M P M} \propto N_t. \quad (4.78d)$$

Generally the power of N_t is the same as the number of independent contractions. This is true only when N_t is large, as the number of free temporal slices must be large enough for the contractions to be separate. Since we are interested in the $N_t \gg 1$ range, we will disregard contributions from contractions not consisting of a single PM pair.

At this stage in the computation we will dispense with the notion that hops in positive and negative spatial directions are distinguishable. In contrast to the temporal hops, which get boosted by baryon chemical potential, there is no asymmetry between positive and negative spatial hops. We therefore switch to a notation which focusses on the dominant pairings

$$\text{tr} X_i Y_i = \text{tr} X \overbrace{P Y} M + \text{tr} X M \overbrace{Y P}, \quad (4.79)$$

in which X and Y symbolise the remainder of the matrix, which are disallowed from having spatial hops overlapping with the i -pairing. Every contracted PM pair is labelled

by an arbitrary symbol i , and is invariant under relabelling. Of the terms in TABLE 4.1, the six terms which consists of pairings only can in this notation be reduced to the three terms

$$\text{tr } 112233, \quad \text{tr } 123321, \quad \text{tr } 123123. \quad (4.80)$$

To be a bit more explicit we will quickly go through the notation at NLO. In the old notation the kinetic determinant would read

$$\det Q_{\text{kin}} = 1 - \text{tr}(\text{PM}) + \frac{1}{2}(\text{tr}(\text{PM}))^2 - \text{tr}(\text{PPMM}) - \frac{1}{2}\text{tr}(\text{PMPM}) + \mathcal{O}(\kappa^6) \quad (4.81)$$

which would give

$$\begin{aligned} \det Q_{\text{kin}} = 1 - \frac{1}{2}\text{tr}(11) + \frac{1}{8}\text{tr}(11)\text{tr}(22) \\ + \frac{1}{4}\text{tr}(12)\text{tr}(12) - \frac{1}{2}\text{tr}(1122) + \mathcal{O}(\kappa^6, N_t^{-1}). \end{aligned} \quad (4.82)$$

The pairing notation might seem lengthier, but it contains more information than the previous PM notation. When counting terms one has to be careful not to over count. For instance, the final term of EQ (4.82) can be expanded into four terms in the PM notation

$$\text{tr}(\text{PMPM}), \quad \text{tr}(\text{PMMP}), \quad \text{tr}(\text{MPPM}), \quad \text{tr}(\text{MPMP}), \quad (4.83)$$

one should however note that the third term is identical to the second under cyclic permutations and relabelling, and should therefore be discarded. The separate traces are however distinct, and the invariant relabelling must be considered on a trace by trace basis. The combinatorial prefactors $1/g$ can be computed with the following formula

$$\frac{1}{g} = \frac{\text{\# of unique cyclic permutations of the traces}}{n_2!n_4! \dots n_N! 2^{n_2}4^{n_4} \dots N^{n_N}}. \quad (4.84)$$

The numerator is the number of cyclic permutations within the traces that remain different under relabelling, e.g. $\text{tr}(1122)$ has two distinct permutations, the one already mentioned and $\text{tr}(1221)$. The n_m in the numerator is the number of trace factors with m matrices. E.g. $\text{tr}(12)\text{tr}(12)$ has $n_2 = 2, n_4 = 0, \dots, n_N = 0$, while $\text{tr}(1122)$ has $n_2 = 0, n_4 = 1, \dots, n_N = 0$.

4.8.2 Dirac indices

In this subsection we will study the spin structure of the terms dominating the cold regime, and subsequently discover that it is in fact trivial in this limit. In the limit of high baryon chemical potential, we see from EQS (4.28-4.33) that the static propagator simplifies to

$$Q_{\text{stat}, t_y t_x}^{-1} \approx (1 - \kappa T^+)^{-1}_{t_y t_x} = \delta_{t_y t_x} + \frac{1 + \gamma_0}{2} B_{t_y t_x}^+, \quad (4.85)$$

in which the matrix B has no spin dependence. We see from the definition of a contraction, EQS (4.77a, 4.77b), that the $\delta_{t_y t_x}$ in Q_{stat}^{-1} would impose additional constraints on the

temporal index and will therefore produce terms which are subleading when N_t is large. The only exception is a contraction

$$\overbrace{P_{xy} M_{yz}} = P_{xy} M_{yz} \delta_{\bar{z}z} \delta_{t_y t_z} \quad (4.86)$$

in which the $\delta_{t_y t_x}$ condition of the Q_{stat}^{-1} matrix of the M factor is already fulfilled. However this would apply no temporal movement and is therefore disallowed because the hopping expansion of Wilson fermions does not allow backtracking, $(1 + \gamma_\mu)(1 - \gamma_\mu) = 0$. We can therefore to leading order use the following expression for the static propagator

$$Q_{\text{stat}, t_y t_x}^{-1} \stackrel{\text{leading order}}{=} \frac{1 + \gamma_0}{2} B_{t_y t_x}^+ \quad (4.87)$$

Since the B^\pm matrix has no spin structure, we can easily identify the full Dirac trace of any contributing term as

$$\text{tr}_{xsc}(X_{xsc}) = \text{tr}_s \left((1 + \gamma_0)(1 \pm \gamma_i)(1 + \gamma_0)(1 \pm \gamma_j) \cdots \right) \text{tr}_{xc}(X'_{xc}). \quad (4.88)$$

where every P would contribute with a factor $(1 + \gamma_0)(1 + \gamma_i)$ and every M a factor $(1 + \gamma_0)(1 - \gamma_j)$. To shorten the notation we introduce the alias $g_\mu = (1 + \gamma_\mu)$ and $\bar{g}_\mu = (1 - \gamma_\mu)$. In this notation the spin trace of a polymer X gives

$$\text{tr}_s(X'_s) = \text{tr}_s(g_0 g_i g_0 \bar{g}_j \cdots) \quad (4.89)$$

We can expand the first product

$$\begin{aligned} \text{tr}_s((1 + \gamma_0 \pm \gamma_i \pm \gamma_0 \gamma_i) g_0 \cdots) \\ = \text{tr}_s(g_0 \cdots) + \text{tr}_s(\gamma_0 g_0 \cdots) \pm \text{tr}_s(\gamma_i g_0 \cdots) \pm \text{tr}_s(\gamma_0 \gamma_i g_0 \cdots). \end{aligned} \quad (4.90)$$

Using the anti-commutation relation of the Dirac matrices, together with the expression $\gamma_0 g_0 = \gamma_0(1 + \gamma_0) = (\gamma_0 + 1) = g_0$, we see that the spin structure simplifies to

$$\text{tr}_s(g_0 \cdots) + \text{tr}_s(g_0 \cdots) \pm \text{tr}_s(\gamma_i g_0 \cdots) \mp \text{tr}_s(\gamma_i g_0 \cdots) = 2 \text{tr}_s(g_0 \cdots). \quad (4.91)$$

We therefore replace every $g_0 g_i$ and every $g_0 \bar{g}_j$ pair with a factor 2 until there is only one pair left. The trace of the final pair is simply the dimension of the system, in this case 4. The spin trace of the large- N_t limit can thus be considered trivial

$$\text{tr}_s(X'_s) = \underbrace{\text{tr}(g_0 g_i g_0 \bar{g}_j \cdots)}_{n \text{ pairs}} = 2^{n-1} \text{tr}(g_0 g_i) = 2^{n+1}. \quad (4.92)$$

4.8.3 A comment on gauge corrections

Before we finally state the $N^3\text{LO}$ effective action for the cold and dense regime we need to examine a final set of apparently low order graphs which have yet to be discussed. They are the result of new geometries only possible to construct with the insertion of plaquettes. The first of these appears at $\mathcal{O}(\kappa^4 u)$ and is depicted to the far left in FIGURE 4.6. This particular contribution arises in the following integral

$$\kappa^4 u \int [dU]_\mu \chi(U) \text{tr}_{xsc}(P_i P_j M_i M_j), \quad \text{for } i \neq j. \quad (4.93)$$

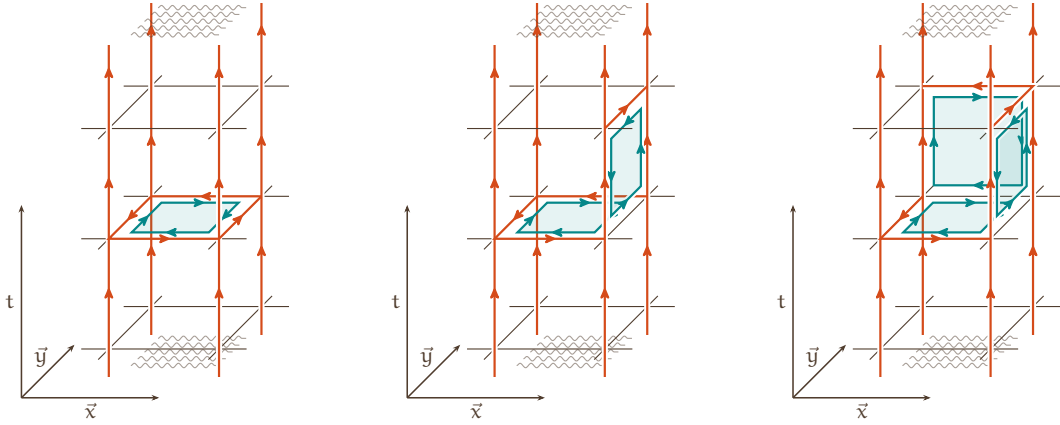


Figure 4.6.: The three first non-trivial gauge corrections to $\mathcal{O}(\kappa^4)$

This however restricts the four quark hops to occupy the same temporal slice and therefore only gives a single factor of N_t , while the dominating $\mathcal{O}(\kappa^4)$ terms give contributions proportional to N_t^2 . It is possible to shift the quark hops on the slices by inserting plaquettes as can be seen in the two other graphs in FIGURE 4.6, and that would give a correction to the formula above

$$\kappa^4 \mathbf{u} \left(1 + 2 \frac{\mathbf{u} \kappa^2 - (\mathbf{u} \kappa^2)^{N_t}}{1 - \mathbf{u} \kappa^2} \right)^4 (1 + 4\mathbf{u}^5) \int [d\mathbf{U}]_\mu \chi(\mathbf{U}) \text{tr}_{xsc}(\mathbf{P}_i \mathbf{P}_j \mathbf{M}_i \mathbf{M}_j), \quad (4.94)$$

which of course would be highly suppressed as \mathbf{u} is also a small parameter. This specific geometry will indeed appear at $\mathcal{O}(\kappa^8)$ where the plaquette can be replaced by a quark loop including windings which can shift the links arbitrarily in the temporal coordinate.

4.8.4 The $\mathcal{O}(\kappa^8)$ effective action

We finally turn our attention to the higher order contributions to the effective theory. Although the groundwork has been laid, the combinatorics still have to be carried out. As the number of terms grow exponentially, so does their complexity, there is little chance for a straightforward computation ever to get all the prefactors correct. Due to this, a computer program has been developed as part of the present work. The aim is to compute the effective theory in the limit of cold QCD [Glesaaen, 2016].

The software computes the effective theory terms in a series of easily understandable steps

1. Computes all permutations of \mathbf{P} and \mathbf{M} that can enter a trace to a given order.
2. Finds and collects all identical terms.
3. Computes all combinations of traces of lower orders which give a contribution to the given order.
4. Computes all contractions of \mathbf{P} 's and \mathbf{M} 's which can be realised spatially.
5. Computes all spatial realisations of ambiguous multi trace contractions.

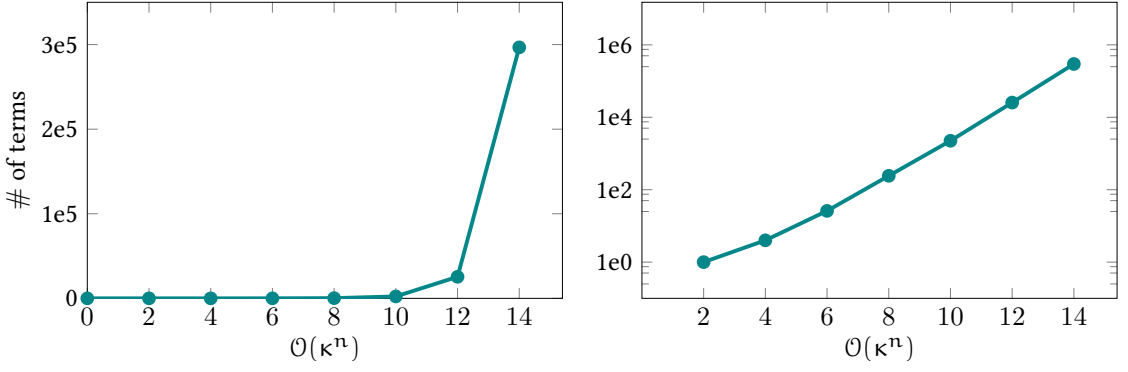


Figure 4.8.: Number of terms generated by the software at varying orders in κ .

the expansion order. This is a roadblock for the numerical evaluation as the number of operations one has to carry out to compute the Monte Carlo weight / Complex Langevin force at some point will overtake even that of computing the fermion determinant in full. The number of terms can be reduced by around one order of magnitude by expressing sums over coordinates such that the link indices can run over both positive and negative directions. This is conceptually similar to the earlier switch between the PM notation and the pairing notation. However, this rewriting is a simplification for analytic evaluation only, as the net numerical work stays constant.

In [Glesaaen et al., 2015, 2016], as well as in this thesis we work with the effective action up to $\mathcal{O}(\kappa^8 u^5)$. Since the analytic expression is rather lengthy, we give the effective action in a graphical representation. This will also serve as a convenient notation for the analytic evaluation, which we will tackle in the next session. The full expression is given in a more conventional notation in APPENDIX B.1. We symbolise factors of $W_{n,m}(\vec{x})$ by vertices where n is the number of bonds entering a vertex and m is the number indicated on the node. Furthermore, vertices connected by one or more nodes are nearest neighbours on the lattice =2mu

$$\begin{aligned}
 S_{\text{eff}} = & S_0 + h_2 N_f \sum_{\text{dof}} \begin{array}{c} \textcircled{1} \\ | \\ \textcircled{1} \end{array} - h_2^2 N_f \sum_{\text{dof}} \begin{array}{c} \textcircled{1} \\ / \quad \backslash \\ \textcircled{1} \quad \textcircled{1} \end{array} - h_2^2 N_f^2 \sum_{\text{dof}} \begin{array}{c} \textcircled{1} \\ | \\ \textcircled{1} \end{array} + h_2^3 N_f \sum_{\text{dof}} \begin{array}{c} \textcircled{1} \quad \textcircled{1} \\ / \quad \backslash \\ \textcircled{1} \quad \textcircled{1} \end{array} \\
 & + \frac{1}{3} h_2^3 N_f \sum_{\text{dof}} \left(\begin{array}{c} \textcircled{1} \\ / \quad \backslash \\ \textcircled{1} \quad \textcircled{1} \end{array} - \begin{array}{c} \textcircled{1} \\ / \quad \backslash \\ \textcircled{1} \quad \textcircled{2} \end{array} \right) + 2h_2^3 N_f^2 \sum_{\text{dof}} \left(\begin{array}{c} \textcircled{1} \\ / \quad \backslash \\ \textcircled{1} \quad \textcircled{1} \end{array} - \begin{array}{c} \textcircled{2} \\ / \quad \backslash \\ \textcircled{1} \quad \textcircled{1} \end{array} \right) \\
 & + \frac{1}{6} h_2^3 N_f \sum_{\text{dof}} \left(\begin{array}{c} \textcircled{1} \\ | \\ \textcircled{1} \end{array} - \begin{array}{c} \textcircled{2} \\ | \\ \textcircled{1} \end{array} \right) - \frac{4}{3} h_2^3 N_f^3 \sum_{\text{dof}} \begin{array}{c} \textcircled{1} \\ | \\ \textcircled{2} \end{array} - h_2^4 N_f \sum_{\text{dof}} \begin{array}{c} \textcircled{1} \quad \textcircled{1} \\ / \quad \backslash \\ \textcircled{1} \quad \textcircled{1} \end{array} \\
 & - \frac{1}{12} h_2^4 N_f \sum_{\text{dof}} \left(\begin{array}{c} \textcircled{1} \quad \textcircled{1} \\ / \quad \backslash \\ \textcircled{1} \quad \textcircled{1} \end{array} - 2 \begin{array}{c} \textcircled{1} \quad \textcircled{1} \\ / \quad \backslash \\ \textcircled{1} \quad \textcircled{2} \end{array} + \begin{array}{c} \textcircled{1} \quad \textcircled{1} \\ / \quad \backslash \\ \textcircled{1} \quad \textcircled{3} \end{array} \right) - h_2^4 N_f \sum_{\text{dof}} \left(\begin{array}{c} \textcircled{1} \quad \textcircled{1} \\ / \quad \backslash \\ \textcircled{1} \quad \textcircled{1} \end{array} - \begin{array}{c} \textcircled{1} \quad \textcircled{1} \\ / \quad \backslash \\ \textcircled{1} \quad \textcircled{2} \end{array} \right) \\
 & - h_2^4 N_f^2 \sum_{\text{dof}} \left(\begin{array}{c} \textcircled{1} \\ / \quad \backslash \\ \textcircled{1} \quad \textcircled{1} \end{array} - 4 \begin{array}{c} \textcircled{1} \\ / \quad \backslash \\ \textcircled{1} \quad \textcircled{2} \end{array} + \begin{array}{c} \textcircled{1} \\ / \quad \backslash \\ \textcircled{1} \quad \textcircled{3} \end{array} \right) - h_2^4 N_f^2 \sum_{\text{dof}} \begin{array}{c} \textcircled{1} \quad \textcircled{1} \\ | \\ \textcircled{1} \quad \textcircled{1} \end{array} \\
 & - 2h_2^4 N_f^2 \sum_{\text{dof}} \left(\begin{array}{c} \textcircled{1} \quad \textcircled{1} \\ / \quad \backslash \\ \textcircled{1} \quad \textcircled{1} \end{array} - \begin{array}{c} \textcircled{2} \quad \textcircled{1} \\ / \quad \backslash \\ \textcircled{1} \quad \textcircled{1} \end{array} \right) - h_2^4 N_f^2 \sum_{\text{dof}} \left(\begin{array}{c} \textcircled{1} \quad \textcircled{1} \\ / \quad \backslash \\ \textcircled{1} \quad \textcircled{1} \end{array} - 2 \begin{array}{c} \textcircled{1} \quad \textcircled{1} \\ / \quad \backslash \\ \textcircled{1} \quad \textcircled{2} \end{array} + \begin{array}{c} \textcircled{2} \quad \textcircled{1} \\ / \quad \backslash \\ \textcircled{1} \quad \textcircled{2} \end{array} \right)
 \end{aligned}$$

$$\begin{aligned}
& -\frac{1}{3}h_2^4N_f \sum_{\text{dof}} \left(\begin{array}{c} \textcircled{1} \\ \textcircled{1} \textcircled{1} \end{array} - 2 \begin{array}{c} \textcircled{2} \\ \textcircled{1} \textcircled{1} \end{array} + 2 \begin{array}{c} \textcircled{2} \\ \textcircled{2} \textcircled{1} \end{array} - \begin{array}{c} \textcircled{3} \\ \textcircled{2} \textcircled{1} \end{array} \right) \\
& + \frac{4}{3}h_2^4N_f^3 \sum_{\text{dof}} \left(\begin{array}{c} \textcircled{1} \\ \textcircled{2} \textcircled{1} \end{array} - 2 \begin{array}{c} \textcircled{2} \\ \textcircled{2} \textcircled{1} \end{array} + 2 \begin{array}{c} \textcircled{2} \\ \textcircled{1} \textcircled{1} \end{array} - \begin{array}{c} \textcircled{3} \\ \textcircled{1} \textcircled{1} \end{array} \right) \\
& - \left(\frac{1}{12}N_f + \frac{2}{3}N_f^3 \right) h_2^4 \sum_{\text{dof}} \left(\begin{array}{c} \textcircled{1} \\ \textcircled{1} \textcircled{1} \end{array} - 4 \begin{array}{c} \textcircled{2} \\ \textcircled{1} \textcircled{1} \end{array} + \begin{array}{c} \textcircled{3} \\ \textcircled{1} \textcircled{1} \end{array} \right) \\
& - \frac{2}{3}h_2^4N_f^4 \sum_{\text{dof}} \left(\begin{array}{c} \textcircled{1} \\ \textcircled{3} \end{array} + 2 \begin{array}{c} \textcircled{2} \\ \textcircled{2} \end{array} \right) - \frac{1}{12}h_2^4N_f^2 \sum_{\text{dof}} \left(\begin{array}{c} \textcircled{1} \\ \textcircled{1} \end{array} + 12 \begin{array}{c} \textcircled{2} \\ \textcircled{2} \end{array} + \begin{array}{c} \textcircled{3} \\ \textcircled{3} \end{array} \right) \\
& + \frac{2}{3}h_2^4N_f^2 \sum_{\text{dof}} \left(\begin{array}{c} \textcircled{1} \\ \textcircled{2} \end{array} + \begin{array}{c} \textcircled{2} \\ \textcircled{3} \end{array} \right) + \mathcal{O}(\kappa^{10}, \frac{1}{N_\tau}). \quad (4.99)
\end{aligned}$$

The sums over "degrees of freedom" represent the remaining spatial trace and sums over directions, which remains to be carried out either for analytic computations or during numerical evaluation. We see that all the higher order interactions appear with a coupling constant equal to some power of the nearest neighbour coupling constant h_2 . This is not very hard to realise from the mathematics, as every new spatial link contributes a combinatorial factor of N_t , a hopping factor of κ^2 and the gauge integration results in a factor of N_c^{-1} for every integrated link. Since no spatial links ever overlap, we can apply gauge corrections on a link by link basis regardless of whether they connect the same nearest neighbour sites. Corrections to this will appear at NLO in N_t^{-1} . The gauge corrections are therefore given by replacing $h_2 \rightarrow h_2(\beta)$ as shown in EQ (4.56).

4.8.5 Application region of the large- N_t approximation

Although there is no questioning the dense approximation for its region of applicability when studying the cold and dense regime due to its exponential nature, one might ask the validity of the expansion around $N_t^{-1} \rightarrow 0$. The lowest order correction to this limit comes at order $\kappa^4 N_t$. If we choose a somewhat extreme scenario for our parameters, $h_2 = 0.15$ and $N_t = 50$, we see that the $\kappa^4 N_t$ and h_2^4 have about the same order of magnitude, meaning that the next order in N_t^{-1} should contribute about the same as the κ^8 terms do. To analyse this effect we plot the ratio of the baryon number density computed at fixed h_1 and h_2 using the $\mathcal{O}(h_2^4)$ action with and without the $\mathcal{O}(\kappa^4 N_t)$ terms, shown in FIGURE 4.9. Although the prefactor of the expansion coefficients are around the same order of magnitude, it is clear that the contributions from these higher order terms give small corrections to the final result. Already at $N_t \leq 13$ the contribution is less than 5%, which is insignificant when compared to the contribution from the $\mathcal{O}(h_2^4)$ term at these extreme parameter choices. We thus conclude that the large- N_t limit is well under control for the physical region we are studying.

4.9 NUMERICAL EVALUATION

Although the focus of this thesis is the analytic evaluation of the effective theory, a couple of remarks on the numerical evaluation is still in order. At the beginning of this chapter we stated the nefarious sign problem as a motivation for developing the effective

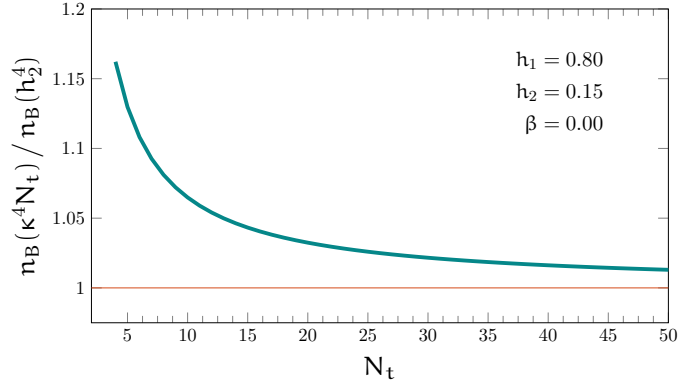


Figure 4.9.: Ratio of baryon number density at $\mathcal{O}(h_2^4, \kappa^4 N_t)$ and at $\mathcal{O}(h_2^4)$ for fixed h_1 and h_2 in the strong coupling limit. Computed with the analytic treatment of CHAPTER 5.

3D theory. And although the effective theory still suffers from a conceptual sign problem in the sense that the action takes complex values, we are in a regime where methods such as reweighting work well. A thorough review of the theory's numerical properties can be found in [Neuman, 2015].

The effective theory offers multiple advantages for numerical evaluation over full lattice calculations besides the apparent resolution of the sign problem.

- First and foremost we have replaced the very expensive fermion determinant with a discrete sum over the volume and a handful of terms, an overall much cheaper computation.
- Second, the temporal direction has been integrated out and its remnant is encoded in N_t , which is a parameter, reducing the dimensionality of the variable space by one.
- Finally, the remaining field variables are traces of group elements of SU(3) which can be represented by two real angles in comparison to the eight generators needed to represent a gauge link in full lattice QCD.

Regardless of whether one chooses to do a reweighted *Monte Carlo* (MC) or a *Complex Langevin* (CL) simulation to deal with the trivial sign problem, it is advantageous to rewrite the partition function to depend on the angular representation of the group characters, as outlined in APPENDIX A.1. For SU(3) we replace the characters with

$$L(\vec{x}) \equiv \chi_1 = e^{i\theta_{\vec{x}}} + e^{i\phi_{\vec{x}}} + e^{-i(\theta_{\vec{x}} + \phi_{\vec{x}})} \quad (4.100)$$

and the integration measure by

$$\int [dW]_{\vec{x}} = \frac{1}{(2\pi)^2 N_c!} \int \prod_{\vec{x}} d\theta_{\vec{x}} d\phi_{\vec{x}} H(\theta_{\vec{x}}, \phi_{\vec{x}}) \quad (4.101)$$

where H is the reduced Haar measure given by EQ (A.13). This induces a Polyakov Loop potential in the action

$$\int [d\theta d\phi]_{\vec{x}} e^{-S_{\text{eff}} + V[L]}, \quad (4.102)$$

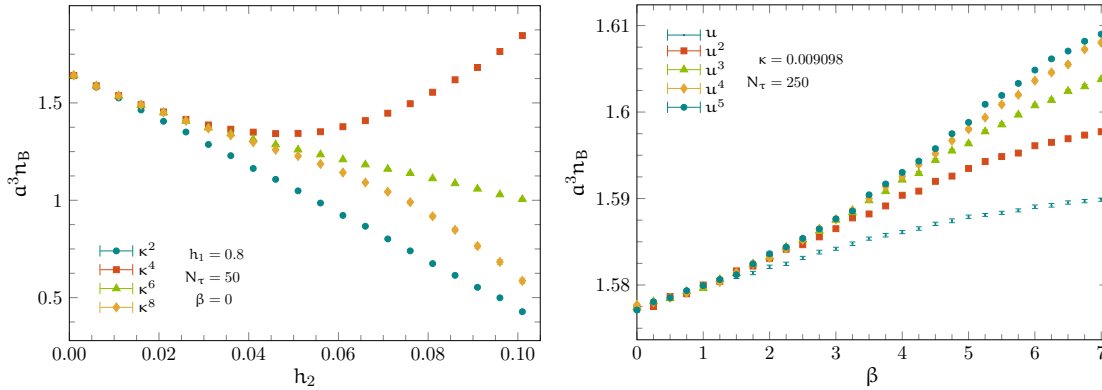


Figure 4.10.: Left: Convergence of baryon number density in lattice units as a function of the nearest neighbour coupling h_2 in various orders of the hopping expansion at strong coupling. Right: Corresponding convergence plot at different orders in the character expansion parameter u .⁽⁴⁾

with the potential as stated in the appendix

$$V[L] = \log \left(\sum_{\vec{x}} 27 - 18|L(\vec{x})|^2 + 8\text{Re} L(\vec{x})^3 - |L(\vec{x})|^4 \right). \quad (4.103)$$

The effective theory is also easily extendable to other $SU(N_c)$, possibly other gauge groups. For the former, one simply has to give the proper reduced Haar measure and the definition for the new Polyakov loop variable

$$L_{N_c}(\vec{x}) = \sum_{n=1}^{N_c-1} e^{i\theta_n(\vec{x})} + e^{-i\sum_{n=1}^{N_c-1} \theta_n(\vec{x})}. \quad (4.104)$$

We see that an effective theory using the gauge group $SU(N_c)$ has $N_s^3(N_c - 1)$ degrees of freedom as compared to the $4N_s^3N_t(N_c^2 - 1)$ degrees of freedom one would have in a full lattice gauge theory simulation. Therefore, on top of the reduced computation cost the theory also scales linearly in complexity with the number of colours as compared to quadratic in a full simulation.

The simulations were carried out using both algorithms, MC with reweighting and CL, and the results were cross checked [Langelage et al., 2014]. Both methods give compatible results within the parameter range for which the effective theory is well defined. Our first task is to assess the range of validity of the strong coupling, heavy quark action. One expects the additional orders in κ to extend the convergence region, within which the description of thermodynamic functions by the effective action is reliable. We test this by computing the baryon number density at fixed values of the coupling h_1 and N_τ . Varying κ then allows us to assess the convergence of the expansion of the kinetic quark determinant. FIGURE 4.10 (left) shows the results obtained with effective actions of increasing order in κ . One clearly observes how two adjacent orders stay together for larger values of $h_2(\kappa)$ as the order increase, thus extending the range where our effective action is reliable. FIGURE 4.10 (right) shows the same exercise for the largest κ considered with the numerics, this time increasing the orders of the character expansion. We

⁽⁴⁾Simulation data courtesy of Mathias Neuman

observe good convergence up to $\beta \sim 6$, which is a sufficiently weak coupling to allow for continuum extrapolations. It is interesting to note that the convergence properties are not determined by the size of the expansion parameters alone. Even though the $u(\beta)$ -values far exceed the κ -values employed in the figures, convergence in $u(\beta)$ appears to be faster. The gain in convergence region by the additional orders in the effective action can be exploited to study the systematics of our effective theory.

We will leave the numerical evaluation for now and will shift our focus to a purely analytical treatment of the effective 3D theory using graphical methods borrowed from the linked cluster formalism.

ANALYTIC EVALUATION OF THE EFFECTIVE THEORY

In CHAPTER 4 we introduced the dimensionally reduced effective theory for heavy quarks at strong coupling. The chapter ended with a section on the numerical handling of the theory and its advantages over full lattice gauge theory simulations. Although a lot of progress has been made evaluating the predictions of the theory [Fromm et al., 2012, 2013; Langelage et al., 2014], we see from the convergence plots in FIGURE 4.10 that convergence is slow and other approaches should be considered.

It was discovered in one of the previous studies of the effective theory [Langelage et al., 2014] that it is possible to treat the effective theory purely analytically, which provides a plethora of useful methods to be explored in this chapter. First and foremost the analytical evaluation gives insight into the mathematical and physical structure of the effective theory and serves as a cross check for the numerical methods. In SECTION 5.1 we present the linked cluster expansion which provides the building blocks for a systematic study of the analytic evaluation. We will see how one can transform the language of spin statistics and nearest neighbour systems to that of the strong coupling, heavy quark formalism. In SECTION 5.4 we introduce a new resummation scheme, which is inaccessible to numerical methods.

In SECTION 5.4.4 we use the full power of the analytic expressions to study the various aspects of the theory at hand, comparing with numerical results, studying lattice artefacts and more.

Finally, in SECTIONS 5.5.1, and 5.5.2, we carry out two exploratory studies in which the analytic evaluation is paramount. Although these still pose a lot of open questions, we build foundations which future studies can use as a basis.

5.1 LINKED CLUSTER EXPANSION

We start once more on a more fundamental level by introducing the linked cluster formalism for scalar fields with nearest neighbour interactions. Although the following section gives a complete overview, we refer to introductory texts on the subject for more details, e.g. [Wortis, 1974; Reisz, 1995], and [Domb, 1974; Martin, 1974] for a physics focused presentation of simple graph theoretical practices. After the fundamentals are out of the way, we study how the formalism can be extended to include n -point interactions with finite spatial extent – a system in which the effective theory can then be expressed.

5.1.1 *Classical linked cluster expansion for nearest neighbour interactions*

To introduce the framework we consider a scalar field with a two-point coupling

$$\mathcal{Z} = \int [d\phi] e^{-S_0[\phi] + \frac{1}{2} \sum_{x,y} \phi(x) v(x,y) \phi(y)}, \quad \text{and} \quad v(x,x) = 0, \quad (5.1)$$

where the function $v(x, y)$ encodes the coupling information. We will assume that the coupling strength is small enough to justify an expansion around the free theory. To facilitate the expansion we introduce source fields $J(x)$ and define the generating functional

$$\mathcal{Z}[J] = \int [d\phi] e^{-S[\phi] + \sum_x J(x) \phi(x)}. \quad (5.2)$$

Since our goal is to study thermodynamic quantities, we shift our attention to the computation of the grand canonical potential \mathcal{W} , also known as the generating functional of connected correlation functions

$$\mathcal{W}[J, v] = \log \mathcal{Z}[J, v]. \quad (5.3)$$

A linked cluster expansion (*LCE*) of the grand canonical potential is then defined as the Taylor expansion with respect to the coupling $v(x, y)$ around the free theory

$$\mathcal{W}[J, v] = \left(\exp \left(\frac{1}{2} \sum_{x,y} v(x,y) \frac{\delta}{\delta \hat{v}(x,y)} \right) \right) \mathcal{W}[J, \hat{v}] \Big|_{\hat{v}=0}. \quad (5.4)$$

The derivative of \mathcal{W} with respect to the couplings can be expressed as derivatives with respect to the sources

$$\frac{\delta \mathcal{W}}{\delta v(x,y)} = \frac{\delta^2 \mathcal{W}}{\delta J(x) \delta J(y)} + \frac{\delta \mathcal{W}}{\delta J(x)} \frac{\delta \mathcal{W}}{\delta J(y)}. \quad (5.5)$$

We also know that $\mathcal{W}[J]$ is the generating functional of the connected n -point functions

$$\frac{\delta \mathcal{W}}{\delta J(x)} \Big|_{J=0} = \frac{1}{\mathcal{Z}} \int [d\phi] \phi(x) e^{-S[\phi]} \equiv \langle \phi(x) \rangle, \quad (5.6)$$

which for higher order derivatives produces the cumulants

$$\frac{\delta^2 \mathcal{W}}{\delta J(x) \delta J(y)} \Big|_{J=0} = \langle \phi(x) \phi(y) \rangle - \langle \phi(x) \rangle \langle \phi(y) \rangle. \quad (5.7)$$

To second order the expansion in EQ (5.4) is

$$\begin{aligned} \mathcal{W}[J, v] = \mathcal{W}[J, 0] &+ \frac{1}{2} \sum_{x,y} v(x,y) \frac{\delta \mathcal{W}[J, \hat{v}]}{\delta \hat{v}(x,y)} \Big|_{\hat{v}=0} \\ &+ \frac{1}{8} \sum_{x,y} \sum_{z,w} v(x,y) v(z,w) \frac{\delta^2 \mathcal{W}[J, \hat{v}]}{\delta \hat{v}(x,y) \delta \hat{v}(z,w)} \Big|_{\hat{v}=0} + \dots \end{aligned} \quad (5.8)$$

We define the coupled n -point functions by

$$\mathcal{M}_n(x_1, x_2, \dots, x_n) = \frac{\delta^n \mathcal{W}[J, v]}{\delta J(x_1) \delta J(x_2) \cdots \delta J(x_n)}, \quad (5.9)$$

which in turn define the free n -point functions

$$\mathcal{M}_n(x_1, x_2, \dots, x_n)|_{v=0} \equiv M_n(x_1) \delta(x_1, x_2, \dots, x_n) \quad (5.10)$$

where the Kronecker deltas naturally arise in the free theory

$$x \neq y \Rightarrow \langle \phi(x) \phi(y) \rangle|_{v=0} = \langle \phi(x) \rangle \langle \phi(y) \rangle. \quad (5.11)$$

We can easily see from the deltas that the cluster expansion constitutes an expansion in connected graphs as any disconnected graphs would give vanishing contributions. We can rewrite the second order derivative in v in EQ (5.8) in terms of derivatives w.r.t. the sources, and thus the free n -point functions, obtaining

$$\begin{aligned} \mathcal{W}[v] = \mathcal{W}[0] + \frac{1}{2} \sum_{x,y} M_1(x) v(x, y) M_1(y) + \frac{1}{4} \sum_{x,y} M_2(x) v^2(x, y) M_2(y) \\ + \frac{1}{2} \sum_{x,y,z} M_1(x) v(x, y) M_2(y) v(y, z) M_1(z) + \dots \end{aligned} \quad (5.12)$$

5.1.2 Graphical definitions

Although the coefficients for the v^n term can be computed systematically from EQ (5.4), as we showed to second order in EQ (5.8), the process is tedious. However, there exists a formalism in which the terms and their prefactors can be written down immediately in an intuitive way.

Definition 5.1. *Connected graph*

A graph is a set of vertices and bonds where every bond connects two distinct vertices. An n -rooted graph has n fixed, distinguishable, external vertices, while all non-rooted vertices are free. A vertex is said to be n -valent if it has n bonds attached to it.

A connected graph has the property that one can always move from one vertex to another through a continuous set of movements along the graph's bonds. A graph which is not connected is disconnected.

Two n -rooted graphs are isomorphic if there exists a labelling of the bonds and vertices so that the bonds and vertices of the two graphs can be made identical. The number of distinct isomorphic labellings of a graph is called the graph's symmetry factor.

To compute \mathcal{W} one simply takes the set of all topologically distinct 0-rooted connected graphs. The order counting is on the bond level, meaning that at $\mathcal{O}(v^3)$ we only take 0-rooted connected graphs with three or fewer bonds. The final ingredient is a rule for transforming between the graphical representation and the mathematical expression for the grand canonical potential

Rule 5.1. *Grand canonical potential \mathcal{W}*

1. Assign a symbol, x_1, x_2, \dots, x_n to every vertex.

2. To every bond connecting vertices x_i and x_j add a factor $v(x_i, x_j)$.
3. For every vertex x_i with valence p , add a factor $M_p(x_i)$.
4. Add a sum over the entire lattice for every vertex symbol x_i .
5. Divide by the symmetry factor of the graph.

Using this rule we can write the grand canonical potential in EQ (5.12) in terms of graphs

$$\mathcal{W}[v] = \bullet + \frac{1}{2} \text{---} \text{---} + \frac{1}{2} \text{---} \text{---} \text{---} + \frac{1}{4} \text{---} \text{---} \text{---} + \dots \quad (5.13)$$

The equality between RULE 5.1 and the grand canonical potential LCE EQ (5.4) is in no way trivial, and proofs for the equality are given in e.g. [Englert, 1963; Bloch and Langer, 1965]. The geometry of the interaction is yet to be specified, and the sum over the symbols $\{x_1, \dots, x_n\}$ runs over the entire lattice. Further simplification can be achieved by choosing e.g. a uniform nearest neighbour coupling

$$v(x, y) = \begin{cases} v & \text{if } x \text{ and } y \text{ are nearest neighbours} \\ 0 & \text{else.} \end{cases} \quad (5.14)$$

It was shown in [Pordt and Reisz, 1997] that a graphical expansion for non-nearest neighbour couplings (albeit uniform) can be reordered in such a way that the class of graphs is identical to the nearest neighbour case, and thus the procedure is in practice more general than the one stated here. Regardless, choosing nearest neighbour interactions the grand canonical potential simplifies further

$$\mathcal{W}[v] = NM_0 + \frac{q}{2}vNM_1^2 + \frac{q}{4}v^2NM_2^2 + \frac{q^2}{2}v^2NM_1^2M_2 + \dots \quad (5.15)$$

where q is $2d$ for a d -dimensional square lattice. The prefactor of a term that arise from the spatial sum is called the embedding number⁽¹⁾ of a graph onto the lattice, and will differ from lattice to lattice. For every graph arising from an action with a uniform two-point interaction, the sum over the symbols / coordinates will yield N , the number of lattice sites, times the (free) embedding number of the graph. It might seem wrong at first to include all possible embeddings, as e.g. the q^2 in the $M_1^2M_2$ term will naturally include the embedding corresponding to the M_2^2 term. This is however not a problem, as the M_n factors are given in terms of cumulants, and consulting SECTION 4.7.1 we see that the system resolves these issues automatically. The embedding number is dependent on the lattice, so that e.g. the three bond graph

$$\triangle \quad (5.16)$$

has embedding number zero on a square lattice, given that there is no way to resolve the nearest neighbour requirement of RULE 5.1. On a triangular lattice on the other hand, it would have a non-zero embedding number. A table of all four bond graphs, as well as their symmetry factors and embeddings on a square lattice can be found in TABLE 5.1. When we later extrapolate the graphical methods to the effective theory, we will see that these are all the graphs needed to carry out a computation to order κ^8 .

In the next section we will see how to map the effective theory onto an LCE framework and which additional considerations have to be taken into account.

⁽¹⁾Also referred to as the *lattice constant* in the lattice community.










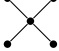










Graph	Symmetries	Embeddings	Graph	Symmetries	Embeddings
	2	2d		3!	(2d) ³
	2	(2d) ²		6	0
	4	2d		2	(2d) ²
	2	(2d) ³		2×3!	2d
	2	(2d) ⁴		4!	(2d) ⁴
	2	(2d) ⁴		8	3(2d) ² − 6d
	2×2!	(2d) ³		2	(2d) ³
	2×2!	(2d) ³		2×2!	0
	2	0		2×(2!) ²	(2d) ²
	3!	(2d) ²		2×4!	2d

Table 5.1.: Graphs with up to four bonds with symmetry factor and embeddings on a d dimensional square lattice.

5.1.3 LCE for the effective theory at LO

We first analyse the leading order action, and see how to establish a correspondence between the parameters of the effective action to the ones of the LCE. In the dense regime ($\mu \gg T$) the LO effective partition function is

$$\mathcal{Z}_2 = \int [d\mathbf{U}]_0 \det Q_{\text{stat}}^{N_f} \exp \left(-h_2 N_f \sum_{\langle \mathbf{x}, \mathbf{y} \rangle} W_{11}(\mathbf{x}) W_{11}(\mathbf{y}) \right), \quad (5.17)$$

as shown in CHAPTER 4. Comparing the above equation to the scalar field partition function we used to introduce the LCE, EQ (5.1), we see that there is an approximate one-to-one correspondence between the two systems

$$\phi \Leftrightarrow W_{11}, \quad v \Leftrightarrow 2h_2 N_f, \quad e^{-S_0[\phi]} \Leftrightarrow \mathcal{J}(\mathbf{U}_0, W_{11}) \det Q_{\text{stat}}, \quad (5.18)$$

where $\mathcal{J}(\mathbf{U}_0, W_{11})$ is the Jacobian determinant for the variable change. There is however no need to compute $S_0[W_{11}]$ explicitly, as the free energy depends only on the n-point functions M_n , which in turn depend on the expectation values of the free theory. We

define the n -point functions in terms of z -functions, which are (for $N_f = 1$)

$$z_0 = \int dW \det Q_{\text{stat}} = 1 + 4h_1^3 + h_1^6, \quad (5.19a)$$

$$z_{(11)} = \int dW \det Q_{\text{stat}} W_{11} = 6h_1^3 + 3h_1^6, \quad (5.19b)$$

$$z_{(11)^2} = \int dW \det Q_{\text{stat}} W_{11}^2 = 4h_1^3 + 9h_1^6, \quad (5.19c)$$

$$z_{(11)^3} = \int dW \det Q_{\text{stat}} W_{11}^3 = h_1^3 + 17h_1^6 + h_1^9, \quad (5.19d)$$

$$z_{(11)^4} = \int dW \det Q_{\text{stat}} W_{11}^4 = 21h_1^6 + 6h_1^9, \quad (5.19e)$$

while for $N_f = 2$ they take the values

$$z_0 = \int dW \det Q_{\text{stat}}^2 = 1 + 20h_1^3 + 50h_1^6 + 20h_1^9 + h_1^{12}, \quad (5.20a)$$

$$z_{(11)} = \int dW \det Q_{\text{stat}}^2 W_{11} = 15h_1^3 + 75h_1^6 + 45h_1^9 + 3h_1^{12}, \quad (5.20b)$$

$$z_{(11)^2} = \int dW \det Q_{\text{stat}}^2 W_{11}^2 = 6h_1^3 + 95h_1^6 + 96h_1^9 + 9h_1^{12}, \quad (5.20c)$$

$$z_{(11)^3} = \int dW \det Q_{\text{stat}}^2 W_{11}^3 = h_1^3 + 90h_1^6 + 188h_1^9 + 27h_1^{12}, \quad (5.20d)$$

$$z_{(11)^4} = \int dW \det Q_{\text{stat}}^2 W_{11}^4 = 60h_1^6 + 312h_1^9 + 81h_1^{12}. \quad (5.20e)$$

The z 's have a fairly convoluted naming scheme. The reason for this is that upon including more orders in the effective action, sets of $W_{\{n_m\}}$ must be placed in the integrand. The z 's follow the naming scheme

$$z_{(n_1 m_1)^{k_1} \dots (n_p m_p)^{k_p}} = \int dW \det Q_{\text{stat}}^{N_f} W_{n_1 m_1}^{k_1} \dots W_{n_p m_p}^{k_p}. \quad (5.21)$$

A list of all the integrated z 's needed to compute the results presented later is given in APPENDIX B.2. The n -point functions are then given by

$$M_0 = \log z_0, \quad (5.22a)$$

$$M_1 = \frac{z_{(11)}}{z_0}, \quad (5.22b)$$

$$M_2 = \frac{z_{(11)^2}}{z_0} - \frac{z_{(11)}^2}{z_0^2}, \quad (5.22c)$$

$$M_3 = \frac{z_{(11)^3}}{z_0} - 3 \frac{z_{(11)^2} z_{(11)}}{z_0^2} + 2 \frac{z_{(11)}^3}{z_0^3}, \quad (5.22d)$$

$$M_4 = \frac{z_{(11)^4}}{z_0} - 4 \frac{z_{(11)^3} z_{(11)}}{z_0^2} - 3 \frac{z_{(11)^2}^2}{z_0^2} + 12 \frac{z_{(11)^2} z_{(11)}^2}{z_0^3} - 6 \frac{z_{(11)}^4}{z_0^4}. \quad (5.22e)$$

With the full analytic result for the \mathcal{Z}_2 partition function at hand, we can start comparing thermodynamic quantities with results from the numerical evaluation. However, we first need to establish the observables.

5.2 OBSERVABLES

The definitions of the observables were given in SECTION 3.1, but just as they were defined on the lattice in SECTION 3.3, we have to give them in terms of the parameters we are working with in the analytic treatment of the effective theory. We exploit the fact that \mathcal{W} is linear in volume in the thermodynamic limit, which means that the pressure is given simply as

$$\mathcal{P} = \mathbb{T} \left(\frac{\partial}{\partial V} \log \mathcal{Z} \right)_{\mathbb{T}, z} = \frac{\mathbb{T}}{V} \mathcal{W}. \quad (5.23)$$

Similarly, taking the derivative with respect to fugacity is also straightforward. We simplify it further by using

$$z \frac{\partial}{\partial z} \Big|_{\mathbb{T}, V} = h_1 \frac{\partial}{\partial h_1} \Big|_{\mathbb{T}, V} \quad (5.24)$$

which means that the baryon number density is defined as

$$n_B = \frac{1}{3} n_q = h_1 \frac{1}{3} \left(\frac{\partial}{\partial h_1} \frac{\mathcal{W}}{V} \right)_{\mathbb{T}, V}. \quad (5.25)$$

To compute the energy density e we need to calculate the derivative

$$e = \mathbb{T}^2 \left(\frac{\partial}{\partial \mathbb{T}} \frac{\log \mathcal{Z}}{V} \right)_{z, V}. \quad (5.26)$$

We know that $\frac{\log \mathcal{Z}}{V}$ is volume independent, and therefore the requirement of keeping V constant is automatically fulfilled. We replace the derivative in \mathbb{T} by a derivative in α , and thus have

$$e = - \frac{1}{N_t} \left(\frac{\partial}{\partial \alpha} \frac{\mathcal{W}}{V} \right)_z. \quad (5.27)$$

The derivative with respect to the lattice spacing must be handled with some care. One option is to define the derivative at constant baryon mass

$$\alpha \frac{\partial}{\partial \alpha} (\alpha m_B) = \alpha m_B. \quad (5.28)$$

We base the baryon and meson masses on the full heavy quark results from [Smit, 2002], and later with the additional gauge corrections from [Langelage et al., 2014]

$$\alpha m_M = \operatorname{arcosh} \left(1 + \frac{(M^2 - 4)(M^2 - 1)}{2M^2 - 3} \right) - 24\kappa^2 \frac{u}{1 - u}, \quad (5.29)$$

$$\alpha m_B = \log \left(\frac{M^3(M^3 - 2)}{M^3 - \frac{5}{4}} \right) - 18\kappa^2 \frac{u}{1 - u}, \quad (5.30)$$

where $M = \frac{1}{2\kappa}$. In the strong coupling limit we can use this to determine $\frac{\partial \kappa}{\partial \alpha}$

$$\begin{aligned} \alpha \frac{\partial \kappa}{\partial \alpha} &= \alpha m_B / \frac{\partial \alpha m_B}{\partial \kappa} \\ &= - \frac{\alpha m_B e^{-\alpha m_B} (e^{\alpha m_B} - 8 + 4\sqrt{4 + e^{\alpha m_B} (e^{\alpha m_B} - 1)})}{6 \times 20^{1/3} \sqrt{4 + e^{\alpha m_B} (e^{\alpha m_B} - 1)} (e^{-\alpha m_B} (2 + e^{\alpha m_B} - \sqrt{4 + e^{\alpha m_B} (e^{\alpha m_B} - 1)}))^{2/3}}. \end{aligned} \quad (5.31)$$

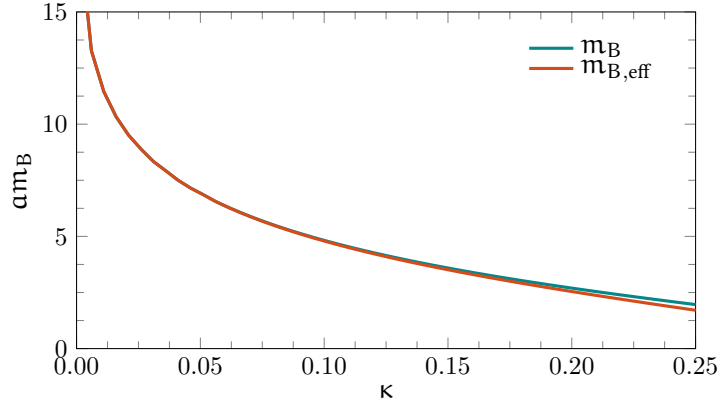


Figure 5.1.: Comparison of the effective and full baryon mass used in the definition of ϵ .

Away from strong coupling the derivative in a must be defined in terms of a derivative in β through the use of implicit functions

$$a \frac{d\beta}{da} \frac{d\kappa}{d\beta} = -a \frac{d\beta}{da} \frac{\partial am_B}{\partial \beta} / \frac{\partial am_B}{\partial \kappa}. \quad (5.32)$$

Assuming strong coupling for now, we observe that the energy density is given in terms of the two parameters of the theory, h_1 and h_2

$$e = -\frac{1}{aN_t} a \frac{\partial \kappa}{\partial a} \frac{\partial h_1}{\partial \kappa} \frac{\partial}{\partial h_1} \frac{\mathcal{W}}{V} \Big|_z - \frac{1}{aN_t} a \frac{\partial \kappa}{\partial a} \frac{\partial h_2}{\partial \kappa} \frac{\partial}{\partial h_2} \frac{\mathcal{W}}{V} \Big|_z. \quad (5.33)$$

We use the fact that

$$\frac{\partial h_1}{\partial \kappa} \Big|_z = \frac{N_t}{\kappa} h_1 \quad (5.34)$$

to see that the first part of EQ (5.33) is

$$-\frac{1}{aN_t} a \frac{\partial \kappa}{\partial a} \frac{\partial h_1}{\partial \kappa} \frac{\partial}{\partial h_1} \frac{\mathcal{W}}{V} \Big|_z = -\frac{1}{a} \frac{\partial \kappa}{\partial a} h_1 \frac{\partial}{\partial h_1} \frac{\mathcal{W}}{V} = -3 \frac{1}{a} \frac{\partial \kappa}{\partial a} n_B \quad (5.35)$$

after inserting the definition of n_B . Using that to first order in κ , $\frac{\partial \kappa}{\partial a} \sim -\kappa \frac{m_B}{3}$, we notice the first term to be somehow related to the rest energy of the system. We subtract this shift from the energy density, and the resulting quantity should give a good estimate for the binding energy of the system at low temperatures where thermal fluctuations are suppressed. We define the dimensionless ratio of the binding energy density to the rest energy to be

$$\epsilon = \frac{e - m_{B,\text{eff}} n_B}{m_{B,\text{eff}} n_B}, \quad (5.36)$$

where

$$m_{B,\text{eff}} = -3 \frac{1}{\kappa} \frac{\partial \kappa}{\partial a}. \quad (5.37)$$

We plot the effective baryon mass vs the real baryon mass in the strong coupling limit for different values of κ in FIGURE 5.1, and see that they mostly agree all the way to κ_{crit} ,

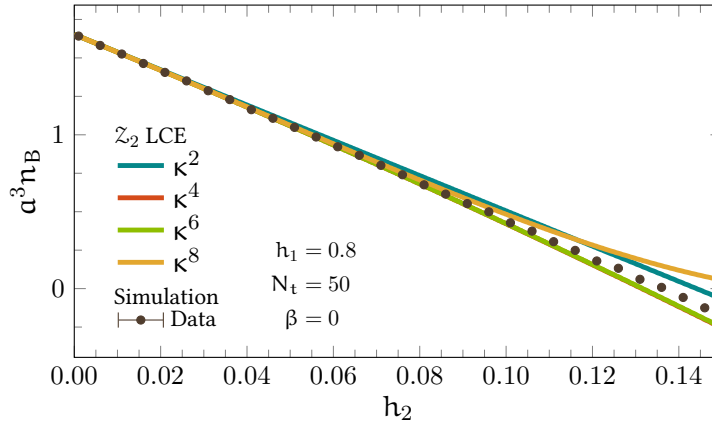


Figure 5.2.: Convergence of LCE carried out on the LO effective theory \mathcal{Z}_2 , compared to numerical data for the same parameters.

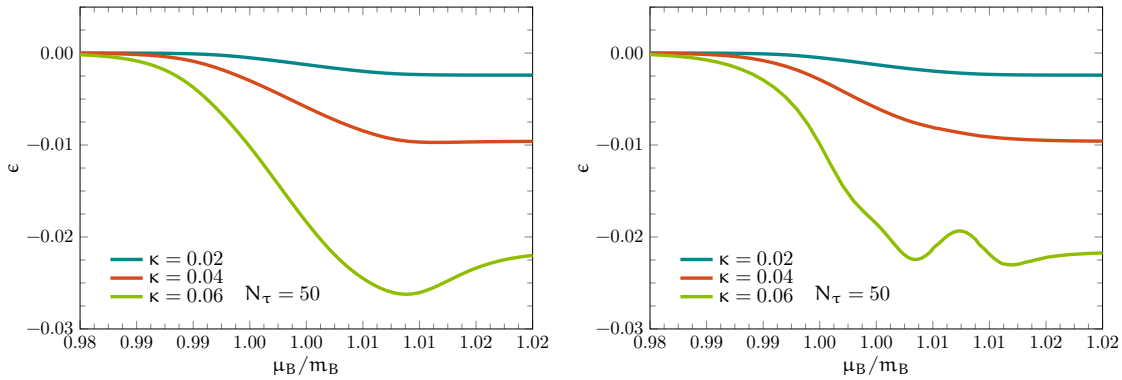


Figure 5.3.: Binding energy ϵ for three different values of κ with the $\mathcal{O}(\kappa^2)$ LCE of \mathcal{Z}_2 on the left and $\mathcal{O}(\kappa^8)$ LCE of \mathcal{Z}_2 on the right.

which is far enough from the parameter range in this study for the two to be interchangeable.

FIGURE 5.2 shows the baryon number density in the strong coupling limit at varying coupling parameter h_2 . This can be used to test the convergence of the expansion, similar to what we did in CHAPTER 4 with FIGURE 4.10 (left). We see that the higher order linked cluster contribution has a small effect on the convergence, and that it agrees with the results from the simulations.

At this point, a note on the multi level expansions is in order. Using the methods outlined in CHAPTER 4, we compute the effective theory to some order in the expansion parameters κ and u . This defines a unique system with a unique action, which can then be simulated with Monte Carlo or Langevin algorithms. Another alternative is to analyse the partition function at the given expansion order and determine the new expansion parameters (in this case h_2). A second expansion can then be carried out to evaluate this specific system order by order in the expansion parameter. If the simulation converges to the correct result it is expected to reproduce the full (all orders) linked cluster expansion result of the effective theory at a given order.

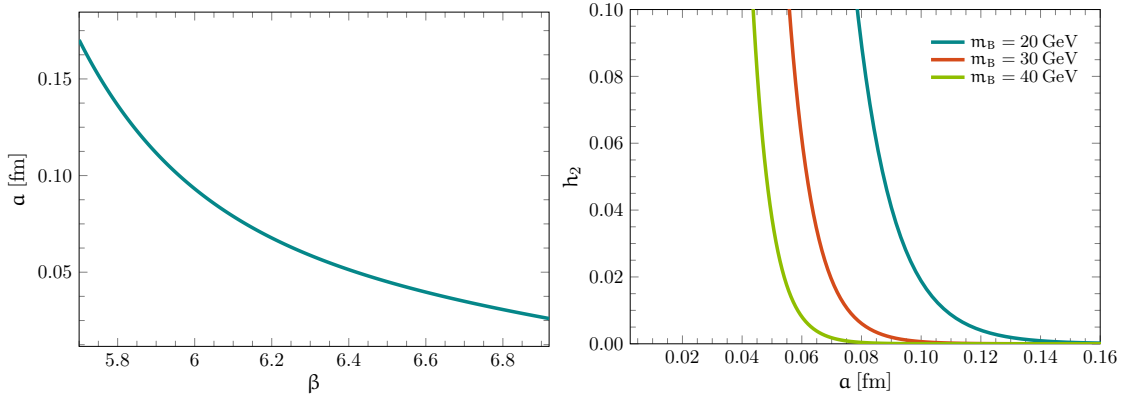


Figure 5.4.: Left: The scale range accessible to the Necco-Sommer interpolation formula for strong coupling QCD. Right: The effective nearest neighbour coupling h_2 as a function of the lattice spacing keeping m_B fixed at $T = 10$ MeV.

Finally, we plot the binding energy ratio ϵ as a function of the chemical potential for various values of κ in FIGURE 5.3. We see that the binding energy decreases together with the constituent quark masses (increased κ), which is what one would expect. The plot on the left is to leading order in h_2 , while the plot on the right shows the fourth order, h_2^4 , of the expansion. The higher order solution shows interesting behaviour at higher values of κ as we pass the $\mu_B/m_B = 1$ line. It is however beyond convergence, and we need more orders in the effective theory before we can say anything about the behaviour at higher chemical potential.

5.2.1 Scale setting and the continuum limit

Until now we have only considered observables at finite lattice spacing, and these observables have always been computed as dimensionless ratios of the, thus far unspecified, lattice spacing. However, for us to be able to make any connections to other fields, we first have to determine the physical scale of the problem. As outlined in SECTION 2.6, we need to determine the scale generated by the regulator a . One way to do this is to analyse the static potential and link the curvature of this potential to the characteristic length scale of QCD interactions (the so called *Sommer parameter* [Sommer, 1994]). In this way we can determine a function $a(\beta, \kappa)$ that encodes the scale information. We assume that the heavy quarks have little influence on the running of the coupling, and so for small κ we assume $a(\beta, \kappa) \approx a(\beta)$. We make use of the interpolation formula for $a(\beta)$ [Necco and Sommer, 2002]

$$a = r_0 \exp(-1.6804 - 1.7331(\beta - 6) + 0.7849(\beta - 6)^2 - 0.4428(\beta - 6)^3),$$

for $\beta \in [5.7, 6.29]$, (5.38)

using the Sommer parameter $r_0 = 0.5$ fm. The interpolation formula is plotted in FIGURE 5.4 (left).

With respect to the continuum limit, it is important to alter the variables in such a way that the physical system remains unchanged, in other words move along curves of constant physics. Analogous to how we defined the energy density by taking the

β	a [fm]	N_t	κ	β	a [fm]	N_t	κ
5.70	0.170	116	0.000089	6.00	0.093	212	0.004419
5.75	0.152	130	0.000224	6.05	0.086	231	0.006488
5.80	0.136	145	0.000491	6.10	0.077	250	0.009100
5.85	0.123	160	0.000964	6.15	0.073	270	0.012278
5.90	0.112	177	0.001724	6.20	0.068	291	0.016030
5.95	0.102	194	0.002851	6.25	0.063	313	0.020348

Table 5.2.: Tabulated values of the parameters of interest for the continuum study, computed at $T = 10$ MeV and $m_B = 30$ GeV.

a derivative in such a way that m_B remained constant, we now vary the parameters $\kappa(a), \beta(a), N_t(a)$ in such a way that $\partial_a m_B = 0$ and $\partial_a T = 0$. Some of the values at different lattice spacings are shown in TABLE 5.2, where we have fixed the baryon mass at 30 GeV. We observe that moving towards the continuum limit not only increases the hopping parameter, but also increases the number of temporal slices needed to fix the temperature. These two effects combine when computing the effective coupling constant $h_2 = \kappa^2 N_t / N_c$, as is clearly shown in FIGURE 5.4 (right).

Finally, we demonstrate how the continuum limit is approached. We first compute the desired observable at multiple values for β , whose upper limit is determined by the convergence limit of our theory. For instance the convergence plot FIGURE 4.10 (left) tells us that $h_2 \lesssim 0.04$ for \mathcal{Z}_2 if we demand at most 10% deviation. If we fix $m_B = 30$ GeV and $T = 10$ MeV, we find an upper limit for $\beta \lesssim 6.02$. Afterwards, the scaling of the observable with respect to the lattice spacing is analysed

$$O_{\text{lattice}} = O_{\text{continuum}} + O_1 a + O_2 a^2 + \mathcal{O}(a^3). \quad (5.39)$$

As the expansion is based on unimproved Wilson fermions, the lattice spacing corrections enter already at the linear level. We somewhat conservatively assume that we still have $\mathcal{O}(a^2)$ remnants in the observables. The observables are then fitted to the quadratic function, and the continuum limit results are extracted from an extrapolation to $a = 0$. The fit is carried out with two sets of data points, which are chosen based on the observable and the value for μ . A common choice here is $\Delta\beta = 0.01$ and then using the final 10 and 6 points respectively for the two fits. One then averages over the two values, and takes the difference as an error estimate for the systematic error. The importance of a data point for the fit is weighted by the difference in the computed observable at a fixed lattice spacing for two consecutive orders. The fitting procedure is illustrated in FIGURE 5.5 (left). In the right hand plot is the continuum extrapolated baryon number density of the \mathcal{Z}_2 partition function expanded to four bonds using the linked cluster expansion.

5.3 LINKED CLUSTER EXPANSION FOR POLYMER INTERACTIONS

Before we can apply the cluster expansion formalism to the full $\mathcal{O}(u^5 \kappa^8)$ effective action, we must be able to handle interactions more complicated than two-point couplings. In this section we develop a new method for our tool belt to handle polymer interactions

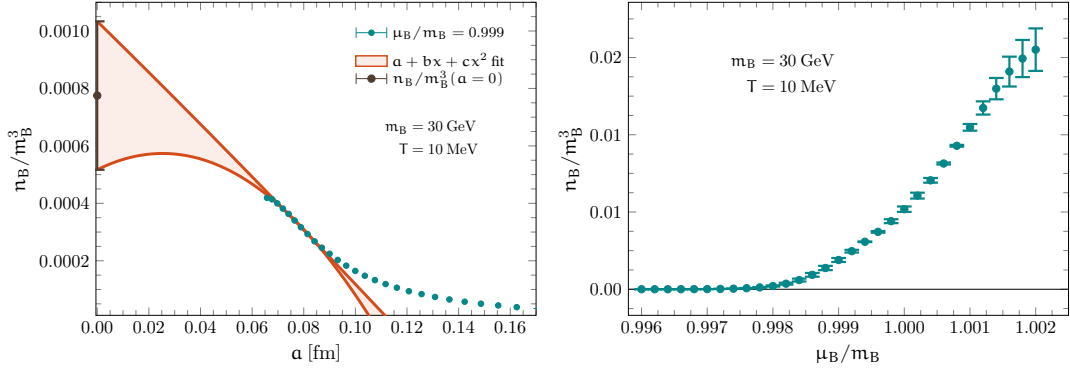


Figure 5.5.: Left: Plot demonstrating the continuum limit which is taken at the smallest accessible lattice spacing extrapolated with two different data sets. Right: The continuum limit of n_B/m_B^3 for the LO effective theory to four bond LCE.

with the linked cluster formalism. We then establish the necessary mappings and apply it to the higher order effective theories.

5.3.1 Generalisation of the LCE to polymer interactions

We start with a generalised partition function for n component fields ϕ_i

$$\mathcal{Z} = \int [d\phi_i] \exp \left(-S_0[\phi_i] + \frac{1}{2!} \sum_{x,y} \sum_{i,j} v_{ij}(x,y) \phi_i(x) \phi_j(y) + \frac{1}{3!} \sum_{x,y,z} \sum_{i,j,k} u_{ijk}(x,y,z) \phi_i(x) \phi_j(y) \phi_k(z) + \dots \right). \quad (5.40)$$

We introduce sources J_i similarly to how they were introduced in SECTION 5.1.1. This gives us a linked cluster expansion for the grand canonical potential

$$\mathcal{W}[v, u] = \left[\exp \left(\frac{1}{2!} \sum_{x,y} \sum_{i,j} v_{ij}(x,y) \frac{\delta}{\delta \tilde{v}_{ij}(x,y)} \right) \times \exp \left(\frac{1}{3!} \sum_{x,y,z} \sum_{i,j,k} u_{ijk}(x,y,z) \frac{\delta}{\delta \tilde{u}_{ijk}(x,y,z)} \right) \dots \right] \mathcal{W}[\tilde{v}, \tilde{u}] \Big|_{\substack{\tilde{v}=0 \\ \tilde{u}=0 \\ \dots}}. \quad (5.41)$$

The derivative with respect to the three-point coupling u can be expressed in terms of derivatives w.r.t. the sources

$$\frac{\delta \mathcal{W}}{\delta u_{ijk}(x,y,z)} = \frac{\delta^3 \mathcal{W}}{\delta J_i(x) \delta J_j(y) \delta J_k(z)} + \frac{\delta \mathcal{W}}{\delta J_i(x)} \frac{\delta^2 \mathcal{W}}{\delta J_j(y) \delta J_k(z)} + \frac{\delta \mathcal{W}}{\delta J_j(y)} \frac{\delta^2 \mathcal{W}}{\delta J_i(x) \delta J_k(z)} + \frac{\delta \mathcal{W}}{\delta J_k(z)} \frac{\delta^2 \mathcal{W}}{\delta J_i(x) \delta J_j(y)} + \frac{\delta \mathcal{W}}{\delta J_i(x)} \frac{\delta \mathcal{W}}{\delta J_j(y)} \frac{\delta \mathcal{W}}{\delta J_k(z)}, \quad (5.42)$$

the same is also true for all the higher n -point interactions. To $\mathcal{O}(v^2, u)$ (two bonds) we get

$$\begin{aligned}
 \mathcal{W}[v, u] = & \mathcal{W}[0] + \frac{1}{2} \sum M_i(x) v_{ij}(x, y) M_j(y) + \frac{1}{4} \sum M_{ij}(x) v_{ik}(x, y) v_{jl}(x, y) M_{jl}(y) \\
 & + \frac{1}{2} \sum M_i(x) v_{ij}(x, y) M_{jk}(y) v_{kl}(y, z) M_l(z) \\
 & + \frac{1}{3!} \sum u_{ijk}(x, y, z) M_i(x) M_j(y) M_k(z) \\
 & + \frac{1}{2} \sum u_{ijk}(x, y, y) M_i(x) M_{jk}(y) + \dots \quad (5.43)
 \end{aligned}$$

where the sums have been shortened for the sake of brevity, and we have assumed that the three-point coupling is cyclic. Just as with the two-point LCE, one can systematically carry out the linked cluster expansion, rewriting the derivatives in the couplings $\{v, u, \dots\}$ order by order and evaluate \mathcal{W} . A graphical method is however desired, as it would greatly benefit the expansion. To do this we need to further specify the geometry of the three-point interaction. One natural choice that is compatible with the already defined nearest neighbour interaction v , is a set of two nearest neighbour interactions

$$u(x, y, z) = \begin{cases} u & \text{if } \langle x, y \rangle \text{ and } \langle y, z \rangle \text{ are nearest neighbours,} \\ u & \text{if } \langle x, y \rangle \text{ and } \langle x, z \rangle \text{ are nearest neighbours,} \\ u & \text{if } \langle x, z \rangle \text{ and } \langle y, z \rangle \text{ are nearest neighbours,} \\ 0 & \text{else,} \end{cases} \quad (5.44)$$

where we have reverted to the one-components fields for simplicity. Using this definition for u , \mathcal{W} evaluates to

$$\begin{aligned}
 \mathcal{W}[v, u] = & NM_0 + \frac{q}{2} v NM_1^2 + \frac{q^2}{2} v^2 NM_1^2 M_2 \\
 & + \frac{q}{4} v^2 NM_2^2 + \frac{q^2}{2} u NM_1^3 + \frac{q}{2} u NM_1 M_2 + \dots \quad (5.45)
 \end{aligned}$$

The above expression can be represented graphically as

$$\mathcal{W}[v] = \bullet + \frac{1}{2} \text{---} \text{---} + \frac{1}{2} \text{---} \text{---} + \frac{1}{4} \text{---} \text{---} + \frac{1}{2} \text{---} \text{---} + \frac{1}{2} \text{---} \text{---} + \dots, \quad (5.46)$$

where the v bonds are coloured blue and the u bond pair red. The nodes are represented by concentric circles, where every additional node from a base interaction adds an additional circle of appropriate colour. This is necessary to distinguish e.g. the nodes in the final term. An alternative three-point coupling could be a triangular nearest neighbour coupling

$$u(x, y, z) = \begin{cases} u & \text{if } \langle x, y \rangle, \langle y, z \rangle, \text{ and } \langle x, z \rangle \text{ are nearest neighbours,} \\ 0 & \text{else,} \end{cases} \quad (5.47)$$

in which case the final term in EQ (5.46) would be excluded, given that it is not geometrically realisable. It would actually be better to represent this particular version of the three-point interaction with a three bond diagram

$$\text{---} \text{---} \text{---} \quad (5.48)$$

as the bonds are intended to encode the nearest neighbour restriction. Regardless of which geometry the n -point interactions have, there are numerous paths onward. One option is to compute the derivatives explicitly order by order and sum over the coordinates explicitly. Alternatively one can write down all mixed graphs that respect the chosen geometry and compute the modified symmetry factor. For instance we see that the two bond nearest neighbour graph for the v and u interactions

$$\frac{1}{4} \begin{array}{c} \circ \\ | \\ \circ \end{array}, \quad \frac{1}{2} \begin{array}{c} \circ \\ \diagup \diagdown \\ \circ \end{array} \quad (5.49)$$

have different symmetry factors since the node relabelling symmetry is broken. A third alternative, and the one we will focus on, is through a second embedding step

Rule 5.2. *Grand canonical potential \mathcal{W} for n point interactions*

1. *Represent the geometry of the n -point interaction $v_n(x_{n_1}, x_{n_2}, \dots, x_{n_n})$ as a graph according to DEFINITION 5.1.*
2. *Construct all graphs with the necessary number of bonds and geometry to the desired order (we refer to these as skeleton graphs).*
3. *Embed all n -point interaction graphs onto the skeleton graphs.*
4. *For every embedded n -point graph that visits $x_{n_1}, x_{n_2}, \dots, x_{n_n}$, add a factor $v_n(x_{n_1}, x_{n_2}, \dots, x_{n_n})$.*
5. *For every vertex with modified valence⁽²⁾ p , add a factor $M_p(x_i)$.*
6. *The correct symmetry factor will be the symmetry factor of the skeleton graph times the number of unique isomorphic embeddings.*

Let us consider the embedding of a v -link and a u -"wedge" from EQ (5.44) on the three bond graph

$$\frac{1}{2} \begin{array}{c} \bullet \\ \diagup \diagdown \\ \bullet \end{array} \quad (5.50)$$

This can be done in four different ways

$$\frac{1}{2} \begin{array}{c} \circ \\ \diagup \diagdown \\ \circ \end{array} + \frac{1}{2} \begin{array}{c} \circ \\ \diagdown \diagup \\ \circ \end{array} + \frac{1}{2} \begin{array}{c} \circ \\ \diagup \diagdown \\ \circ \end{array} + \frac{1}{2} \begin{array}{c} \circ \\ \diagdown \diagup \\ \circ \end{array} \quad (5.51)$$

where the first two are isomorphic and can be collected in one term. Hence there are three unique embeddings of this combination onto the skeleton graph, of which one has a non-unit embedding number, and thus a modified symmetry factor. With these two ingredients we present the full three bond free energy

$$\begin{aligned} \mathcal{W}[v] = & \bullet + \frac{1}{2} \begin{array}{c} | \\ | \\ | \end{array} + \frac{1}{2} \begin{array}{c} \diagup \diagdown \\ \diagdown \diagup \end{array} + \frac{1}{4} \begin{array}{c} \circ \\ | \\ \circ \end{array} + \frac{1}{2} \begin{array}{c} \diagup \diagdown \\ \diagdown \diagup \end{array} + \frac{1}{2} \begin{array}{c} \circ \\ \diagup \diagdown \\ \circ \end{array} + \frac{1}{3!} \begin{array}{c} \circ \\ \diagup \diagdown \\ \circ \end{array} \\ & + \frac{1}{2} \begin{array}{c} \circ \\ \diagdown \diagup \\ \circ \end{array} + \frac{1}{6} \begin{array}{c} \circ \\ \diagup \diagdown \\ \circ \end{array} + \frac{1}{2} \begin{array}{c} \circ \\ \diagup \diagdown \\ \circ \end{array} + \frac{1}{2 \times 3!} \begin{array}{c} \circ \\ \diagup \diagdown \\ \circ \end{array} + \frac{1}{2} \begin{array}{c} \circ \\ \diagdown \diagup \\ \circ \end{array} \\ & + \begin{array}{c} \diagup \diagdown \\ \diagdown \diagup \end{array} + \frac{1}{2} \begin{array}{c} \circ \\ \diagup \diagdown \\ \circ \end{array} + \frac{1}{2} \begin{array}{c} \circ \\ \diagdown \diagup \\ \circ \end{array} + \frac{1}{2} \begin{array}{c} \circ \\ \diagup \diagdown \\ \circ \end{array} + \frac{1}{2} \begin{array}{c} \circ \\ \diagdown \diagup \\ \circ \end{array} + \dots \quad (5.52) \end{aligned}$$

⁽²⁾Modified valence is the number of bonds entering a vertex originating from *different* n -point interactions.

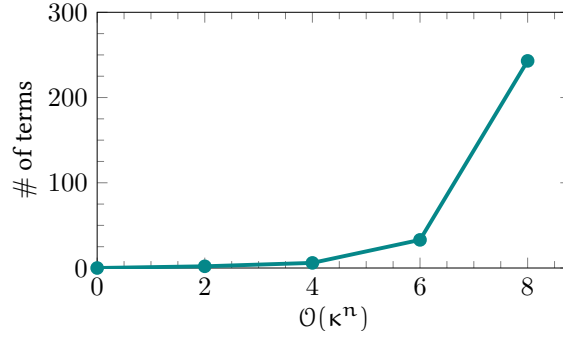


Figure 5.6.: Number of analytic terms from the LCE of the effective theory

5.3.2 Application to the effective theory, graph embeddings

Once more, we will compare the effective theory partition function to the one of the LCE and create a correspondence. We will increase the order of the effective theory by one, working with \mathcal{Z}_4 . The method is easily generalisable, and the \mathcal{Z}_8 effective theory partition function has been considered for the upcoming result. The $\mathcal{O}(\kappa^4)$ partition function is

$$\begin{aligned} \mathcal{Z}_4 = \int [d\mathbf{U}]_0 \det \mathbf{Q}_{\text{stat}}^{\mathbf{N}_f} \exp \left(-2h_2 \mathbf{N}_f \sum_{\langle x, y \rangle} W_{11}(x) W_{11}(y) \right. \\ \left. + 2h_2^2 \mathbf{N}_f \sum_{\langle x, y \rangle} \sum_{\langle y, z \rangle} W_{11}(x) W_{21}(y) W_{11}(z) + 2h_2^2 \mathbf{N}_f^2 \sum_{\langle x, y \rangle} W_{21}(x) W_{21}(y) \right). \end{aligned} \quad (5.53)$$

The correspondence is now between the two component field ϕ_i in the following manner

$$\phi_i \Leftrightarrow (W_{11}, W_{21})_i, \quad e^{-S_0[\phi]} \Leftrightarrow \mathcal{J}(\mathbf{U}_0, W_{11}, W_{21}) \det \mathbf{Q}_{\text{stat}}^{\mathbf{N}_f}. \quad (5.54)$$

The two and three-point interactions are given by

$$v_{ij}(x, y) = \delta(\langle x, y \rangle) \begin{pmatrix} -2h_2 \mathbf{N}_f & 0 \\ 0 & 2h_2^2 \mathbf{N}_f^2 \end{pmatrix}_{ij} \quad (5.55)$$

and

$$u_{1jk}(x, y, z) = 2h_2^2 \mathbf{N}_f \begin{pmatrix} 0 & \delta(\langle x, z \rangle) \delta(\langle y, z \rangle) \\ \delta(\langle x, y \rangle) \delta(\langle y, z \rangle) & 0 \end{pmatrix}_{jk}, \quad (5.56)$$

$$u_{2jk}(x, y, z) = 2h_2^2 \mathbf{N}_f \begin{pmatrix} \delta(\langle x, y \rangle) \delta(\langle x, z \rangle) & 0 \\ 0 & 0 \end{pmatrix}_{jk}. \quad (5.57)$$

At \mathcal{Z}_6 we see that we have to expand the set of fields to four, $\phi_i \Leftrightarrow (W_{11}, W_{21}, W_{31}, W_{32})_i$, which would result in the following two-point interaction matrix

$$v_{ij}(x, y) = \delta(\langle x, y \rangle) \begin{pmatrix} -2h_2 \mathbf{N}_f & 0 & 0 & 0 \\ 0 & 2h_2^2 \mathbf{N}_f^2 & 0 & 0 \\ 0 & 0 & -\frac{1}{3} h_2^3 \mathbf{N}_f^3 & \frac{4}{3} h_2^3 \mathbf{N}_f^3 \\ 0 & 0 & \frac{4}{3} h_2^3 \mathbf{N}_f^3 & -\frac{1}{3} h_2^3 \mathbf{N}_f^3 \end{pmatrix}_{ij}. \quad (5.58)$$

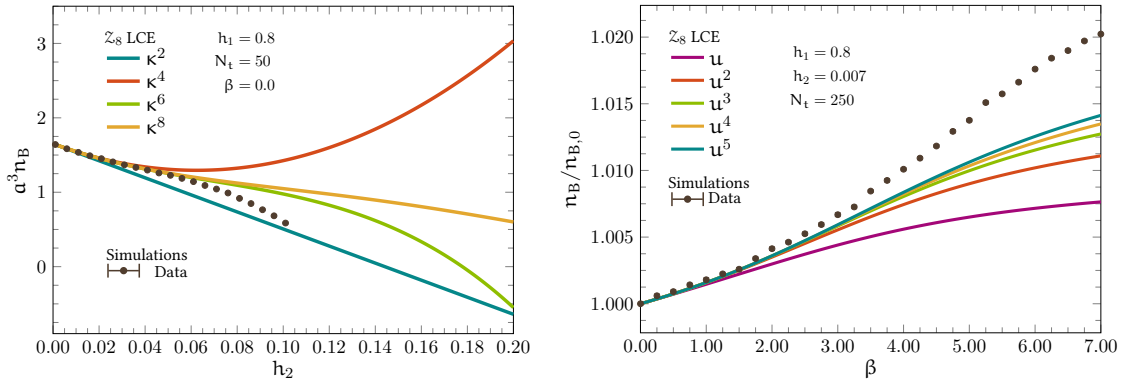


Figure 5.7.: Convergence of the analytic expressions in h_2 (left) and β (right) overlaid with the simulation results at highest order. The normalised baryon number density has been used in the right plot.

The other n -point functions are too long to list. The computation of the analytic formula for \mathcal{W} has been carried out using all three methods outlined above (calculating derivatives, computing graphs directly as well as using the embedding method). This was done to verify the result. The number of terms contributing to the analytic function describing \mathcal{Z}_{QCD} at a given order in our expansion scheme is plotted in FIGURE 5.6, and we see once more that the number of terms grows exponentially with increasing order. Pushing this to higher order would require the development software to carry out the graphical combinatorics. This would be a similar task e.g. to the one undertaken by Lüscher and Weisz in their groundbreaking work on the $\lambda\phi^4$ lattice theory [Lüscher and Weisz, 1988, 1989] where they carried out a LCE to 14th order, and showed the triviality of the theory. One should however note the added difficulty due to the additional polymer interaction, and the geometry. For instance, the four bond LCE on a square lattice gives 17 graphs, while our effective theory has 243 graphs at the four bond level.

5.3.3 Results

We are now in a position where we can evaluate thermodynamic functions fully analytically. Using the LCE we have computed the grand canonical partition function in the thermodynamic limit through $\mathcal{O}(\kappa^8 u^5)$ to first order in N_t^{-1} . We first compare the convergence of the theory in the two parameters to that obtained through simulating the effective theory. The convergence in the nearest neighbour effective coupling, h_2 , is shown in FIGURE 5.7 (left). Comparing it to FIGURE 4.10 (left), we see that the analytic convergence range matches that of the simulated data and shows good quantitative agreement. FIGURE 5.7 (right) shows the corresponding convergence plot in the strong coupling parameter β . We see that the analytic computation underestimates the strong coupling contributions. One should however note the axis scales, that the finite coupling corrections are much smaller than the corrections in κ , and that the main contribution of finite β ultimately appears indirectly through a rescaling of the system.

Next we explore the convergence properties of the theory as we move towards lighter quarks and smaller lattice spacings. FIGURE 5.8 shows the baryon number density at ever smaller lattice spacings. The error bars are estimates of the systematic error, computed as the difference between two subsequent orders in the expansion. The first observation

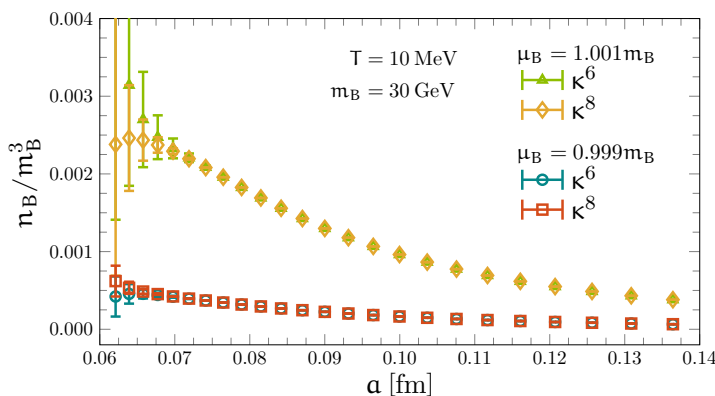


Figure 5.8.: Convergence of the baryon number density at smaller and smaller lattice spacings. Shows similar limitations to the extrapolation plot of the \mathbb{Z}_2 theory in FIGURE 5.5 (left).

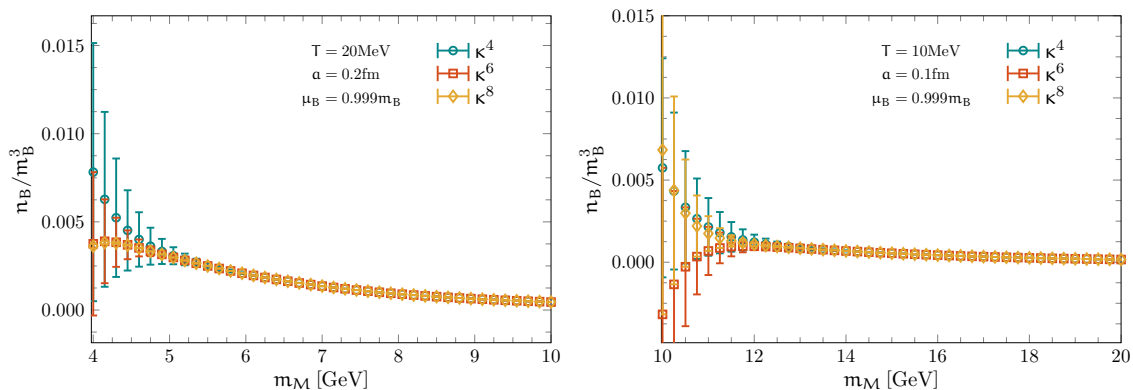


Figure 5.9.: Order by order convergence as a function of the meson mass of the system exposing the heavy quark limits of the system. Left plot at $T = 20$ MeV and $a = 0.2$ fm, right plot at $T = 10$ MeV and $a = 0.1$ fm.

is that at conservative quark masses of ~ 10 GeV, the continuum extrapolation is limited by extrapolation from data taken at ~ 0.07 fm. However, we note that the convergence improves at higher orders of the expansion in all cases, demonstrating the stability of the expansion. The second observation is that convergence is worse at higher chemical potential. This, combined with the fact that the slope increases, makes accessing the denser systems more difficult. This is a manifestation of fermion saturation on the lattice, as was discussed in SECTION 3.4.1.

FIGURE 5.9 shows the convergence of the different orders of the expansion at varying meson mass at fixed temperature and lattice spacing. This plot demonstrates the difficulty the effective theory has in reaching smaller quark masses. Although higher orders do indeed help the convergence, we see that the effect of two more orders is small compared to the relevant scales of the problem. We can therefore not envision an extension to smaller quark masses through brute force order by order computations.

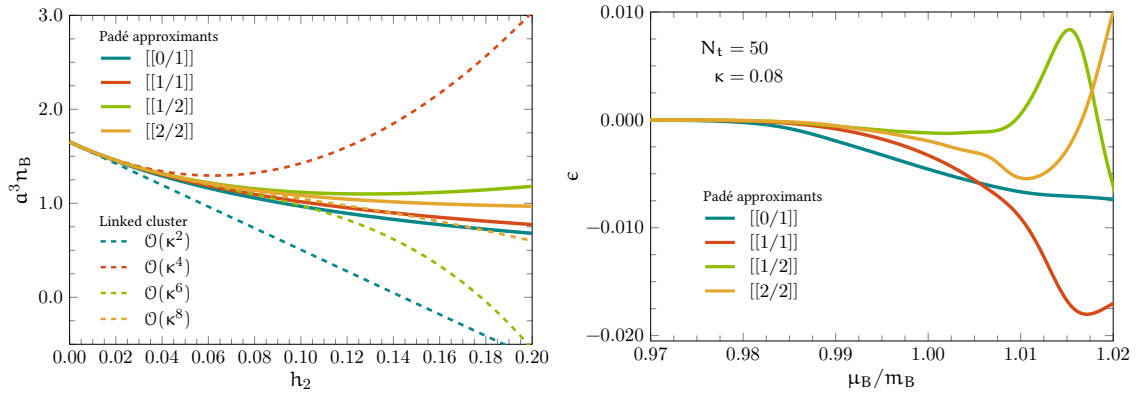


Figure 5.10.: Results from the Padé approximants. Left: Convergence plot at strong coupling compared to the normal series from the LCE. Right: The nucleon binding energy as a function of chemical potential at different orders.

5.3.4 Padé approximants

An alternative, but very powerful tool for series analyses is the *Padé approximants*. It is simply a reordering of the power series into a rational expression

$$[L/M](z) = \frac{a_0 + a_1 z + \dots + a_L z^L}{b_0 + b_1 z + \dots + b_M z^M}, \quad (5.59)$$

so that its Maclaurin series agrees with the original series to $(L + M)^{\text{th}}$ order

$$\sum_{i=0}^{L+M} c_i z^i = [L/M](z) + \mathcal{O}(z^{L+M+1}). \quad (5.60)$$

An extensive introduction to Padé approximants, their uses and properties can be found in [Baker and Graves-Morris, 1996]. If the approximants are well defined, they tend to show better convergence properties than their corresponding Maclaurin series. If one considers a long enough series it is also possible to use the Padé formulation to analyse critical points and non-analyticities of the theory. One should however be careful, as the Padé series will pick up both the real physical singularities as well as artificial singularities due to the fractional nature of the expression. To resolve this one can e.g. study the different Padé approximants, as the L-M ratio can be set freely. It is however known that the diagonals ($[[L/L]]$ and $[[L - 1/L]]$) possess various favourable properties [Gaunt and Guttman, 1974; Guttman, 1989, and references therein].

In our case the Padé variable is h_2 , and the highest order is $L + M = 4$. After discarding the approximants with artificial singularities, we can compare the convergence to that of the Maclaurin series. This is shown in FIGURE 5.10 (left) where we have once more used the baryon number density to investigate convergence. We see that the order by order convergence rate of the Padé approximants is far superior to that of the pure linked cluster expansion, as expected.

Finally we plot the binding energy per nucleon, ϵ , as defined in EQ (5.36) with the Padé series in FIGURE 5.10 (right). We observe that this quantity displays the *silver blaze* problem, namely that it is zero up until onset transition, where it in this case becomes

negative, as demonstrated in [Langelage et al., 2014]. With the fourth order Padé, we can extend the study to higher densities. Although the quantitative convergence breaks down shortly after the onset transition near $\mu_B \approx m_B$, we see new qualitative behaviour. At higher orders the binding energy has a minimum and reaches a positive value at growing chemical potential, as expected from nuclear physics. This means that we have a qualitative bulk nuclear density, whose quantitative value is still unsettled by the present study.

We refrain from analysing any more results until we have introduced a final improvement to the analytic approach.

5.4 ANALYTIC RESUMMATION

So far we have managed to analytically calculate the grand canonical potential of the effective theory to the same order as the effective theory itself, and thus obtained the thermodynamic quantities analytically. Although this in of itself is both useful due to the permanence of the results, as well as the additional mathematical insight into the theory it admits, we have merely reproduced the simulated results. In this section, further improvements to the theory will be analysed, which will push the analytic evaluation beyond that of the numerically obtained ones. We start by introducing a resummation scheme on the level of the effective theory in SECTION 5.4.1. We then proceed to a resummation on the cluster expansion level in SECTION 5.4.2. Finally, in SECTION 5.4.3, we will review a second hypothetical resummation, again on the level of the effective theory.

5.4.1 Chain resummation

We start with an example. Consider the following four terms from the effective action EQ (4.99)

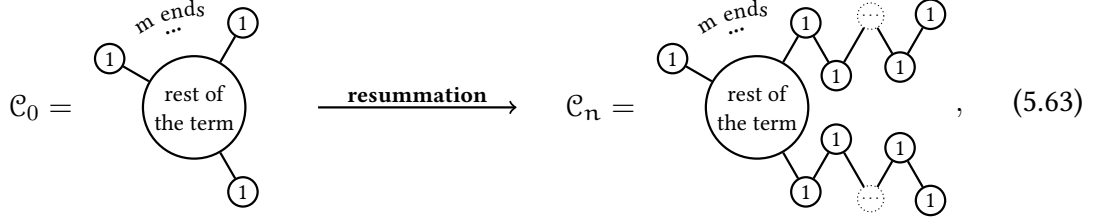
$$h_2 N_f \sum_{\text{dof}} \begin{array}{c} \textcircled{1} \\ | \\ \textcircled{1} \end{array}, -h_2^2 N_f \sum_{\text{dof}} \begin{array}{c} \textcircled{1} \\ / \quad \backslash \\ \textcircled{1} \quad \textcircled{1} \end{array}, h_2^3 N_f \sum_{\text{dof}} \begin{array}{c} \textcircled{1} \quad \textcircled{1} \\ / \quad \backslash \\ \textcircled{1} \quad \textcircled{1} \end{array}, -h_2^4 N_f \sum_{\text{dof}} \begin{array}{c} \textcircled{1} \quad \textcircled{1} \\ / \quad \backslash \\ \textcircled{1} \quad \textcircled{1} \quad \textcircled{1} \end{array}. \quad (5.61)$$

It is clear that these four terms follow a common pattern that generates a chain. Each of the terms above extend the chain by one node while maintaining a common prefactor. By studying the mathematically equivalent formulation, we observe that every new link in the chain contributes a factor $h_2 W_{21}$ to the term, in addition to the necessary spatial geometry. One can check the other terms in the κ^8 action, e.g.

$$2h_2^3 N_f^2 \sum_{\text{dof}} \left(\begin{array}{c} \textcircled{1} \\ / \quad \backslash \\ \textcircled{1} \quad \textcircled{1} \end{array} - \begin{array}{c} \textcircled{2} \\ / \quad \backslash \\ \textcircled{1} \quad \textcircled{1} \end{array} \right), -2h_2^4 N_f^2 \sum_{\text{dof}} \left(\begin{array}{c} \textcircled{1} \quad \textcircled{1} \\ / \quad \backslash \\ \textcircled{1} \quad \textcircled{1} \end{array} - \begin{array}{c} \textcircled{2} \quad \textcircled{1} \\ / \quad \backslash \\ \textcircled{1} \quad \textcircled{1} \end{array} \right), \quad (5.62)$$

all follow this pattern. The conjecture is then that every singly connected node, namely every factor W_{11} , can be extended to a chain of arbitrary length, and that these terms will appear in a predictable form at higher orders. The chain resummation can schematically

be represented as



$$\mathcal{C}_0 = \text{rest of the term} \xrightarrow{\text{resummation}} \mathcal{C}_n = \text{rest of the term} \text{ with extended ends}, \quad (5.63)$$

in which \mathcal{C}_0 represents an arbitrary unsummed term with m singly connected nodes (*open ends*), and \mathcal{C}_n represents the same term where the m open ends have been extended a combined total of n times. We then sum over the extension n of the m open ends which results in a replacement of all open ends

$$W_{11}(x) \rightarrow W_{11}(x) \sum_{n=0}^{\infty} \mathcal{G}(\{x_n\}) \prod_{i=1}^n (-h_2) W_{21}(x_i). \quad (5.64)$$

The factor $\mathcal{G}(\{x_n\})$ represents the geometry of the chain, which we will later embed onto the polymer linked cluster expansion developed in the previous section. Before doing this, we need to review the mathematical structure of the resummation, as well as its origin.

Combinatorial analysis

We already introduced the combinatorics of the cold and dense regime in SECTION 4.8.1, upon which we will build in this section. First, we need to identify which terms, analysed before the spatial gauge link integrals, contribute to the chain. We will simply state the general pattern here and prove it later. We define an *open end* to consist of two consecutive hops that form a pair, such as 1 1. When we earlier introduced the pairing notation, we used the sixth order single trace as an example, which can appear in three combinations (as in EQ (4.80))

$$\text{tr } 1 1 2 2 3 3, \quad \text{tr } 1 2 3 3 2 1, \quad \text{tr } 1 2 3 1 2 3. \quad (5.65)$$

The first term has three open ends, the second has two open ends (including cyclic permutations), while the final term has no open ends. An extension of the chain is obtained by inserting a new pair between the contracted PM pair of an already existing open end. Instead of the quark hopping forth and directly back again, it takes a detour through this new position

$$\dots 1 1 \longrightarrow \dots W_{11}(\vec{x}), \quad (5.66a)$$

$$\dots 1 2 2 1 \longrightarrow \dots W_{21}(\vec{x}) W_{11}(\vec{x} + i), \quad (5.66b)$$

$$\dots 1 2 3 3 2 1 \longrightarrow \dots W_{21}(\vec{x}) W_{21}(\vec{x} + i) W_{11}(\vec{x} + i + j). \quad (5.66c)$$

The prefactors of terms in this resummation can be calculated from symmetry arguments. Assume that we know the symmetry prefactor $1/g$ of a term with N open ends. Extending one of these can be done in N/g distinct ways, which all break the previous symmetry. The sum of all such insertions thus has a prefactor of N/g , which is

N times that of the base diagram. However, instead of counting the number of these permutations, one can make the observation that the problem is equivalent to distributing n indistinguishable objects to N distinguishable bins. This is done assuming that extending any of the chains give the same result. Although this is obviously not true in general, as they result in different geometric objects, when we later embed these objects onto the linked cluster expansion we will only consider the embeddings in which this discrepancy is irrelevant. In this special case, the new symmetry factor from extending a graph with a symmetry factor $1/g$ with N open ends by n links is

$$\frac{1}{g'} = \frac{1}{g} \binom{N-1+n}{n}. \quad (5.67)$$

This is also only true if we consider a *root graph*, which is any graph that does not appear as an extension to any other lower order graph. However, as long as we carry out the resummation on an order by order basis, it does not pose a problem.

With all the ingredients in place, we are ready to carry out the gauge integrals for a chain matrix, and show that the above mentioned expression does indeed appear. As argued, the chain can be express as

$$X \ 1 \ 2 \ 3 \ 4 \ \dots \ n \ n \ \dots \ 4 \ 3 \ 2 \ 1, \quad (5.68)$$

where X represents the remainder of the term, which may or may not include additional open ends, and/or chains. Since the expression has a recursive structure it is natural to define the integrated matrices G_n so that

$$\underbrace{\overbrace{1 \ 2 \ 3 \ 4 \ \dots \ n \ n \ \dots \ 4 \ 3 \ 2 \ 1}^{G_{n-1}}}_{G_n} \quad (5.69)$$

G_{n-2}

The matrix G_n is then defined in terms of G_{n-1} , which is defined in terms of G_{n-2} , and so on. In SECTION 4.8.1 we saw that the static propagator in the cold dense limit had the approximate expression EQ (4.87), meaning that the effective hopping matrices take the form

$$P_{\alpha\beta}^{ab}(\mathbf{y}, \mathbf{x}) = \kappa \left(\frac{1 + \gamma_0}{2} \right)_{\alpha\gamma} B_{\vec{x}}^{ac}(\mathbf{t}_y, \mathbf{t}_x) \sum_{i=1}^3 (1 + \gamma_i)_{\gamma\beta} U_{\vec{x},i}^{cb} \delta_{\vec{y}, \vec{x}+i} \quad (5.70)$$

$$M_{\alpha\beta}^{ab}(\mathbf{y}, \mathbf{x}) = \kappa \left(\frac{1 + \gamma_0}{2} \right)_{\alpha\gamma} B_{\vec{x}}^{ac}(\mathbf{t}_y, \mathbf{t}_x) \sum_{i=1}^3 (1 - \gamma_i)_{\gamma\beta} U_{\vec{x},i}^{\dagger,cb} \delta_{\vec{y}, \vec{x}-i} \quad (5.71)$$

where we have shortened the B^+ notation for brevity. Colour indices are denoted by Roman letters, and Dirac indices by Greek characters. We also saw in SECTION 4.8.2 that the Dirac trace is somewhat trivial. The colour matrix content that enters the integrals is thus

$$B_{\vec{x}}^{ac}(\mathbf{t}_y, \mathbf{t}_x) U_{\vec{x},i}^{cb}, \quad \text{and} \quad B_{\vec{x}}^{ac}(\mathbf{t}_y, \mathbf{t}_x) U_{\vec{x},i}^{\dagger,cb}. \quad (5.72)$$

We are now ready to evaluate the colour integrals over the matrix G_n

$$\begin{aligned}
 G_n^{\text{af}}(\mathbf{t}_1, \mathbf{t}_2; \vec{\mathbf{x}}_0) &= 2\kappa^2 \sum_{i_0, \mathbf{t}_3} \int d\mathbf{U}_{\vec{\mathbf{x}}_0, i_0}(\mathbf{t}_2) B_{\vec{\mathbf{x}}_0}^{\text{ab}}(\mathbf{t}_1, \mathbf{t}_2) \mathbf{U}_{\vec{\mathbf{x}}_0, i_0}^{\text{bc}}(\mathbf{t}_2) \\
 &\quad \times G_{n-1}^{\text{cd}}(\mathbf{t}_2, \mathbf{t}_3; \vec{\mathbf{x}}_0 + \mathbf{i}_0) B_{\vec{\mathbf{x}}_0 + \mathbf{i}_0}^{\text{de}}(\mathbf{t}_3, \mathbf{t}_2) \mathbf{U}_{\vec{\mathbf{x}}_0, i_0}^{\dagger, \text{ef}}(\mathbf{t}_2) \\
 &= \frac{2\kappa^2}{N_c} \sum_{i_0, \mathbf{t}_3} B_{\vec{\mathbf{x}}_0}^{\text{ab}}(\mathbf{t}_1, \mathbf{t}_2) G_{n-1}^{\text{cd}}(\mathbf{t}_2, \mathbf{t}_3; \vec{\mathbf{x}}_0 + \mathbf{i}) B_{\vec{\mathbf{x}}_0 + \mathbf{i}}^{\text{de}}(\mathbf{t}_3, \mathbf{t}_2) \delta_{ce} \delta_{bf} \\
 &= \frac{2\kappa^2}{N_c} \sum_{i_0, \mathbf{t}_3} B_{\vec{\mathbf{x}}_0}^{\text{af}}(\mathbf{t}_1, \mathbf{t}_2) \text{tr}_c [G_{n-1}(\mathbf{t}_2, \mathbf{t}_3; \vec{\mathbf{x}}_0 + \mathbf{i}) B_{\vec{\mathbf{x}}_0 + \mathbf{i}}(\mathbf{t}_3, \mathbf{t}_2)] . \quad (5.73)
 \end{aligned}$$

The coordinate $\vec{\mathbf{x}}_0$ is the coordinate of the beginning of the chain, and we see that we have a recursive structure for these spatial positions as we move along the chain $\vec{\mathbf{x}}_{m+1} = \vec{\mathbf{x}}_m + \mathbf{i}_m$. We use the above equation to express G_{n-1} in terms of G_{n-2}

$$G_{n-1}^{\text{ab}}(\mathbf{t}_2, \mathbf{t}_3; \vec{\mathbf{x}}_1) = \frac{2\kappa^2}{N_c} \sum_{i_1, \mathbf{t}_4} B_{\vec{\mathbf{x}}_1}^{\text{ab}}(\mathbf{t}_2, \mathbf{t}_3) \text{tr}_c [G_{n-2}(\mathbf{t}_3, \mathbf{t}_4; \vec{\mathbf{x}}_2) B_{\vec{\mathbf{x}}_2}(\mathbf{t}_4, \mathbf{t}_3)] . \quad (5.74)$$

Inserting the expression for G_{n-1} into the one for G_n , yields

$$\begin{aligned}
 G_n^{\text{af}}(\mathbf{t}_1, \mathbf{t}_2; \vec{\mathbf{x}}_0) &= \left(\frac{2\kappa^2}{N_c} \right)^2 \sum_{\mathbf{t}_3, \mathbf{t}_4} \sum_{i_0, i_1} B_{\vec{\mathbf{x}}_0}^{\text{af}}(\mathbf{t}_1, \mathbf{t}_2) \text{tr}_c [G_{n-2}(\mathbf{t}_3, \mathbf{t}_4; \vec{\mathbf{x}}_2) B_{\vec{\mathbf{x}}_2}(\mathbf{t}_4, \mathbf{t}_3)] \\
 &\quad \times \underbrace{\text{tr}_c [B_{\vec{\mathbf{x}}_1}(\mathbf{t}_2, \mathbf{t}_3) B_{\vec{\mathbf{x}}_1}(\mathbf{t}_3, \mathbf{t}_2)]}_{-\frac{1}{2} W_{21}(\vec{\mathbf{x}}_1)} . \quad (5.75)
 \end{aligned}$$

We see that the structure of G_n stays the same after one step of the recursion, except for a factor of W_{21} as well as sums over new degrees of freedom. The recursion ends at G_1 , which is the open end of the chain, given by a consecutive, paired hop

$$\begin{aligned}
 G_1^{\text{ae}}(\tau_1, \tau_2; \vec{\mathbf{x}}_n) &= 2\kappa^2 \sum_{i_n} \int d\vec{\mathbf{U}}_{\vec{\mathbf{x}}_n, i_n} B_{\vec{\mathbf{x}}_n}^{\text{ab}}(\mathbf{t}_1, \mathbf{t}_2) \mathbf{U}_{\vec{\mathbf{x}}_n, i_n}^{\text{bc}}(\mathbf{t}_2) B_{\vec{\mathbf{x}}_n + \mathbf{i}}^{\text{cd}}(\mathbf{t}_2, \mathbf{t}_2) \mathbf{U}_{\vec{\mathbf{x}}_n, i_n}^{\dagger, \text{de}}(\mathbf{t}_2) \\
 &= \frac{2\kappa^2}{N_c} \sum_{i_n} B_{\vec{\mathbf{x}}_n}^{\text{ae}}(\mathbf{t}_1, \mathbf{t}_2) \underbrace{\text{tr}_c [B_{\vec{\mathbf{x}}_n + \mathbf{i}}(\mathbf{t}_2, \mathbf{t}_2)]}_{\frac{1}{2} W_{11}(\vec{\mathbf{x}}_{n+1})} . \quad (5.76)
 \end{aligned}$$

Recursively inserting the expressions for the G_m matrices yields the final result for the full chain matrix

$$\begin{aligned}
 G_n^{\text{ab}}(\mathbf{t}_1, \mathbf{t}_2; \vec{\mathbf{x}}_0) &= B_{\vec{\mathbf{x}}_0}^{\text{ab}}(\mathbf{t}_1, \mathbf{t}_2) \left(\frac{2\kappa^2}{N_c} \right)^n \sum_{\substack{\mathbf{t}_3, \mathbf{t}_4, \\ \dots, \mathbf{t}_{n+1}}} \sum_{\substack{i_0, i_1, \\ \dots, i_n}} W_{11}(\vec{\mathbf{x}}_{n+1}) \prod_{k=1}^n (-W_{21}(\vec{\mathbf{x}}_k)) \\
 &= B_{\vec{\mathbf{x}}_0}^{\text{ab}}(\mathbf{t}_1, \mathbf{t}_2) \left(\frac{2\kappa^2}{N_c} \right)^n N_t^{n-1} \sum_{\substack{i_0, i_1, \\ \dots, i_n}} W_{11}(\vec{\mathbf{x}}_{n+1}) \prod_{k=1}^n (-W_{21}(\vec{\mathbf{x}}_k)) . \quad (5.77)
 \end{aligned}$$

The sums over the temporal variables are trivially evaluated because the W_{nm} factors are time independent.

To tie it all together, let us consider a generic contribution with N open ends

$$\mathcal{C}_0 = \frac{1}{g} \text{tr} \left[G_1(t_1, t_2; \vec{x}_1) M_1 G_1(t_3, t_4; \vec{x}_2) M_2 \cdots G_1(t_{2N-1}, t_{2N}; \vec{x}_N) M_N \right], \quad (5.78)$$

where the matrices M_i are the rest of the term, comparable to the left hand side of EQ (5.63). We have only considered a single trace term here, but the analysis can easily be extended to multi trace terms, as a chain can only reside within one fermion trace. Inserting the expression for G_1 gives

$$\begin{aligned} \mathcal{C}_0 = \frac{1}{g} \text{tr} \left[B(t_1, t_2; \vec{x}_1) M_1 B(t_3, t_4; \vec{x}_2) M_2 \cdots B(t_{2N-1}, t_{2N}; \vec{x}_N) M_N \right] \\ \times \left(\frac{\kappa^2}{N_c} \right)^N \sum_{i_1, i_2, \dots, i_N} W_{1,1}(\vec{x}_1 + i_1) W_{1,1}(\vec{x}_2 + i_2) \cdots W_{1,1}(\vec{x}_N + i_N). \end{aligned} \quad (5.79)$$

We can now attach chains of length n_i to each of the N open ends so that the total length of the chain is n , corresponding to the right hand side of EQ (5.63)

$$\begin{aligned} \mathcal{C}_n = \sum_{n_1, n_2, \dots, n_N} \frac{1}{g_{\{n_i\}}} \text{tr} \left[G_{n_1+1}(t_1, t_2; \vec{x}_1) M_1 G_{n_2+1}(t_3, t_4; \vec{x}_2) M_2 \right. \\ \left. \cdots \times G_{n_N+1}(t_{2N-1}, t_{2N}; \vec{x}_N) M_N \right] \delta \left(\sum_{i=1}^N n_i - n \right). \end{aligned} \quad (5.80)$$

This gives a symmetry factor that depends on the partitioning of the attachments $\{n_i\}$. We insert the expression for G_n from EQ (5.77), which yields

$$\begin{aligned} \mathcal{C}_n = \sum_{n_1, n_2, \dots, n_N} \frac{1}{g_{\{n_i\}}} \text{tr} \left[B(t_1, t_2; \vec{x}_1) M_1 B(t_3, t_4; \vec{x}_2) M_2 \cdots B(t_{2N-1}, t_{2N}; \vec{x}_N) M_N \right] \\ \times \left(\frac{\kappa^2}{N_c} \right)^{N+n} N_t^n \sum_{\{\vec{x}_i\}} \prod_{j=1}^N W_{1,1}(\vec{x}_{j(n_j+1)}) \prod_{k=0}^{n_j} (-W_{2,1}(\vec{x}_{jk})) \delta \left(\sum_{i=1}^N n_i - n \right), \end{aligned} \quad (5.81)$$

where we have once more introduced recursive coordinate vectors $\vec{x}_{i(j+1)} = \vec{x}_{ij} + i_{ij}$ which originate from the base position $\vec{x}_{i0} \equiv \vec{x}_i$. There is a remaining sum over all geometries of the extended graphs through the variables $\{\vec{x}_i\}$ which we have to examine further. We see that the base diagram, which is explicitly left in the trace, is the same for the term with and without attachments. This is the crucial observation necessary for the correctness of the chain resummation.

Embeddings

To be able to say anything about the final sum over the chain positions we once more turn to the graph- and lattice embeddings. The snaking chain is in no way a foreign principle to the LCE, as it is the basic ingredient for cluster expansion resummation schemes, which we will analyse further in the next section. For now it is enough to know that

for every chain graph there exists a skeleton graph with the appropriate geometry. For example,

(5.82)

all have the proper geometry to have a chain embedded onto them, given that \bullet denotes a suitable *graph remainder*. Taking the sum of all valid skeleton graphs is unfortunately an impossible task, and we have to restrict the analysis to the subset of graphs we can compute. One such set is all graphs where the chain never overlaps with itself nor the graph remainder. We can thus apply this resummation scheme to all embeddings and combinations of graphs entering the full $\mathcal{O}(\kappa^8)$ polymeric linked cluster expansion. This includes direct map embeddings such as

(5.83)

embeddings where the overlap appears only in sections of the diagram to highest order,

(5.84)

and finally multi-diagram embeddings with free ends

(5.85)

We have introduced the symbol \blacklozenge to indicate a resummed open end in our diagrammatic representation. For this subset of all possible embeddings of the chain, the integrals, embedding factors and symmetry factors can be computed.

We finish the computation of the resummed graph \mathcal{C}_n with this restricted set of embeddings, and label this set \mathcal{C}_n^* . The total symmetry factor after summing over the extension partitions $\{n_i\}$ is exactly the one we argued for in EQ (5.67)

$$\sum_{n_1, n_2, \dots, n_N} \frac{1}{g_{\{n_i\}}} = \frac{1}{g} \binom{N-1+n}{n}. \quad (5.86)$$

The spatial integral over the \mathcal{C}_n^* is

$$\begin{aligned} \int [d\mathbf{U}]_{\mu} \mathcal{C}_n^* = & \frac{1}{g} \binom{N-1+n}{n} \Omega \int [d\mathbf{U}]_0 \det Q_{\text{stat}}^{N_f} \text{tr} [B_1 M_1 B_2 M_2 \cdots B_N M_N] \\ & \times \left(\frac{2d\kappa^2}{N_c} \int [d\mathbf{U}]_0 \det Q_{\text{stat}}^{N_f} W_{11} \right)^N \left(-\frac{2d\kappa^2 N_{\tau}}{N_c} \int [d\mathbf{U}]_0 \det Q_{\text{stat}}^{N_f} W_{21} \right)^n. \end{aligned} \quad (5.87)$$

Here Ω is the embedding factor of the base diagram, and every new node in the chain contributes with a lattice embedding of $(2d)$, as discussed in SECTION 5.1.1. The integrals

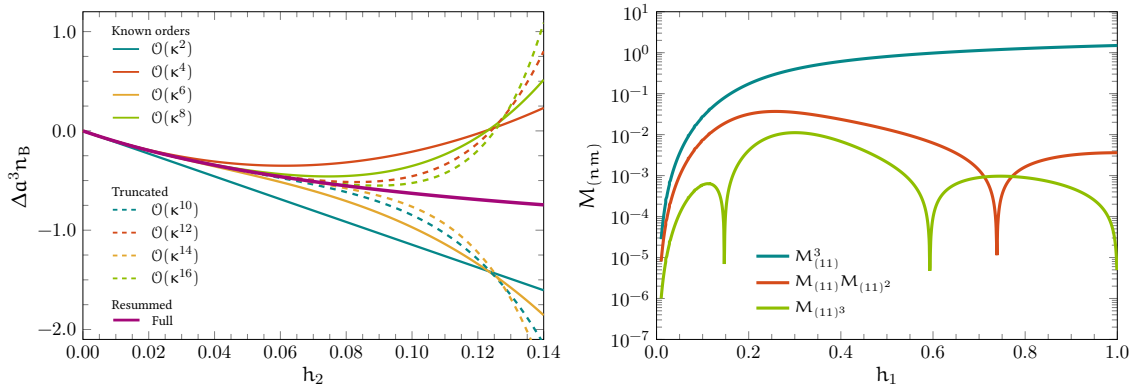


Figure 5.11.: Left: Known and predicted contributions to baryon number density for a single chain single graph embedding. Right: The M -cumulants as a function of h_1 for three different embedding types.

over W_{11} and W_{21} are nothing but the previously defined z -functions. Finally, we sum over the total length of the attachments n

$$\begin{aligned} \sum_{n=0}^{\infty} \int [dU]_{\mu} e_n^* &= \frac{1}{g} \int [dU]_{\mu} \bar{c}_0^* \left(\frac{(2d)\kappa^2}{N_c} z_{(11)} \right)^N \sum_{n=0}^{\infty} \binom{N-1+n}{n} \left(-(2d)h_2 z_{(21)} \right)^n \\ &= \frac{1}{g} \int [dU]_{\mu} \bar{c}_0^* \left(\frac{(2d)\kappa^2}{N_c} \frac{z_{(11)}}{1 + (2d)h_2 z_{(21)}} \right)^N. \end{aligned} \quad (5.88)$$

To highlight the substitution, we have extracted the open ends from the base graph \mathcal{C}_0 , and named the remainder $\bar{\mathcal{C}}_0$. This final equation proves the resummation identity in eq (5.64). At the linked cluster level we make the substitution

$$z_{(11)} \rightarrow \frac{z_{(11)}}{1 + (2d)h_2 z_{(21)}}, \quad (5.89)$$

at an order by order level, making sure we remove the appropriate higher order graphs this resummation predicts. A demonstration of the convergence power of the resummation is shown in FIGURE 5.11 (left), where we have plotted the contribution to the baryon number density of the single chain, single graph terms. We plot the full result up to the highest known order as well as higher order truncated results from the resummation formula, and the resummed result itself. We see that the different orders diverge to $\pm\infty$ at some point at increasing values of h_2 while the full resummed result stays under control.

Finally, the systematic errors introduced by the resummation need to be discussed. In the resummation scheme we chose a specific embedding for the higher order graphs while neglecting other embeddings at the same order. Due to the nature of the method of moments and cumulants this results in a slight overcounting of the number of terms as the embedding factor $(2d)^n$ will naturally include geometries that overlap with itself. One possible way to rectify this is to change the embedding factor to the correct one, given by the theory of the *Self-Avoiding Walk* [see e.g. Janse van Rensburg, 2009, for a review]. This is however not the preferred approach as it would spoil the nice properties of the cluster expansion. We rather regard the cumulants as the primitive objects of the

theory, for which the embedding factor is correct. One may then study the amplitude of the corrections appearing at the same orders as the chain elements. FIGURE 5.11 (right) shows the value of three cumulants as a function of their primary variable, h_1 . We see that the free value is, for all values of h_1 , at least one order of magnitude larger than its overlapping counterparts. This behaviour is due to the fact that the integrals

$$\int dL W_{nm}^N, \quad \text{and} \quad \left(\int dL W_{nm} \right)^N, \quad (5.90)$$

are of the same order of magnitude, resulting in cancellations in the cumulants. This gives us additional confidence in the resummation, and shows that the systematic errors are small.

5.4.2 Cluster resummation

As mentioned earlier, the idea of graph level resummation schemes has been around for the LCE since its conception [see e.g. Wortis, 1974, for a review], and the same machinery is to some extent applicable here as well. We will nonetheless choose a simpler approach to LCE resummations that complements the already incorporated chain resummation. In the previous section we analysed how to create chains on the level of the effective theory. This is however not the only way of creating chains. Instead of extending the base diagrams at the pre-integral level, one can create chains with the LCE ingredients themselves. One example is a chain consisting of nearest neighbour interactions, which can be represented graphically as



$$(5.91)$$

Further improvement is gained by mixing the two expansion schemes and extending every open end by all combinations of chain segments resulting in a chain of a certain length



$$(5.92)$$

This can most easily be achieved by partitioning a chain into $m \in [1, n]$ smaller chains. For instance, one such partition with $m = 4$, $n = 6$, is



$$(5.93)$$

Every cut in the chain will replace a $-h_2 W_{21}$ in the expression by a factor $-2h_2 N_f W_{(11)^2}$, and m replacements on a n long chain can be done in $\binom{n}{m}$ ways. The combined cluster and chain resummation formula is therefore summarised as the replacement

$$\begin{aligned} z_{(11)} &\rightarrow z_{(11)} \sum_{n=0}^{\infty} \sum_{m=0}^n \binom{n}{m} (-2d)h_2^{n+m} z_{(21)}^n (N_f z_{(11)^2})^m \\ &= \frac{z_{(11)}}{1 + 2N_f(2d)h_2 z_{(11)^2} + (2d)h_2 z_{(21)}}. \end{aligned} \quad (5.94)$$

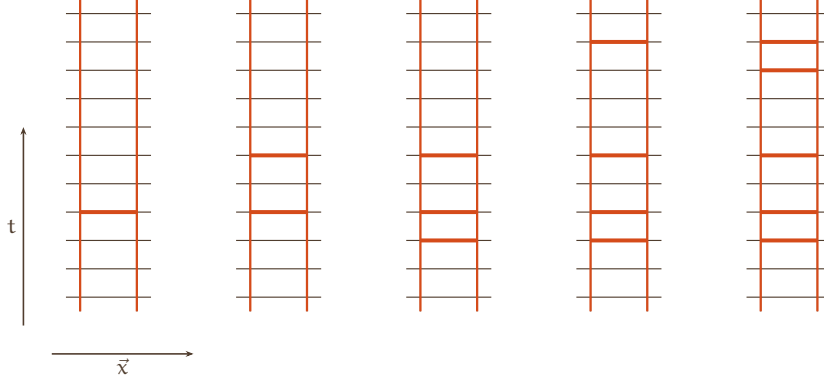


Figure 5.12.: The ladder resummation graphic, illustrating the general principle.

As this is only a fraction of the full LCE resummation scheme, further improvements are expected to appear as one cranks the machinery. Still, this particular subset of cluster resummations synergises well with the already developed chain resummation.

5.4.3 Ladder resummation

The last of the resummation schemes addressed in this thesis is a *ladder resummation*, which is simply a renormalisation scheme for the nearest neighbour coupling constant. The idea behind the ladder resummation is, similarly to the chain resummation, simple, albeit mathematically complicated. The general principle is sketched in FIGURE 5.12, where the details are suppressed. The full ladder is given by the nearest neighbour kinetic determinant

$$\prod_i \det(1 - \kappa^2 P_i M_i) \equiv \det(1 - \kappa^2 \mathcal{M}_{C_2}), \quad (5.95)$$

which represents a different ordering scheme of the spatial hopping expansion. It is possible to express the full static determinant in this path ordering scheme, which is equivalent to the hopping scheme we have used so far. We adopt the same notation as in [Rindlisbacher and de Forcrand, 2016]

$$\det Q_{\text{kin}} = \prod_n \prod_{\{C_n\}} \det(1 - \kappa^n \mathcal{M}_{C_n}), \quad (5.96)$$

where C_s symbolises a spatial path of length s and the product goes over all such paths. The path ordered determinants can then be expanded in traces using the *Faddeev-LeVerrier algorithm*, which truncates at the dimension of the matrix. This formalism does however in no way simplify the computation of the effective theory, as the combinatorics of the spatial gauge integrals, which presents the higher obstacle, remain.

Expanding the nearest neighbour path determinant gives

$$\begin{aligned} \det(1 - \kappa^2 \mathcal{M}_{C_2}) &= 1 - \kappa^2 \text{tr}(\mathcal{M}_{C_2}) - \frac{1}{2} \kappa^4 (\text{tr}(\mathcal{M}_{C_2}^2) - (\text{tr}(\mathcal{M}_{C_2}))^2) \\ &\quad - \frac{1}{6} \kappa^6 ((\text{tr}(\mathcal{M}_{C_2}))^3 - 3 \text{tr}(\mathcal{M}_{C_2}) \text{tr}(\mathcal{M}_{C_2}^2) + 2 \text{tr}(\mathcal{M}_{C_2}^3)) + \dots \end{aligned} \quad (5.97)$$

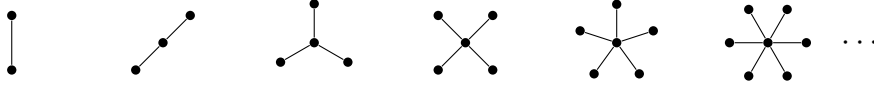
which grants some insight into the terms that will appear in the ladder. It is however impossible to compute the full ladder, and we will have to settle for a computable subset of all graphs. One possible subset is the single trace terms

$$\sum_i \text{tr}(P_i M_i P_i M_i P_i M_i \dots) \quad (5.98)$$

which will include both high order coupled terms as well as close packed embeddings of longer chains. For example all chains of the previous expansion will be one such term, where the chain has been folded onto a nearest neighbour pair. In addition to being restricted by combinatorics, we are restricted by the integrability of the linked cluster integrals. The chain had the advantage that no new integrals (z -functions) were needed, while in a nearest neighbour resummation, new integrals will inevitably appear. We therefore turn to an even smaller subset of all nearest neighbour graphs, namely

$$\text{tr}(1 \ 1 \ 2 \ 2 \ 3 \ 3 \ 4 \ 4 \ 5 \ 5 \dots n \ n). \quad (5.99)$$

From the earlier analysis, we know that these diagrams have n open ends and thus represent the set of *star graphs*



$$\dots \quad (5.100)$$

The structure is the same as a consecutive set of G_1 matrices from earlier

$$\mathcal{A}_n = \text{tr}(1 \ 1 \ 2 \ 2 \dots n \ n) = \underbrace{\text{tr}(G_1 G_1 \dots G_1)}_{n \text{ times}} \quad (5.101)$$

which gives

$$\mathcal{A}_n = \frac{1}{n} \left(\frac{2\kappa^2}{N_c} \right)^n \sum_{\{t_i\}} \text{tr}(B_{\vec{x}}(t_1, t_2) B_{\vec{x}}(t_2, t_3) \dots B_{\vec{x}}(t_n, t_1)) \prod_{i=1}^n \sum_{\{\vec{x}_i\}} \frac{1}{2} W_{11}(\vec{x}_i) \quad (5.102)$$

after inserting the integrated expression for G_1 from EQ (5.76). The positions $\vec{x}_i = \vec{x} + \hat{i}$ are all nearest neighbours to the root position. Finally one has to evaluate the colour trace of all possible partitions of the set of temporal variables $\{t_i\}$. For example the three star term gives

$$\begin{aligned} \mathcal{A}_3 &= \frac{1}{3} \left(\frac{2\kappa^2}{N_c} \right)^3 \sum_{t_1, t_2, t_3} \text{tr}(B_{\vec{x}}(t_1, t_2) B_{\vec{x}}(t_2, t_3) B_{\vec{x}}(t_3, t_1)) \prod_{i=1}^3 \sum_{\{\vec{x}_i\}} \frac{1}{2} W_{11}(\vec{x}_i) \\ &= \frac{1}{3} h_2^3 \left(\frac{1}{2} W_{31} - \frac{1}{2} W_{32} \right) \prod_{i=1}^3 \sum_{\{\vec{x}_i\}} W_{11}(\vec{x}_i), \end{aligned} \quad (5.103)$$

and the four star one results in

$$\mathcal{A}_4 = \frac{1}{4} h_2^4 \left(\frac{1}{4} W_{41} - \frac{1}{2} W_{42} + \frac{1}{4} W_{43} \right) \prod_{i=1}^4 \sum_{\{\vec{x}_i\}} W_{11}(\vec{x}_i). \quad (5.104)$$

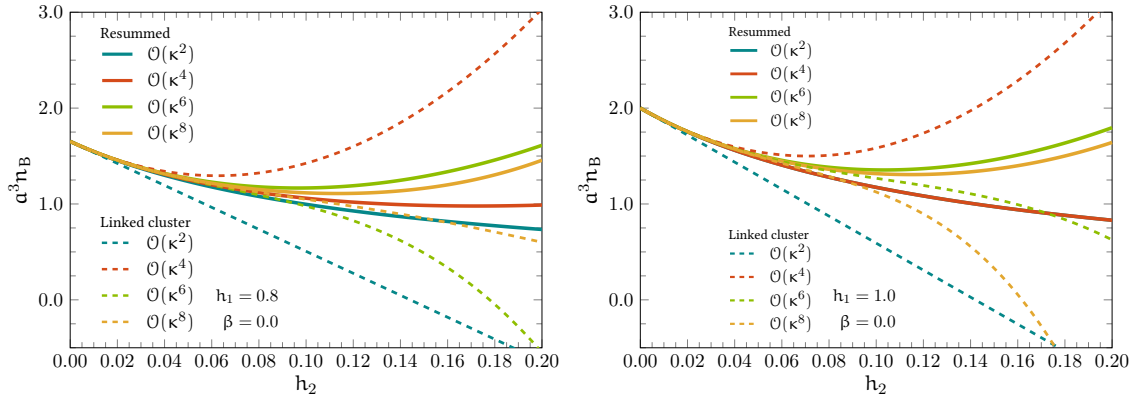


Figure 5.13.: Convergence test of the chain- and cluster resummed effective theory compared to the previous cluster results. Left: At $h_1 = 0.8$. Right: At $h_1 = 1.0$ (resummed κ^2 curve directly behind the κ^4 equivalent).

The partitioning of the temporal sums is currently not known, but the general structure is on the form

$$\mathcal{A}_n = h_2^n \sum_{m=1}^{n-1} p_{nm} W_{nm} \prod_{i=1}^n \sum_{\{\vec{x}_i\}} W_{11}(\vec{x}_i). \quad (5.105)$$

The motivation for choosing this specific set of terms is based on the integrability of the solution. We choose a ladder embedding, meaning that we choose $\vec{x}_i = \vec{x}_1$, and embed the star so that all of its ends lie on the same lattice point. We compute the sum over n for this embedding, assuming that p_{nm} is n independent, for a fixed m

$$\begin{aligned} \sum_{n=1}^{\infty} \mathcal{A}_{nm}^* &= (2d) \sum_{n=1}^{\infty} h_2^n \text{tr} W_{nm} W_{11}^n \\ &= (2d) \text{tr} \left((h_1 W)^m \sum_{n=1}^{\infty} \frac{h_2^n W_{11}^n}{(1 + h_1 W)^n} \right) \\ &= (2d) h_2 W_{11} \text{tr} \left(\frac{(h_1 W)^m}{1 - W_{11} + h_1 W} \right). \end{aligned} \quad (5.106)$$

So whereas the W_{nm} and W_{11}^n by themselves are not integrable in general, the sum is. The assumption that p_{nm} is n independent still has to be investigated and confirmed. If it is inversely proportional to n , the sum would result in a logarithm. The sum over m could also prove beneficial.

5.4.4 Results

With the resummation schemes in place, we are in a position where we can assess their effectiveness by comparing to our previous results. In addition to this we will expand upon the analysis of the thermodynamic functions which we started in SECTION 5.3.3.

Convergence

We first check the convergence of the new results. This is plotted in FIGURE 5.13, where we again plot the strong coupling baryon number density as a function of the effective

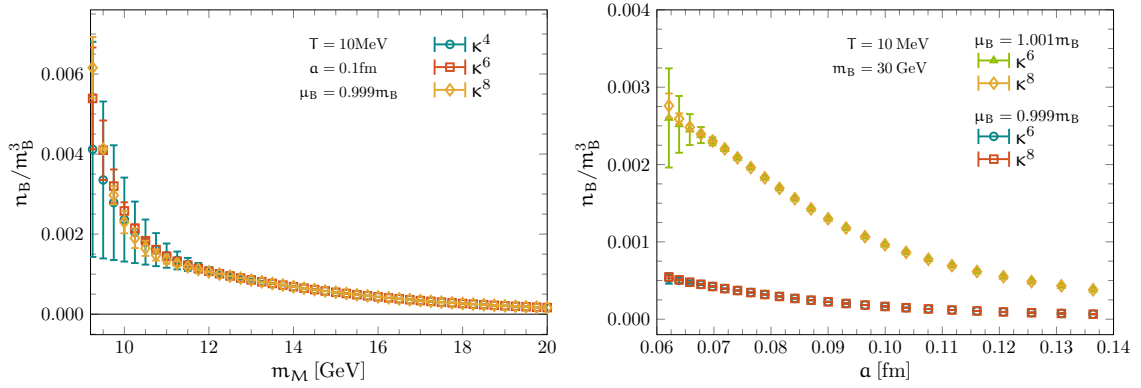


Figure 5.14.: Left: Convergence properties of the resummed theory towards lighter quarks. Right: Continuum extrapolation properties of the resummed theory.

coupling constant. In the left plot we have extended the region of convergence significantly compared to the unsummed result. Comparing the plot to the equivalent Padé plot in FIGURE 5.10 (left), we see a comparable increase in convergence. This is both expected and reassuring as both schemes produce rational expressions for the grand canonical partition function, and the slightly superior convergence of the Padé is also understood, as it is not restricted to any particular set of diagrams and might therefore predict higher order behaviour. The resummed result, on the other hand, has the advantage of being rigorous as well as providing insight into the underlying theory. The right hand side of FIGURE 5.13 shows the convergence behaviour after onset for the resummed and unsummed expressions. We see that the resummation is even more effective at these extreme parameter ranges, whereas convergence is not significantly weakened, as is the case for its unsummed counterpart.

We continue the resummation analysis by checking convergence of physical values as we move towards lighter quarks and finer lattices. The scan in meson mass is plotted in FIGURE 5.14 (left), where we see a significant improvement compared to the previous results, FIGURE 5.9 (right) (notice the difference in scale). The scan in lattice spacing, which is important for the continuum limit extrapolation, is shown in FIGURE 5.14 (right), where we once more see a definite, however smaller, improvement. It is clear from these studies that the resummation schemes provide a much greater improvement to the convergence of the results than additional orders in the expansion, and moving forward, effort should be focussed on structural improvements rather than systematical.

Saturation

Next we want to analyse the issue of lattice saturation discussed in SECTION 3.4.1. Most importantly, we want to verify that this problem vanishes in the continuum, as it has to if our theory is to describe physical systems. FIGURE 5.15 shows the baryon number density as a function of the chemical potential for ever finer lattices. At smaller lattice spacings the baryon number density increases, especially in the onset and half-filling regions. It is therefore clear that we resolve this particular lattice artefact as we move towards the continuum. For instance, the line at $a = 0.12$ fm saturates both quicker, and

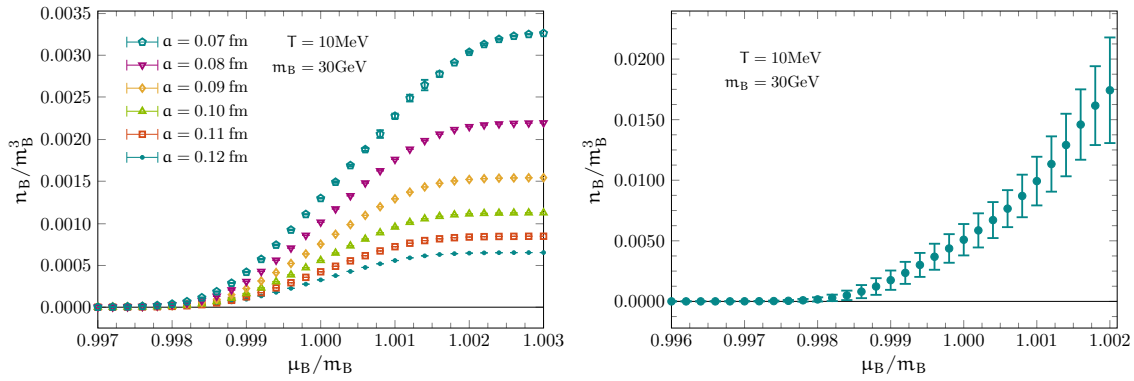


Figure 5.15.: Left: Baryon number density as a function of chemical potential for smaller and smaller lattice sizes. Right: The continuum extrapolation of the same quantity.

at lower densities, than the same system at $a = 0.07$ fm. Another interesting observation regarding the difficulty of studying the dense regime is made by observing the a -scaling of the curves at greater values of μ . We see that they split further and further apart as we increase μ due to saturation, which in turn makes the continuum extrapolation more challenging. This is also reflected in FIGURE 5.14 (right), where the curve at higher chemical potential has a much steeper slope. The right hand side of FIGURE 5.15 shows the continuum extrapolated results for the baryon number density, and we see that this quantity does not saturate.

Equation of state

We finally turn our attention to the study of the *Equation of State* (EoS) for heavy QCD in the cold and dense regime. FIGURE 5.16 shows the path traced out in a pressure vs density plot with varying chemical potential. The finite lattice spacing paths are plotted in red and green, and they clearly eventually curve upwards. This is because of saturation, and with increasing chemical potential above saturation, the density will stay constant, while the pressure will continue to rise. The expected asymptotes are also shown in the same plot, in matching colours to their corresponding plot points, given by

$$n_B(\text{saturation})/m_B^3 = 2N_f/(am_B)^3. \quad (5.107)$$

This curvature disappears in the continuum extrapolation, approaching a straight curve

$$\frac{P}{m_B^4} \propto 0.04929(29) \left(\frac{n_B}{m_B^3} \right)^{5/3}. \quad (5.108)$$

This scaling is the same as for a free gas of non-relativistic fermions, which is remarkable given the fact that we based the computations on a theory of quarks and gluons expanded around the strong coupling regime. The emergence of a system of baryonic degrees of freedom interacting weakly, is fully dynamical, and a result of the computation.

Digging deeper, we can compare the slope to that of the EoS for non-relativistic fermions, which should give some information regarding which degrees of freedom con-

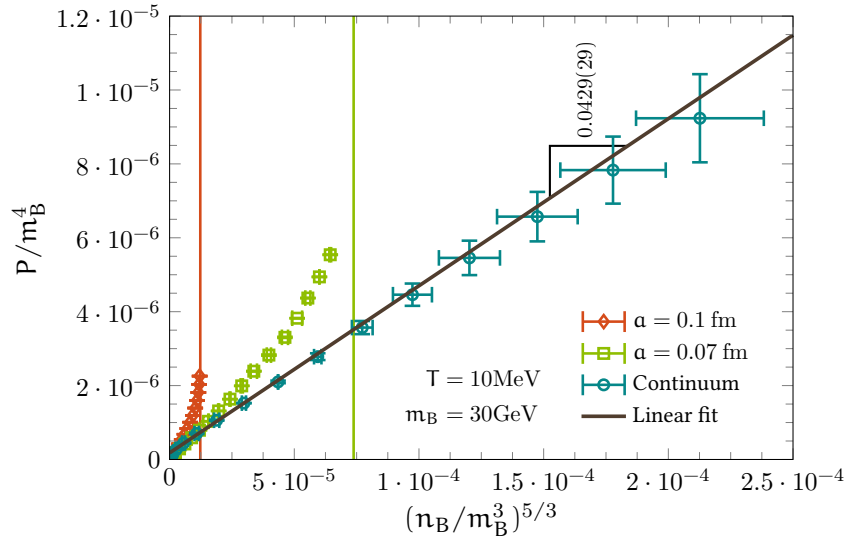


Figure 5.16.: Equation of state for the heavy quark effective theory at two different lattice spacings, and in the continuum. Also plotted, a linear fit of the polytropic EoS (black), as well as the saturation asymptotes for the finite lattice spacing curves (red and green).

tribute to the dynamics. The fermionic EoS is

$$\frac{P_f}{m_f^4} = \frac{1}{5} \left(\frac{6\pi^2}{g_f} \right)^{2/3} \left(\frac{n_f}{m_f^3} \right)^{5/3}, \quad (5.109)$$

where g_f is the number of degrees of freedom. Extracting this number from the fit would give a staggering $g_f = 484(4)$, which is around five times larger than what might be expected from the static theory. The static theory for $N_f = 2$, $N_c = 3$ describes a system of 91 "baryons", including fully degenerate nucleons, as well as all higher excitations, which are all equally weighted as there is no mechanism that favours any particular quark combination. This means that we not only have three quark baryons, but also combination such as hexaquarks (dibaryon), ennequarks (tribaryon) and dodecaquarks (tetrabaryon). We note that the hexaquarks and dodecaquarks are bosonic in nature, which might have an effect on the dense dynamics below half-filling, after which the system only sees the quark degrees of freedom, and the statistics of combinations becomes irrelevant.

To further study this, we plot the density and the pressure separately as a function of chemical potential, and compare their scaling to the predictions of non-interacting fermions. FIGURE 5.17 (left) shows the density as a function of chemical potential, which also scales according to the free fermion hypothesis. However, extracting the degrees of freedom yields $g_f(\mu_b) = 37$. Finally, FIGURE 5.17 (right) shows the pressure scaling, and gives $g_f(P) = 0.02$. This shows that the degrees of freedom are still not properly understood. One possible explanation is that the bosonic baryons condense, and therefore do not contribute to the pressure in the cold and dense regime, however still adding to the baryon number. There are still open questions to be answered regarding this topic, and future studies, such as variations of N_c , might prove to be enlightening.

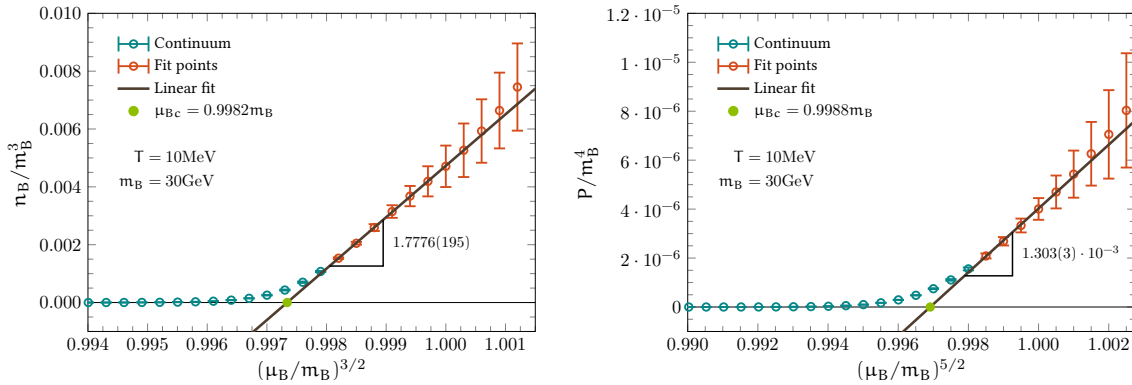


Figure 5.17.: Left: Continuum extrapolated baryon number density as a function of $(\mu_B/m_B)^{3/2}$ together with accompanying linear fits of the onset region. Right: Similar plot for the continuum extrapolated pressure as a function of $(\mu_B/m_B)^{5/2}$.

5.5 FURTHER APPLICATIONS

In this final section, we will review two further applications of the analytic treatment of the effective theories where numerical approaches are less adequate. We first summarise the implementation of different continuous groups, especially higher N_c , in SECTION 5.5.1. Subsequently, in SECTION 5.5.2 we round off this chapter with a look at the extraction of the Yang Lee zeros, which were introduced in SECTION 3.1.2. Both of these topics are in progress, and remain as avenues of future research.

5.5.1 Large- N_c limit

A topic of great interest is the behaviour of gauge theories with fermions, when the number of colours, N_c , is modified. This was first explored by 't Hooft [1974], who discovered that a simplification arises in the large- N_c limit, and that $1/N_c$ could work as a hidden candidate for a possible expansion parameter. More specifically, in this limit the mesons and pure glue states dominate, and are free (in the vacuum). This was further explored by Witten [1979], who hastened the development of this limit's mathematical structure, and its possible implications for QCD. In a sense, QCD sits at the worst possible value for N_c , with $SU(2)$ being much simpler than QCD, as well as not possessing a sign problem. On the other side we have $SU(4)$, $SU(5)$, ..., which are closer to the large- N_c limit, and can thus benefit from the simplifications that arise. There is great interest in higher N_c from a conformal field theory perspective, as there exists a line in the N_f/N_c plane that separates conformal and non-conformal field theories, which is known as the *conformal window* [Dietrich and Sannino, 2007]. An introduction to lattice studies of large- N_c can be found in [Lucini and Panero, 2014].

We already pointed out the reduced numerical cost of simulating the effective theory at higher N_c in SECTION 4.9, as compared to a full scale lattice gauge theory implementation. Furthermore, the graphs that enter analytic computations do not change as we increase N_c . This means that in the strong coupling limit, all we have to do is recompute the z -functions using the methods outlined in the appendices for every N_c . The baryon number density for different gauge groups is plotted in FIGURE 5.18. We see

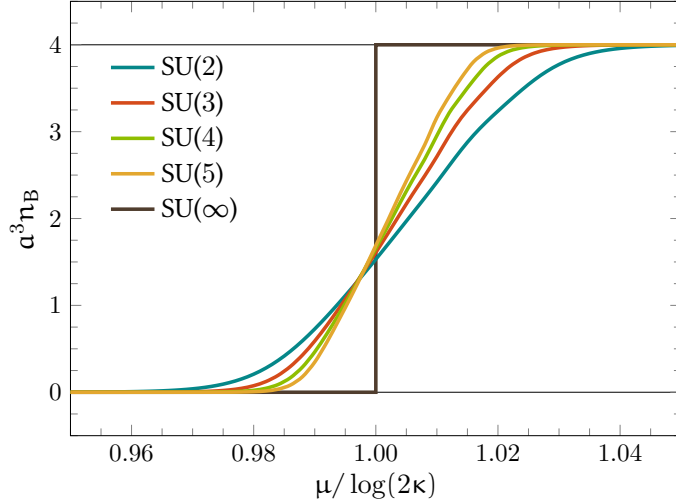


Figure 5.18.: "Baryon" number density as a function of chemical potential at different values of N_c computed with the effective theory. Expected $N_c = \infty$ in black.

that at higher and higher values of N_c , the transition becomes steeper and steeper. We have defined n_B by dividing out a factor of N_c from the quark number density, a colour neutral state requires at least N_c quarks. The behaviour at increasing N_c can be easily seen from the static determinants in TABLE A.2. The static determinant will always have a fugacity coefficient raised to power N_c at highest order. This means that the onset is exponentially suppressed by N_c , and the saturation exponentially enhanced. In the limit this gives a natural transition which matches physical intuition. As the number of quarks needed to form a baryon increases, it becomes more and more energetically expensive to create one. The silver blaze phenomenon is therefore strengthened, and in the actual limit, one will always have a first order transition to nuclear matter, independent of the temperature. It would be very interesting to use the effective theory to find the liquid gas endpoint as a function of N_c , κ and T . Similar to the fact that such an endpoint exists at a critical temperature depending on the quark mass, it also exists for any temperature and κ at a critical N_c . However, this can only be seen if one includes gauge corrections, as the transition point is defined by an interplay between the fermion-gauge interactions. We already see that our effective coupling $h_2 \propto N_c^{-1}$, and will thus become small. The gauge sector on the other hand has graphs that do not suffer from this suppression, and will therefore compete with the quarks.

5.5.2 Yang Lee zeros

Finally we discuss another future prospect of the effective theory, namely the evaluation of its complex Yang Lee zeros. An advantage of the Yang Lee zeros is that it outlines a clear cut systematic procedure for how to approach non-analyticities from a series expansion. Previous studies of zeros of gauge theory partition functions have proven to be fruitful [Barbour et al., 1992, 1993], as well as being successfully applied to random matrix theories [Halasz et al., 1997a], motivating a similar study of the effective theory. Having a fully analytic framework at our disposal is also beneficial for these kinds of

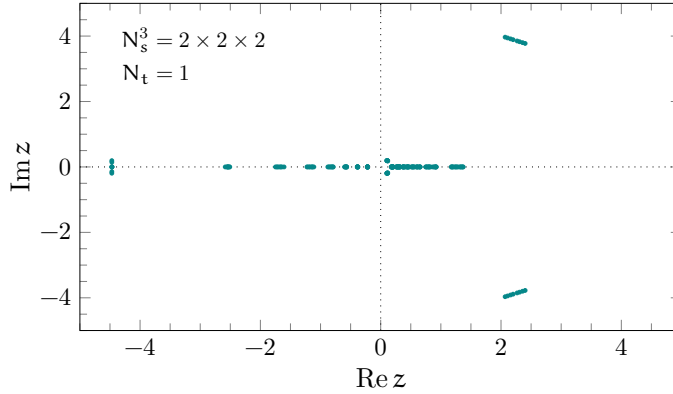


Figure 5.19.: Complex zeros of the \mathcal{Z}_2 partition function on a $2 \times 2 \times 2$ cube with periodic boundaries.

studies.

We start away from the thermodynamic limit, using the logarithmically resummed \mathcal{Z}_2 effective action

$$\mathcal{Z}_2 = \int [d\mathbf{U}]_0 \det Q_{\text{stat}}^{N_f} \prod_{\langle \vec{x}, \vec{y} \rangle} \left(1 - \frac{\kappa^2}{N_c} (W_{11}(\vec{x}) - \bar{W}_{11}(\vec{x})) (W_{11}(\vec{y}) - \bar{W}_{11}(\vec{y})) \right)^{N_t}. \quad (5.110)$$

As the volume increases, approaching the thermodynamic limit, the partition function becomes an ever higher degree polynomial in fugacity, and thus has ever more complex zeros. Similarly, increasing N_t will also alter the degree of the polynomial, showing a more intricate structure when moving towards continuum physics.

The zeros of the \mathcal{Z}_2 partition function on a $2 \times 2 \times 2$ lattice with periodic spatial directions and a temporal extent of 1 is plotted in FIGURE 5.19. Already at these small lattices we see an interesting structure, which starts developing the three-fold symmetry of $SU(3)$. Along with increasing volume, we expect even more complexity, while artificial zeros should disappear. However, due to the need for an exact analytic expression when evaluating the zeros, the integral in EQ (5.110) becomes exceedingly expensive in its evaluation, and the number of terms to evaluate in a naive approach scales as $2^{6N_t N_s^3}$. So, even for a 1×2^3 lattice, the number of terms for the integral would be $\sim 2.8 \cdot 10^{14}$. Most of the terms are of course the same, and we therefore see the need for methods of extracting the zeros that take advantage of these symmetries.

PART III

**DISCUSSION AND
OUTLOOK**

SUMMARY AND DISCUSSION

The effective theory approach to the study of cold and dense QCD manages to probe a region of the phase diagram in which traditional first principle methods fail. The method is based on expanding a system of strongly interacting, heavy quarks around these two limits. By the use of various expansion techniques, the effective theory systematically approaches continuum physics of cold and dense, heavy QCD.

This thesis' main objective has been the continued improvement of the heavy quark effective theory. We started out by introducing both continuum, and lattice gauge theories in CHAPTER 2. We focussed on the symmetry properties of the systems we study, and how these influence large scale dynamics. In CHAPTER 3 we generalised gauge theories to the realm of thermodynamics and statistical mechanics, and saw how these systems regularised on a space-time lattice. Application of lattice methods to dense systems was stressed, and a longer analysis of the difficulty of, and possible remedies to, simulating finite chemical potential physics was given.

CHAPTER 4 was dedicated to a detailed summary of the derivation of the effective theory. The two expansion schemes, namely the character expansion around $\beta = 0$, $g \rightarrow \infty$, and the hopping parameter expansion $\kappa = 0$, $m_q \rightarrow \infty$, were introduced, and their effects on the effective theory discussed. Two important resummation schemes were introduced, an exponential resummation, which improve thermodynamic studies, as well as a logarithmic one, for further analytic evaluation. Then the cold and dense regime, in which the existence of heavy temporal quark lines are favoured over anti-quark lines were introduced, and the combinatorics of the computation of the expansion coefficients simplified. Finally, the full $\mathcal{O}(\kappa^8 u^5 N_t^4)$ effective theory action was derived, followed by a short discussion on its numerical prowess.

In CHAPTER 5 the main objective of the present work was discussed, specifically the fully analytical treatment of the effective theory. We started by introducing the renowned linked cluster expansion for thermodynamic systems, and then showed how one can map the lowest order effective theory, \mathcal{Z}_2 , onto this approach. This was unfortunately not sufficient for a complete study of the higher order effective theory term, and thus a more general, polymer linked cluster expansion, was developed. We used this new systematic approach to map the complete $\mathcal{O}(\kappa^8 u^5 N_t^4)$ effective theory onto this framework, and were consequently able to present an analytic study of the higher order contributions to the cold and dense limit of heavy QCD.

In the subsequent section we employed the full power of the analytic approach and discussed three potent resummation schemes inaccessible to numerical methods. First up was the chain resummation, which makes use of recursive integrability of a specific combination of terms to predict an infinite chain of quark interactions. This specifically adds interactions at arbitrary distances to the effective theory, improving its ability to describe the correct thermodynamics for macroscopic systems. In the same spirit we introduced another resummation on the cluster expansion level, which helps to increase the accuracy of the expansion as compared to numerical methods. This is only a fraction of the full LCE resummation machinery, and can therefore be extended in the future to include additional long range effects, normally beyond the limits of computations based on series expansions. Finally, a hypothetical ladder resummation which would work as a nearest neighbour coupling renormalisation was presented. The results were then re-examined in the fully resummed analytic computation. We showed the equation of state in the continuum, where it has the same scaling as the EoS for non-relativistic weakly interacting fermions. The effective theory dynamically extracts the baryonic degrees of freedom, showing the properties of confinement from a strong coupling, heavy quark foundation. A further analysis of the degrees of freedom predicted by this equation of state shows us that there are still questions left to explore.

Finally, a short overview of further applications of the effective theory was presented. This included the extension to higher N_c gauge groups, which is of great interest to the adS/CFT community, and the analytic evaluation of the Yang Lee zeros. The latter is important to the study of non-analyticities and phase transitions.

The present work demonstrated that the effective theory approach, the spatial hopping expansion, has a rich structure and that there are still undiscovered and unexplored future research topics, which we will discuss next.

RESEARCH PERSPECTIVES

Although we have answered many questions regarding the properties and applications of the effective theory in this thesis, we have also asked new ones, and been organically lead onto the path of new research. First and foremost, applications of the effective theory to large- N_c studies, opening up communication with the adS/CFT community, was elaborated in SECTION 5.5.1. Also, the application of the analytic expressions to studies of Yang Lee zeros was outlined.

Furthermore, questions regarding the nature of the continuum extrapolated results remain unanswered, and additional research is in order. One possible avenue of future investigation is a more thorough analysis of the analytic contributions to said effect. Additional insight could be reached through the large- N_c study, as the *polyquark* states have different statistical properties depending on the gauge group. Finally one could explore the corrections to the ground state energy of the different baryonic states, and see whether it is possible to manipulate the degrees of freedom in such a way that the continuum physics alter, following predictable patterns.

Another research prospect is the computation of susceptibilities, such as Polyakov loop susceptibilities. These quantities are a paramount ingredient in the study of phase transitions for series expansion studies. The linked cluster method proposes a systematic way of computing these quantities in the thermodynamic limit, and is given by the set of n -rooted graphs with connectivity properties depending on the variable of study. We believe that these can be extended to the polymer linked cluster in a straightforward manner, and should prove immediately beneficial to our continued efforts in the Frankfurt lattice group.

Other projects using the same formalism have already been initiated in our working group, for instance the study of isospin chemical potential. This was already explored with the $\mathcal{O}(\kappa^4)$ effective theory action in [Langelage et al., 2014] using numerical methods. It can be extended to the realm of analytics by applying the methods outlined in this thesis. Another project also in progress is the evaluation of the canonical partition function constructed through Fourier transforming the effective theory grand canonical partition function. This could provide an additional extraction point for the nucleon binding energy, which remains a future goal. It could also help illuminate the question of the nature of our continuum physics.

In addition to all of this, we have seen that resummation schemes, as well as system-

atic improvement of the theory are more important than order by order results. Effort should therefore be put towards the development of these methods. This includes applying the cluster expansion resummation strategy, and looking to it for inspiration when devising resummation formulas on the level of the effective action. Recursive improvement patterns, such as coarse graining techniques, are also of great interest. Finally, we have based the study on an unimproved Wilson fermion action. Order α improvement schemes are therefore massively helpful in reducing continuum extrapolation errors.

All in all, we conclude that the powerful approaches described in this thesis are very promising, and are currently being adopted by other groups, showing a broad interest and faith in the approach [Scior and von Smekal, 2015, 2016; Rindlisbacher and de Forcrand, 2016].

PART IV

APPENDIX

A

ANALYTICAL TOOLS FOR SU(N)

The analytic computations contained herein revolve around various SU(N) dependent quantities, and we therefore need a basis for computing these. In this appendix we look at how to compute all the necessary components such as the Haar measure in SECTION A.1, the character integrals in SECTION A.2, integrals over group polynomials in SECTION A.3 and finally the fermionic functions of the effective theory in SECTIONS A.4, and A.5.

A.1 COMPUTING THE HAAR MEASURE

Our first goal is to obtain the invariant group measure of a group element expressed in terms of its spectral decomposition. Any matrix representation of an U(N) matrix has unitary eigenvalues $\lambda_i = e^{i\theta_i}$ only, where $\sum_i \theta_i = 0 \pmod{2\pi}$ for the elements of SU(N). We write a matrix U that is a representation of U(N) in its decomposed form

$$U = W\Lambda W^\dagger, \quad (\text{A.1})$$

where $\Lambda = \text{diag}(e^{i\theta_1}, \dots, e^{i\theta_n})$, and $WW^\dagger = \mathbb{1}_R$. A change in U is therefore

$$dU = Wd\Lambda W^\dagger + W[W^\dagger dW, \Lambda]W^\dagger. \quad (\text{A.2})$$

Using the standard unitary matrix metric, $\|M\|^2 = \text{tr}(M^\dagger M)$, the size of an infinitesimal square in this coordinate space is

$$ds^2 = \text{tr}(dU^\dagger dU) = \sum_i d\theta_i^2 + 2 \sum_{i>j} |e^{i\theta_i} - e^{i\theta_j}|^2 |(W^\dagger dW)_{ij}|^2. \quad (\text{A.3})$$

Since one identifies the set of coordinates to the metric through $ds^2 = g_{\mu\nu} d\xi^\mu d\xi^\nu$, it is natural to construct the measure as

$$dU(x) = \sqrt{\det g(x)} \prod_\mu d\xi^\mu. \quad (\text{A.4})$$

To reconcile these two formulae we use the Baker-Campbell-Hausdorff formula to express $W^\dagger dW$ in terms of the generators of U(d_R)

$$(W^\dagger dW)_{ij} = i(T_a)_{ij} f_{ab}(w) dw_b \equiv Q_{ijk}(w) dw_k \quad (\text{A.5})$$

with f being some function of the parameters of the generator decomposition. The general coordinates will thus be a combination of the eigenvalue angles θ_i and the parameters w_i . The determinant of the metric factorise into parts dependent on these coordinates, and we get

$$\det g(x) \sim (\det Q(w))^2 \prod_{i>j} |e^{i\theta_i} - e^{i\theta_j}|^4. \quad (\text{A.6})$$

Since we are concerned with the integrals over the eigenvalues only, one can integrate out the w_i , and get the invariant measure

$$dU = \underbrace{\prod_{i>j} |e^{i\theta_i} - e^{i\theta_j}|^2}_{H(U)} \prod_i d\theta_i, \quad (\text{A.7})$$

where we have identified the Haar measure, $H(U)$. Although this relation is only true for $U(N)$, it can be trivially extended to $SU(N)$ through the previously mentioned restriction, $\sum_i \theta_i = 0 \pmod{2\pi}$.

The *Vandermonde determinant* is introduced to facilitate the calculation of the Haar measure

$$\prod_{i>j} (z_i - z_j) = \det \mathcal{M} = \begin{vmatrix} 1 & z_1 & \cdots & z_1^{N-1} \\ 1 & z_2 & \cdots & z_2^{N-1} \\ \vdots & \vdots & \ddots & \vdots \\ 1 & z_N & \cdots & z_N^{N-1} \end{vmatrix}, \quad (\text{A.8})$$

which can be used to rewrite the Haar measure

$$H(U) = \prod_{i>j} |z_i - z_j|^2 = \det \mathcal{M}^\dagger \mathcal{M} = \begin{vmatrix} N & \sum_i z_i & \sum_i z_i^2 & \cdots & \sum_i z_i^{N-1} \\ \sum_i z_i^\dagger & N & \sum_i z_i & \cdots & \sum_i z_i^{N-2} \\ \vdots & \vdots & \vdots & \ddots & \vdots \\ \sum_i z_i^{\dagger N-1} & \sum_i z_i^{\dagger N-2} & \sum_i z_i^{\dagger N-3} & \cdots & N \end{vmatrix}. \quad (\text{A.9})$$

The fundamental representation of $SU(N)$ has $N-1$ independent eigenvalues. We know that

$$\sum_i z_i^m = \text{tr } U^m \equiv \chi_m, \quad (\text{A.10})$$

correspond to the m 'th powered character. One can therefore use the Cayley-Hamilton theorem to determine how these angles depend on each other. The Cayley-Hamilton equation reads

$$M^N + c_{N-1} M^{N-1} + \cdots + c_1 M + (-1)^N \det M \mathbb{1}_R = 0, \quad (\text{A.11})$$

where the coefficients can be computed recursively using the *Faddeev-LeVerrier algorithm*

$$c_{N-m} = -\frac{1}{m} \sum_{k=1}^m c_{N-m+k} \text{tr}(M^k). \quad (\text{A.12})$$

The first and last coefficient are $c_N = 1$ and $c_1 = (-1)^N \det M$, as can be inferred from EQ (A.11).

Using the defining properties of $SU(N)$, $\det \mathbf{U} = 1$ and $\mathbf{U}^\dagger \mathbf{U} = \mathbb{1}$, we can multiply EQ (A.11) with powers of \mathbf{U}^\dagger and trace the equation to find relations between the different fundamental characters, and thus reduce the number of unknowns in the Haar measure.

For instance, for $SU(3)$, $\chi_2 = \chi^2 - 2\chi^*$, giving

$$H(\mathbf{U}) = \begin{vmatrix} 3 & \chi & \chi^2 - 2\chi^* \\ \chi^* & 3 & \chi \\ \chi^{*2} - 2\chi & \chi^* & 3 \end{vmatrix} = 27 - 18|\chi|^2 + 8\text{Re}\chi^3 - |\chi|^4. \quad (\text{A.13})$$

A.2 $\chi_r \chi_s$ INTEGRALS

A specific set of integrals we encounter often are integrals of the form

$$I_{nm} = \int d\mathbf{U} \chi(\mathbf{U})^n \chi(\mathbf{U}^\dagger)^m. \quad (\text{A.14})$$

These can be most easily calculated through their trigonometric decomposition. Using

$$\left. \begin{aligned} \chi(\mathbf{U}) &= \sum_{\alpha=1}^N e^{i\theta_\alpha} \\ \chi(\mathbf{U}^\dagger) &= \sum_{\alpha=1}^N e^{-i\theta_\alpha} \end{aligned} \right\} \sum_{\alpha=1}^N \theta_\alpha = 0 \pmod{2\pi}, \quad (\text{A.15})$$

EQ (A.14) yields

$$I_{nm} = \int [d\theta]_i H(\mathbf{U}) \delta(\sum \theta_i = 0) \sum_{\{n_i\}} \sum_{\{m_i\}} \prod_{k=1}^n \prod_{l=1}^m \frac{k!l!}{n_k!m_l!} e^{in_k\theta_k - im_l\theta_l}, \quad (\text{A.16})$$

with sums over integer partitions so that

$$\sum_{i=1}^N (n, m)_i = (n, m). \quad (\text{A.17})$$

As the pure phase integrals give

$$\int_{-\pi}^{\pi} d\alpha e^{in\alpha} = \delta(n), \text{ for } n \in \mathbb{Z}, \quad (\text{A.18})$$

only combinations where the exponential's arguments cancel will give a non-zero contribution, and calculating the integral reduces to finding these combinations.

A.2.1 Integrals over characters of $SU(3)$

As this is not a problem that is solvable in general, we specialise to the group $SU(3)$. In this case we only have two free angles, which we label θ and ϕ . The full integral is

$$\begin{aligned} I_{nm} &= \int d\theta d\phi H(\theta, \phi) (e^{i\theta} + e^{i\phi} + e^{-i(\theta+\phi)})^n (e^{-i\theta} + e^{-i\phi} + e^{i(\theta+\phi)})^m \\ &= \int d\theta d\phi H(\theta, \phi) \sum_{\{l_i\}} \sum_{\{k_i\}} \frac{n!}{l_1!l_2!l_3!} \frac{m!}{k_1!k_2!k_3!} e^{i\theta(l_1-l_3-k_1+k_3)+i\phi(l_2-l_3-k_2+k_3)}. \end{aligned} \quad (\text{A.19})$$

\tilde{I}_{nm}	$\mathbb{1}$	$\chi\chi^*$	$(\chi\chi^*)^2$	$(\chi\chi^*)^3$	$(\chi\chi^*)^4$	$(\chi\chi^*)^5$	$(\chi\chi^*)^6$
$\mathbb{1}$	1	1	2	6	23	103	513
χ^3	1	3	11	47	225	1 173	6529
χ^6	5	21	98	498	2 709	15 565	93 500
χ^9	42	210	1 122	6 336	37 466	230 230	1 461 330
χ^{12}	462	2 574	15 015	91 091	571 428	3 688 932	24 410 334
χ^{15}	6 006	36 036	223 652	1 429 428	9 372 168	62 833 836	429 568 036

Table A.1.: Some integrals over the characters of SU(3) where the integrand is made up of the product of the topmost row with the leftmost column. All other integrals are zero due to the selection rule of EQ (A.35).

We define the measure-less integral $J_{nm} = \int [d\theta]_i \chi^n \chi^{*m}$, which is

$$J_{nm} = (2\pi)^2 \sum_{\{l_i\}} \sum_{\{k_i\}} \frac{n!}{l_1!l_2!l_3!} \frac{m!}{k_1!k_2!k_3!} \delta(l_1 - l_3 - k_1 + k_3) \delta(l_2 - l_3 - k_2 + k_3). \quad (\text{A.20})$$

Carrying out the explicit sums over four variables yields

$$J_{nm} = (2\pi)^2 \sum_{l=0}^n \sum_{k=0}^m \frac{n!}{l! (k + \frac{n-m}{3})! (\frac{2n+m}{3} - l - k)!} \frac{m!}{k! (l + \frac{m-n}{3})! (\frac{2m+n}{3} - l - k)!} \quad (\text{A.21})$$

where the remaining variables l and k are restricted by the requirement that the factorials all have non-negative arguments. Since the Haar measure itself is expressed in terms of the characters, we see from EQ (A.13) that

$$I_{n,m} = 27 J_{n,m} - 18 J_{n+1,m+1} + 4 J_{n+3,m} + 4 J_{n,m+3} - J_{n+2,m+2}. \quad (\text{A.22})$$

It is easy to see that J_{nm} is symmetric in its indices, $J_{nm} = J_{mn}$, and by extension, so is I_{nm} . We introduce the normalised integral, $\tilde{I}_{nm} = I_{nm}/I_{00}$, the value of some of which are listed in TABLE A.1. Analysing the sequences one notices that they have deep combinatorial connections [OEIS, 2011]. For instance, the first row of this table is the sequence of permutations of S_n with longest increasing subsequence length ≤ 3 (A005802). The first column of the table on the other hand corresponds to the 3 dimensional Catalan numbers (A005789). A more thorough review of the combinatorics of SU(3) can be found in [Unger, 2014].

A.2.2 Characters of plaquettes

Another set of integrals that appears often, are those of characters over plaquettes sharing a common link, such as the ones in SECTION 4.3. These integrals are of the form

$$F_{nm}^r(V, W) = \int dU \chi_r(VU)^n \chi_r(WU^\dagger)^m. \quad (\text{A.23})$$

In [Bars and Green, 1979] the authors introduced a recursive formula to evaluate the diagonal integrals of this form in the fundamental representation of U(N), namely the

integrals $F_{n,n}^f(V, V^\dagger)$. The procedure is as follows. First one introduces a new integral

$$G_n(\{V_i\}) = \int dU \chi_f(V_1 U) \cdots \chi_f(V_n U) \chi_f(V_1^\dagger U^\dagger) \cdots \chi_f(V_n^\dagger U^\dagger), \quad (A.24)$$

and verifies that by using the special form $(A_n)_{kl} = \delta_{ik}\delta_{lq}$, $(A_n^\dagger)_{kl} = \delta_{qk}\delta_{lj}$ for some of the integers i, j, q , the final factors of G simplify when summing over k

$$\sum_k G_n(\{V_i\}) = \delta_{ij} G_{n-1}(\{V_i\}'). \quad (A.25)$$

Due to the properties of the integrand of G , it has to be $U(N) \times U(N)$ invariant, and we can therefore decompose any G into its invariant combinations. For instance, the two lowest orders yield

$$\begin{aligned} G_1(A_1) &= \int dU \chi_f(A_1 U) \chi_f(A_1^\dagger U^\dagger) = C_1 \chi_f(A_1 A_1^\dagger), \quad (A.26) \\ G_2(A_1, A_2) &= \int dU \chi_f(A_1 U) \chi_f(A_2 U) \chi_f(A_1^\dagger U^\dagger) \chi_f(A_2^\dagger U^\dagger) \\ &= C_1 (\chi_f(A_1 A_1^\dagger) \chi_f(A_2 A_2^\dagger) + \chi_f(A_1 A_2^\dagger) \chi_f(A_2 A_1^\dagger)) \\ &\quad + C_2 (\chi_f(A_1 A_1^\dagger A_2 A_2^\dagger) + \chi_f(A_1 A_2^\dagger A_2 A_1^\dagger)). \quad (A.27) \end{aligned}$$

One then inserts the special form for A_n on the left and right hand side of the equations and systematically determine the unknown parameters C_i .

A.3 $g^n(g^{-1})^m$ INTEGRALS

In this section we present a method of computing integrals over matrix representations of the $SU(N)$ members, namely integrals of the form EQ (2.25)

$$I_{i_1, j_1, \dots, i_n, j_n}^{k_1, l_1, \dots, k_m, l_m} = \int dU u_{i_1 j_1} \cdots u_{i_n j_n} u_{k_1 l_1}^\dagger \cdots u_{k_m l_m}^\dagger. \quad (A.28)$$

Although there are multiple ways to approach this, we will closely follow the paper of Creutz [1978a; 1978b]. First we introduce the generating functional

$$\mathcal{W}(J, K) = \int dU \exp \left(\text{tr} (JU + KU^\dagger) \right) \quad (A.29)$$

noting that we can use it to reexpress I

$$I_{i_1, j_1, \dots, i_n, j_n}^{k_1, l_1, \dots, k_m, l_m} = \left(\frac{\delta}{\delta J_{i_1 j_1}} \cdots \frac{\delta}{\delta J_{i_n j_n}} \frac{\delta}{\delta K_{k_1 l_1}} \cdots \frac{\delta}{\delta K_{k_m l_m}} \right) \mathcal{W}(J, K) \Big|_{J=K=0}. \quad (A.30)$$

We then use the cofactor expansion of U^\dagger to remove the dependence on K

$$\begin{aligned} U_{ij}^\dagger &= \frac{1}{\det U} (\text{cof } U^T)_{ij} \\ &= \frac{1}{(N-1)!} \epsilon_{j, i_1, \dots, i_{N-1}} \epsilon_{i, j_1, \dots, j_{N-1}} u_{i_1 j_1} \cdots u_{i_{N-1} j_{N-1}}. \quad (A.31) \end{aligned}$$

where we have introduced the completely anti-symmetric tensors ϵ . We factor out the dependence on K of the generating functional

$$\mathcal{W}(J, K) = \exp \left(\text{tr} \left(K \text{cof} \frac{\delta}{\delta J} \right) \right) \underbrace{\int d\mathbf{U} \exp(\text{tr}(J\mathbf{U}))}_{\mathcal{W}(J)}. \quad (\text{A.32})$$

Using a determinant expansion of $\mathcal{W}(J)$, which is allowed due to the fact that $\mathcal{W}(V\mathbf{U}W) = \mathcal{W}(\mathbf{U})$ for arbitrary matrices $W, V \in \text{SU}(3)$ [Creutz, 1978a], we finally obtain

$$\mathcal{W}(J) = \sum_{i=0}^{\infty} \frac{2! \cdots (N-1)!}{i! \cdots (i+N-1)!} (\det J)^i. \quad (\text{A.33})$$

Although this expression is a little unwieldy, we immediately see a selection rule for the integrals. Using the fact that the determinant of an $N \times N$ matrix is a polynomial of N 'th power of its elements

$$\det M = \frac{1}{N!} \epsilon_{i_1, \dots, i_N} \epsilon_{j_1, \dots, j_N} M_{i_1 j_1} \cdots M_{i_N j_N}, \quad (\text{A.34})$$

only factors of N 'th power derivatives of \mathcal{W} will survive when we set $J = 0$. Since the cofactor is a $N - 1$ 'th power polynomial we get the selection rule

$$\int d\mathbf{U} \mathbf{U}^n \mathbf{U}^{\dagger m} \neq 0 \iff n + (N-1)m = 0 \pmod{N}. \quad (\text{A.35})$$

Finally, we compute the most used integral of this thesis

$$\begin{aligned} I_{ij}^{kl} &= \int d\mathbf{U} \mathbf{U}_{ij} \mathbf{U}_{kl}^{\dagger} \\ &= \frac{1}{(N-1)!} \epsilon_{l, i_1, \dots, i_{N-1}} \epsilon_{k, j_1, \dots, j_{N-1}} \int d\mathbf{U} \mathbf{U}_{ij} \mathbf{U}_{i_1 j_1} \cdots \mathbf{U}_{i_{N-1} j_{N-1}} \\ &= \frac{1}{(N-1)!} \epsilon_{l, i_1, \dots, i_{N-1}} \epsilon_{k, j_1, \dots, j_{N-1}} \left(\frac{\delta}{\delta J_{ij}} \frac{\delta}{\delta J_{i_1 j_1}} \cdots \frac{\delta}{\delta J_{i_{N-1} j_{N-1}}} \right) \mathcal{W}(J) \Big|_{J=0} \\ &= \frac{1}{N!(N-1)!} \epsilon_{l, i_1, \dots, i_{N-1}} \epsilon_{k, j_1, \dots, j_{N-1}} \epsilon_{i, i_1, \dots, i_{N-1}} \epsilon_{j, j_1, \dots, j_{N-1}} \\ &= \frac{1}{N!(N-1)!} (N-1)! \delta_{il} (N-1)! \delta_{jk} = \frac{1}{N} \delta_{il} \delta_{jk}. \end{aligned} \quad (\text{A.36})$$

A.4 STATIC DETERMINANT

With the measure and various link integrals at hand, it is time we approach the two fundamental fermionic quantities of the effective theory, namely the static determinant and one-site interactive loop terms. The latter we will cover in the next section, and we will focus on the static determinant here, namely

$$\det Q_{\text{stat}} = \prod_{\vec{x}} \det(1 + h_1 \mathcal{W}(\vec{x}))^2 \det(1 + \bar{h}_1 \mathcal{W}^{\dagger}(\vec{x}))^2. \quad (\text{A.37})$$

SU(N)	$\det(1 + h_1 W)$
1	$1 + h_1$
2	$1 + h_1^2 + h_1 \chi_1$
3	$1 + h_1^3 + h_1 \chi_1 + \frac{1}{2} h_1^2 (\chi_1^2 - \chi_2)$
4	$1 + h_1^4 + h_1 \chi_1 + \frac{1}{2} h_1^2 (\chi_1^2 - \chi_2) + \frac{1}{6} h_1^3 (\chi_1^3 - 3\chi_1 \chi_2 + 2\chi_3)$
5	$1 + h_1^5 + h_1 \chi_1 + \frac{1}{2} h_1^2 (\chi_1^2 - \chi_2) + \frac{1}{6} h_1^3 (\chi_1^3 - 3\chi_1 \chi_2 + 2\chi_3) + \frac{1}{24} h_1^4 (\chi_1^4 - 6\chi_1^2 \chi_2 + 3\chi_2^2 + 8\chi_1 \chi_3 - 6\chi_4)$

Table A.2.: Static determinants calculated in various groups SU(N) with the independent characters $\chi_i = \text{tr}(U^i)$.

Since these factors are all independent quantities, we can focus on determining a single determinant $\det(1 + h_1 W)$, restricting ourselves to $W \in \text{SU}(N)$ for the current study. The determinant can be rewritten using the trace log identity together with the Mercator series, giving

$$\det(1 + h_1 W) = \sum_{n=0}^N \sum_{\{k_i\}_n} \prod_{l=1}^N \frac{(-1)^{(l+1)k_l}}{l^{k_l} k_l!} h_1^{l k_l} \text{tr}(W^l)^{k_l}, \quad (\text{A.38})$$

with indices $\{k_i\}_n$ summed over a range bounded by the equations

$$\sum_{i=1}^N k_i = n, \quad \text{and} \quad \sum_{i=1}^N i k_i \leq N. \quad (\text{A.39})$$

The highest power term of the Mercator series is fixed by the fact that $\det W = 1$, and we can thus reduce it out of the problem using the Cayley-Hamilton equation (A.11). The static determinants of groups SU(1 \rightarrow 5) are listed in TABLE A.2.

A.5 W_{nm} TERMS

The last group dependent quantity of interest is the effective theory nodes, which have the form

$$W_{nm} = \text{tr} \frac{(h_1 W)^m}{(1 + h_1 W)^n}, \quad (\text{A.40})$$

and need to be rewritten in terms of the characters. There are multiple ways to work with these quantities. First of all, they can be studied directly through their series expansion

$$W_{nm} = \text{tr} \left((h_1 W)^m \sum_{k=0}^{\infty} \binom{k+n-1}{k} (-h_1 W)^k \right) \quad (\text{A.41})$$

which is useful for some particular identities. Alternately one can rewrite it in terms of its independent factors

$$W_{nm} = \sum_{i=0}^{N-1} a_i \text{tr} W^i, \quad (\text{A.42})$$

then use a combination of its series expansion and the Cayley-Hamilton theorem to manipulate the expression and solve for α_i . Finally, one can construct a generating functional to convert between the different variables. One such functional can conveniently be constructed using the expression for the static determinant

$$G(\alpha, \beta) = \log \det(\alpha + \beta h_1 W), \quad (\text{A.43})$$

from which

$$W_{nm} = \frac{(-1)^{n-1}}{(n-1)!} \frac{\partial^{(n-m)}}{\partial \alpha^{(n-m)}} \frac{\partial^m}{\partial \beta^m} G(\alpha, \beta) \Big|_{\alpha=\beta=1}. \quad (\text{A.44})$$

The generating functional can in turn be calculated with the methods outlined in the previous sections.

B

ADDITIONAL ANALYTIC RESULTS

In this chapter we summarise all additional analytic results which are either too lengthy, or do not fit in the main text.

B.1 NON GRAPHICAL $\mathcal{O}(\kappa^8)$ EFFECTIVE ACTION

The effective action to $\mathcal{O}(\kappa^8 N_f^{-1})$

$$S_{\text{eff}} = S_0 + S_2 + S_4 + S_6 + S_8 + \mathcal{O}\left(\kappa^{10}, \frac{1}{N_f}\right) \quad (\text{B.1})$$

$$S_0 = - \sum_{\mathbf{x}} \log \det Q_{\text{stat}}(\mathbf{x}), \quad (\text{B.2})$$

$$S_2 = h_2 N_f \sum_{\mathbf{x}} \sum_{\mathbf{i}} W_{1,1}(\mathbf{x}) W_{1,1}(\mathbf{x} + \mathbf{i}), \quad (\text{B.3})$$

$$\begin{aligned} S_4 = & - h_2^2 N_f \sum_{\mathbf{x}} \sum_{\mathbf{i}, \mathbf{j}} W_{2,1}(\mathbf{x}) W_{1,1}(\mathbf{x} + \mathbf{i}) W_{1,1}(\mathbf{x} + \mathbf{j}) \\ & - h_2^2 N_f^2 \sum_{\mathbf{x}} \sum_{\mathbf{i}} W_{2,1}(\mathbf{x}) W_{2,1}(\mathbf{x} + \mathbf{i}), \end{aligned} \quad (\text{B.4})$$

$$\begin{aligned} S_6 = & + \frac{1}{3} h_2^3 N_f \sum_{\mathbf{x}} \sum_{\mathbf{i}, \mathbf{j}, \mathbf{k}} [W_{3,1}(\mathbf{x}) - W_{3,2}(\mathbf{x})] W_{1,1}(\mathbf{x} + \mathbf{i}) W_{1,1}(\mathbf{x} + \mathbf{j}) W_{1,1}(\mathbf{x} + \mathbf{k}) \\ & + h_2^3 N_f \sum_{\mathbf{x}} \sum_{\mathbf{i}, \mathbf{j}, \mathbf{k}} W_{2,1}(\mathbf{x}) W_{2,1}(\mathbf{x} + \mathbf{i}) W_{1,1}(\mathbf{x} + \mathbf{i} + \mathbf{j}) W_{1,1}(\mathbf{x} + \mathbf{k}) \\ & + 2 h_2^3 N_f^2 \sum_{\mathbf{x}} \sum_{\mathbf{i}, \mathbf{j}} [W_{3,1}(\mathbf{x}) - W_{3,2}(\mathbf{x})] W_{2,1}(\mathbf{x} + \mathbf{i}) W_{1,1}(\mathbf{x} + \mathbf{j}) \\ & + \frac{1}{6} h_2^3 N_f \sum_{\mathbf{x}} \sum_{\mathbf{i}} [W_{3,1}(\mathbf{x}) W_{3,1}(\mathbf{x} + \mathbf{i}) + W_{3,2}(\mathbf{x}) W_{3,2}(\mathbf{x} + \mathbf{i})] \\ & - \frac{4}{3} h_2^3 N_f^3 \sum_{\mathbf{x}} \sum_{\mathbf{i}} W_{3,1}(\mathbf{x}) W_{3,2}(\mathbf{x} + \mathbf{i}), \end{aligned} \quad (\text{B.5})$$

$$\begin{aligned}
 S_8 = & + \frac{1}{12} h_2^4 N_f \sum_x \sum_{i,j,k,l} [W_{4,1}(x) - 4W_{4,2}(x) + W_{4,3}(x)] W_{1,1}(x+i) W_{1,1}(x+j) \\
 & \quad \times W_{1,1}(x+k) W_{1,1}(x+l) \\
 & + h_2^4 N_f \sum_x \sum_{i,j,k,l} [W_{3,1}(x) - W_{3,2}(x)] W_{2,1}(x+i) W_{1,1}(x+i+j) \\
 & \quad \times W_{1,1}(x+k) W_{1,1}(x+l) \\
 & + h_2^4 N_f \sum_x \sum_{i,j,k,l} W_{2,1}(x) W_{2,1}(x+i) W_{2,1}(x+j) \\
 & \quad \times W_{1,1}(x+i+k) W_{1,1}(x+j+l) \\
 & + h_2^4 N_f^2 \sum_x \sum_{i,j,k} [W_{4,1}(x) - 4W_{4,2}(x) + W_{4,3}(x)] W_{2,1}(x+i) \\
 & \quad \times W_{1,1}(x+j) W_{1,1}(x+k) \\
 & + h_2^4 N_f^2 \sum_x \sum_{i,j,k} [W_{3,1}(x) W_{3,1}(x+i) - 2W_{3,1}(x) W_{3,2}(x+i) + W_{3,2}(x) W_{3,2}(x+i)] \\
 & \quad \times W_{1,1}(x+j) W_{1,1}(x+i+k) \\
 & + 2h_2^4 N_f^2 \sum_x \sum_{i,j,k} [W_{3,1}(x) - W_{3,2}(x)] W_{2,1}(x+i) W_{2,1}(x+j) W_{1,1}(x+j+k) \\
 & + h_2^4 N_f^2 \sum_x \sum_{i,j} W_{2,1}(x) W_{2,1}(x) W_{2,1}(x+i) W_{2,1}(x+j) \\
 & + \frac{1}{2} h_2^4 N_f^2 \sum_x \sum_{i,j} W_{2,1}(x) W_{2,1}(x+i) W_{2,1}(x+j) W_{2,1}(x+i+j) \\
 & + \frac{1}{3} h_2^4 N_f \sum_x \sum_{i,j} [W_{4,1}(x) W_{3,1}(x+i) - 2W_{4,2}(x) W_{3,1}(x+i) + 2W_{4,2}(x) W_{3,2}(x+i) \\
 & \quad - W_{4,3}(x) W_{3,2}(x+i)] W_{1,1}(x+j) \\
 & - \frac{4}{3} h_2^4 N_f^3 \sum_x \sum_{i,j} [2W_{4,2}(x) W_{3,1}(x+i) - W_{4,3}(x) W_{3,1}(x+i) + W_{4,1}(x) W_{3,2}(x+i) \\
 & \quad - 2W_{4,2}(x) W_{3,2}(x+i)] W_{1,1}(x+j) \\
 & + \frac{1}{12} h_2^4 N_f \sum_x \sum_{i,j} [W_{4,1}(x) - 4W_{4,2}(x) + W_{4,3}(x)] W_{2,1}(x+i) W_{2,1}(x+j) \\
 & + \frac{2}{3} h_2^4 N_f^3 \sum_x \sum_{i,j} [W_{4,1}(x) - 4W_{4,2}(x) + W_{4,3}(x)] W_{2,1}(x+i) W_{2,1}(x+j) \\
 & + \frac{1}{12} h_2^4 N_f^2 \sum_x \sum_i [W_{4,1}(x) W_{4,1}(x+i) + 12W_{4,2}(x) W_{4,2}(x+i) \\
 & \quad + W_{4,3}(x) W_{4,3}(x+i)] \\
 & + \frac{2}{3} h_2^4 N_f^4 \sum_x \sum_i [W_{4,1}(x) W_{4,3}(x+i) + 2W_{4,2}(x) W_{4,2}(x+i)] \\
 & - \frac{2}{3} h_2^4 N_f^2 \sum_x \sum_i [W_{4,1}(x) W_{4,2}(x+i) + W_{4,2}(x) W_{4,3}(x+i)]. \tag{B.6}
 \end{aligned}$$

The sums over the spatial indices $\{i, j, k, l\}$ are over all spatial directions. At the leading order in temperature all gauge corrections come from rescaling the coupling constants h_1 and h_2 . Away from the low temperature limits new gauge corrections will appear as was demonstrated in SECTION 4.8.3.

B.2 INTEGRATED LCE n -POINT FUNCTIONS

Below are all z -functions needed for the analytical calculation of the $\mathcal{O}(\kappa^8)$ action; evaluated with $N_c = 3$ and $N_f = 2$. The definition of the z -functions is found in EQ (5.21). The integrals can be computed with the methods outlined in APPENDIX A,

$$z_0 = 1 + 20h_1^3 + 50h_1^6 + 20h_1^9 + h_1^{12}, \quad (\text{B.7a})$$

$$z_{(11)} = 15h_1^3 + 75h_1^6 + 45h_1^9 + 3h_1^{12}, \quad (\text{B.7b})$$

$$z_{(21)} = 21h_1^3 + 70h_1^6 + 21h_1^9, \quad (\text{B.7c})$$

$$z_{(31)} = 28h_1^3 + 35h_1^6 - 7h_1^9, \quad (\text{B.7d})$$

$$z_{(32)} = -7h_1^3 + 35h_1^6 + 28h_1^9, \quad (\text{B.7e})$$

$$z_{(41)} = 36h_1^3 - 40h_1^6 + h_1^9, \quad (\text{B.7f})$$

$$z_{(42)} = -8h_1^3 + 75h_1^6 - 8h_1^9, \quad (\text{B.7g})$$

$$z_{(43)} = h_1^3 - 40h_1^6 + 36h_1^9, \quad (\text{B.7h})$$

$$z_{(11)^2} = 6h_1^3 + 95h_1^6 + 96h_1^9 + 9h_1^{12}, \quad (\text{B.7i})$$

$$z_{(11)(21)} = 7h_1^3 + 105h_1^6 + 56h_1^9, \quad (\text{B.7j})$$

$$z_{(11)(31)} = 8h_1^3 + 100h_1^6 - 20h_1^9, \quad (\text{B.7k})$$

$$z_{(11)(32)} = -h_1^3 + 5h_1^6 + 76h_1^9, \quad (\text{B.7l})$$

$$z_{(11)^3} = h_1^3 + 90h_1^6 + 188h_1^9 + 27h_1^{12}, \quad (\text{B.7m})$$

$$z_{(21)^2} = 8h_1^3 + 135h_1^6 + 8h_1^9, \quad (\text{B.7n})$$

$$z_{(11)^2(21)} = h_1^3 + 100h_1^6 + 148h_1^9, \quad (\text{B.7o})$$

$$z_{(11)^4} = 60h_1^6 + 312h_1^9 + 81h_1^{12}. \quad (\text{B.7p})$$

 B.3 HIGHER ORDER z -FUNCTIONS

So far we have only encountered z -functions of order $\leq 2N_f$. This has the advantage that the resulting integrals over the characters enter only in polynomial form. This is due to the fact that the W_{nm} term is

$$W_{nm} = \frac{w_{nm}}{\det^n(1 + h_1 W)} \quad (\text{B.8})$$

where w_{nm} is a polynomial in the characters. As the denominator enters to power $2N_f$ in the integrand from the static determinant, the resulting integral only has polynomials of the characters, which we saw how to solve in APPENDIX A.2. For higher orders, an expansion is needed. The simplest option is to expand the expression for W_{nm} directly

$$W_{nm} = \text{tr} \left(\frac{(h_1 W)^m}{(1 + h_1 W)^n} \right) = \text{tr} \left((h_1 W)^m \sum_{k=0}^{\infty} \binom{k+n-1}{k} (-h_1 W)^k \right) \quad (\text{B.9})$$

In this case the expression is a series in W , and the higher powers of the W matrices have to be rewritten to lower order ones using the Cayley-Hamilton equation. A direct computation of $z_{(11)^5}$ has been carried out as an example, and the order by order results are compared to the full result in FIGURE B.1 (left).

ADDITIONAL ANALYTIC RESULTS

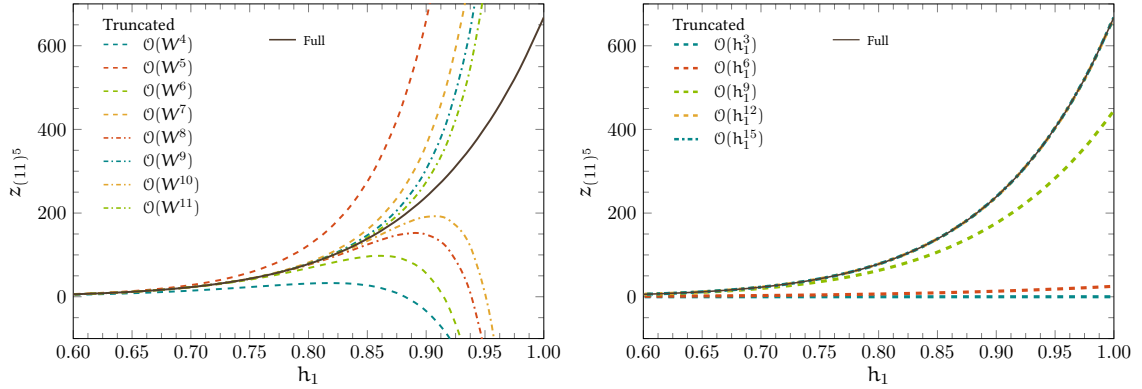


Figure B.1.: Expansions schemes for the higher order z -functions at $N_f = 2$. Left: Direct expansion in the W matrices. Right: Reshuffling of the expansion to a series in h_1 .

Unfortunately, the convergence of this series is particularly slow, and will for any finite order diverge from the correct result at $h_1 = 1$. To amend this, one can shuffle the expansion either into a series in the full characters by including the lower orders from the static determinant, or one can reorder it into a pure expansion in h_1 , also here taking the already existing orders of the static determinant into account. The latter choice is plotted in FIGURE B.1 (right), where the improved convergence is clearly visible. At 12th order the expression is almost exact, and it reaches the full result at 15th order. Above this order the remainder of the series' coefficients are all zero.

Bibliography

- G. Aarts, F. Attanasio, B. Jäger, and D. Sexty. The QCD phase diagram in the limit of heavy quarks using complex Langevin dynamics. 2016.
- C. R. Allton, S. Ejiri, S. J. Hands, O. Kaczmarek, F. Karsch, E. Laermann, and C. Schmidt. The Equation of state for two flavor QCD at nonzero chemical potential. *Phys. Rev.*, D68:014507, 2003. doi: 10.1103/PhysRevD.68.014507.
- J. Ambjorn and S. K. Yang. Numerical Problems in Applying the Langevin Equation to Complex Effective Actions. *Phys. Lett.*, B165:140, 1985. doi: 10.1016/0370-2693(85)90708-7.
- Y. Aoki, G. Endrodi, Z. Fodor, S. D. Katz, and K. K. Szabo. The Order of the quantum chromodynamics transition predicted by the standard model of particle physics. *Nature*, 443:675–678, 2006. doi: 10.1038/nature05120.
- G. A. Baker, Jr. and P. Graves-Morris. *Padé approximants*, volume 59 of *Encyclopedia of Mathematics and its Applications*. Cambridge University Press, Cambridge, second edition, 1996. ISBN 0-521-45007-1. doi: 10.1017/CBO9780511530074. URL <http://dx.doi.org/10.1017/CBO9780511530074>.
- I. M. Barbour, A. J. Bell, M. Bernaschi, G. Salina, and A. Vladikas. Complex zeros of the partition function for compact lattice QED. *Nucl. Phys.*, B386:683–700, 1992. doi: 10.1016/0550-3213(92)90633-M.
- I. M. Barbour, A. J. Bell, E. G. Klepfish, R. Burioni, A. Vladikas, and G. Salina. The Behavior of the Lee-Yang zeros for SU(3) and compact U(1). *Nucl. Phys. Proc. Suppl.*, 30:339–342, 1993. doi: 10.1016/0920-5632(93)90222-R.
- I. Bars and F. Green. Complete Integration of U(N) Lattice Gauge Theory in a Large N Limit. *Phys. Rev.*, D20:3311, 1979. doi: 10.1103/PhysRevD.20.3311.
- G. Bergner, J. Langelage, and O. Philipsen. Numerical corrections to the strong coupling effective Polyakov-line action for finite T Yang-Mills theory. *JHEP*, 11:010, 2015. doi: 10.1007/JHEP11(2015)010.
- C. Bloch and J. S. Langer. Diagram Renormalization, Variational Principles, and the Infinite-Dimensional Ising Model. *Journal of Mathematical Physics*, 6:554–572, April 1965. doi: 10.1063/1.1704307.

BIBLIOGRAPHY

- A. S. Christensen, J. C. Myers, and P. D. Pedersen. Large N lattice QCD and its extended strong-weak connection to the hypersphere. *JHEP*, 02:028, 2014. doi: 10.1007/JHEP02(2014)028.
- A. S. Christensen, J. C. Myers, P. D. Pedersen, and J. Rosseel. Calculating the chiral condensate of QCD at infinite coupling using a generalised lattice diagrammatic approach. *JHEP*, 03:068, 2015. doi: 10.1007/JHEP03(2015)068.
- T. D. Cohen. Functional integrals for QCD at nonzero chemical potential and zero density. *Phys. Rev. Lett.*, 91:222001, 2003. doi: 10.1103/PhysRevLett.91.222001.
- M. Creutz. Feynman Rules for Lattice Gauge Theory. *Rev. Mod. Phys.*, 50:561, 1978a. doi: 10.1103/RevModPhys.50.561.
- M. Creutz. On Invariant Integration Over $SU(N)$. *J. Math. Phys.*, 19:2043, 1978b. doi: 10.1063/1.523581.
- F. Cuteri, C. Czaban, O. Philipsen, C. Pinke, and A. Sciarra. Roberge-Weiss transition in $N_f = 2$ QCD with Wilson fermions and $N_\tau = 6$. *Phys. Rev.*, D93(5):054507, 2016. doi: 10.1103/PhysRevD.93.054507.
- P. H. Damgaard and H. Huffel. Stochastic Quantization. *Phys. Rept.*, 152:227, 1987. doi: 10.1016/0370-1573(87)90144-X.
- P. de Forcrand. Simulating QCD at finite density. *PoS*, LAT2009:010, 2009.
- P. de Forcrand and O. Philipsen. The QCD phase diagram for small densities from imaginary chemical potential. *Nucl. Phys.*, B642:290–306, 2002. doi: 10.1016/S0550-3213(02)00626-0.
- P. de Forcrand, S. Kim, and T. Takaishi. QCD simulations at small chemical potential. *Nucl. Phys. Proc. Suppl.*, 119:541–543, 2003. doi: 10.1016/S0920-5632(03)80451-6. [541(2002)].
- M. D’Elia and M.-P. Lombardo. Finite density QCD via imaginary chemical potential. *Phys. Rev.*, D67:014505, 2003. doi: 10.1103/PhysRevD.67.014505.
- F. Di Renzo and G. Eruzzi. Thimble regularization at work: from toy models to chiral random matrix theories. *Phys. Rev.*, D92(8):085030, 2015. doi: 10.1103/PhysRevD.92.085030.
- D. D. Dietrich and F. Sannino. Conformal window of $SU(N)$ gauge theories with fermions in higher dimensional representations. *Phys. Rev.*, D75:085018, 2007. doi: 10.1103/PhysRevD.75.085018.
- C. Domb. Graph Theory and Embeddings. In C. Domb and M. S. Green, editors, *Phase Transitions and Critical Phenomena*, volume 3, pages 1–95. London, England: Academic Press 694p, 1974.
- J.-M. Drouffe and J.-B. Zuber. Strong Coupling and Mean Field Methods in Lattice Gauge Theories. *Phys. Rept.*, 102:1, 1983. doi: 10.1016/0370-1573(83)90034-0.

- F. Englert. Linked Cluster Expansions in the Statistical Theory of Ferromagnetism. *Physical Review*, 129:567–577, January 1963. doi: 10.1103/PhysRev.129.567.
- Z. Fodor, S. D. Katz, D. Sexty, and C. Török. Complex Langevin dynamics for dynamical QCD at nonzero chemical potential: A comparison with multiparameter reweighting. *Phys. Rev.*, D92(9):094516, 2015. doi: 10.1103/PhysRevD.92.094516.
- M. Fromm, J. Langelage, S. Lottini, and O. Philipsen. The QCD deconfinement transition for heavy quarks and all baryon chemical potentials. *JHEP*, 01:042, 2012. doi: 10.1007/JHEP01(2012)042.
- M. Fromm, J. Langelage, S. Lottini, M. Neuman, and O. Philipsen. Onset Transition to Cold Nuclear Matter from Lattice QCD with Heavy Quarks. *Phys. Rev. Lett.*, 110(12):122001, 2013. doi: 10.1103/PhysRevLett.110.122001.
- W. Fulton and J. Harris. *Representation Theory: A First Course*. Graduate Texts in Mathematics. Springer New York, 2013. ISBN 9781461209799.
- C. Gattringer and C. Lang. *Quantum Chromodynamics on the Lattice: An Introductory Presentation*. Lecture Notes in Physics. Springer Berlin Heidelberg, 2009. ISBN 9783642018497.
- D. S. Gaunt and A. J. Guttmann. Asymptotic Analysis and Coefficients. In C. Domb and M. S. Green, editors, *Phase Transitions and Critical Phenomena*, volume 3, pages 181–243. London, England: Academic Press 694p, 1974.
- M. Gell-Mann. Symmetries of baryons and mesons. *Phys. Rev.*, 125:1067–1084, 1962. doi: 10.1103/PhysRev.125.1067.
- M. Gell-Mann. A Schematic Model of Baryons and Mesons. *Phys. Lett.*, 8:214–215, 1964. doi: 10.1016/S0031-9163(64)92001-3.
- M. Gell-Mann and M. Lévy. The axial vector current in beta decay. *Nuovo Cim.*, 16:705, 1960. doi: 10.1007/BF02859738.
- H. Georgi. *Lie Algebras in Particle Physics: From Isospin to Unified Theories*. Frontiers in Physics Series. Westview Press, 1999. ISBN 9780813346113.
- P. H. Ginsparg and K. G. Wilson. A Remnant of Chiral Symmetry on the Lattice. *Phys. Rev.*, D25:2649, 1982. doi: 10.1103/PhysRevD.25.2649.
- J. Glesaaen. hopping-large-nt: First release, June 2016. URL <http://dx.doi.org/10.5281/zenodo.56319>.
- J. Glesaaen, M. Neuman, and O. Philipsen. Heavy dense QCD from a 3d effective lattice theory. In *Proceedings, 33rd International Symposium on Lattice Field Theory (Lattice 2015)*, 2015. URL <http://inspirehep.net/record/1402598/files/arXiv:1511.00967.pdf>.
- J. Glesaaen, M. Neuman, and O. Philipsen. Equation of state for cold and dense heavy QCD. *JHEP*, 03:100, 2016. doi: 10.1007/JHEP03(2016)100.

BIBLIOGRAPHY

- O. W. Greenberg. Spin and Unitary Spin Independence in a Paraquark Model of Baryons and Mesons. *Phys. Rev. Lett.*, 13:598–602, 1964. doi: 10.1103/PhysRevLett.13.598.
- A. J. Guttmann. Asymptotic Analysis of Power-Series Expansions. In C. Domb and M. S. Green, editors, *Phase Transitions and Critical Phenomena*, volume 13, pages 1–234. London, England: Academic Press 320p, 1989.
- A. M. Halasz, A. D. Jackson, and J. J. M. Verbaarschot. Yang-Lee zeros of a random matrix model for QCD at finite density. *Phys. Lett.*, B395:293–297, 1997a. doi: 10.1016/S0370-2693(97)00015-4.
- A. M. Halasz, A. D. Jackson, and J. J. M. Verbaarschot. Fermion determinants in matrix models of QCD at nonzero chemical potential. *Phys. Rev.*, D56:5140–5152, 1997b. doi: 10.1103/PhysRevD.56.5140.
- P. Hasenfratz and F. Karsch. Chemical Potential on the Lattice. *Phys. Lett.*, B125:308, 1983. doi: 10.1016/0370-2693(83)91290-X.
- H. Huffer and G. Kelnhöfer. QED revisited: Proving equivalence between path integral and stochastic quantization. *Phys. Lett.*, B588:145–150, 2004. doi: 10.1016/j.physletb.2004.03.036.
- E. J. Janse van Rensburg. Monte Carlo methods for the self-avoiding walk. *J. Phys. A*, 42(32):323001, 97, 2009. ISSN 1751-8113. doi: 10.1088/1751-8113/42/32/323001.
- D. B. Kaplan. A Method for simulating chiral fermions on the lattice. *Phys. Lett.*, B288:342–347, 1992. doi: 10.1016/0370-2693(92)91112-M.
- J.I. Kapusta and C. Gale. *Finite-Temperature Field Theory: Principles and Applications*. Cambridge Monographs on Mathematical Physics. Cambridge University Press, 2, revised edition, 2006. ISBN 9781139457620.
- J. B. Kogut, H. Matsuoka, M. Stone, H. W. Wyld, S. H. Shenker, J. Shigemitsu, and D. K. Sinclair. Chiral Symmetry Restoration in Baryon Rich Environments. *Nucl. Phys.*, B225:93, 1983. doi: 10.1016/0550-3213(83)90014-7.
- L.D. Landau and E.M. Lifshitz. *Statistical Physics*. Number volume 5. Elsevier Science, 3 edition, 2013. ISBN 9780080570464.
- J. Langelage, S. Lottini, and O. Philipsen. Centre symmetric 3d effective actions for thermal SU(N) Yang-Mills from strong coupling series. *JHEP*, 02:057, 2011. doi: 10.1007/JHEP07(2011)014,10.1007/JHEP02(2011)057. [Erratum: JHEP07,014(2011)].
- J. Langelage, M. Neuman, and O. Philipsen. Heavy dense QCD and nuclear matter from an effective lattice theory. *JHEP*, 09:131, 2014. doi: 10.1007/JHEP09(2014)131.
- B. Lucini and M. Panero. Introductory lectures to large-N QCD phenomenology and lattice results. *Prog. Part. Nucl. Phys.*, 75:1–40, 2014. doi: 10.1016/j.pnpnp.2014.01.001.
- M. Lüscher and P. Weisz. Application of the Linked Cluster Expansion to the N Component ϕ^4 Theory. *Nucl. Phys.*, B300:325–359, 1988. doi: 10.1016/0550-3213(88)90602-5.

- M. Lüscher and P. Weisz. Scaling Laws and Triviality Bounds in the Lattice ϕ^4 Theory. 3. N Component Model. *Nucl. Phys.*, B318:705–741, 1989. doi: 10.1016/0550-3213(89)90637-8.
- M. Maggiore. *A Modern Introduction to Quantum Field Theory*. Oxford Master Series in Physics. OUP Oxford, 2004. ISBN 9780191036996.
- J. L. Martin. Computer Techniques for Evaluating Lattice Constants. In C. Domb and M. S. Green, editors, *Phase Transitions and Critical Phenomena*, volume 3, pages 97–112. London, England: Academic Press 694p, 1974.
- I. Montvay and G. Münster. *Quantum Fields on a Lattice*. Cambridge Monographs on Mathematical Physics. Cambridge University Press, 1997. ISBN 9780521599177.
- G. Münster. High Temperature Expansions for the Free Energy of Vortices, Respectively the String Tension in Lattice Gauge Theories. *Nucl. Phys.*, B180:23–60, 1981. doi: 10.1016/0550-3213(81)90153-X.
- K. Nagata, J. Nishimura, and S. Shimasaki. Gauge cooling for the singular-drift problem in the complex Langevin method –a test in Random Matrix Theory for finite density QCD. 2016a.
- K. Nagata, J. Nishimura, and S. Shimasaki. The argument for justification of the complex Langevin method and the condition for correct convergence. 2016b.
- Y. Nambu and G. Jona-Lasinio. Dynamical Model of Elementary Particles Based on an Analogy with Superconductivity. 1. *Phys. Rev.*, 122:345–358, 1961. doi: 10.1103/PhysRev.122.345.
- S. Necco and R. Sommer. The $N(f) = 0$ heavy quark potential from short to intermediate distances. *Nucl. Phys.*, B622:328–346, 2002. doi: 10.1016/S0550-3213(01)00582-X.
- Y. Ne’eman. Derivation of strong interactions from a gauge invariance. *Nucl. Phys.*, 26: 222–229, 1961. doi: 10.1016/0029-5582(61)90134-1.
- H. Neuberger. Exactly massless quarks on the lattice. *Phys. Lett.*, B417:141–144, 1998a. doi: 10.1016/S0370-2693(97)01368-3.
- H. Neuberger. More about exactly massless quarks on the lattice. *Phys. Lett.*, B427:353–355, 1998b. doi: 10.1016/S0370-2693(98)00355-4.
- M. Neuman. *Effective theory for heavy quark QCD at finite temperature and density with stochastic quantization*. PhD thesis, Goethe University Frankfurt, 2015.
- H. B. Nielsen and M. Ninomiya. Absence of Neutrinos on a Lattice. 1. Proof by Homotopy Theory. *Nucl. Phys.*, B185:20, 1981a. doi: 10.1016/0550-3213(81)90361-8.
- H. B. Nielsen and M. Ninomiya. Absence of Neutrinos on a Lattice. 2. Intuitive Topological Proof. *Nucl. Phys.*, B193:173, 1981b. doi: 10.1016/0550-3213(81)90524-1.
- OEIS Foundation Inc. OEIS. The On-Line Encyclopedia of Integer Sequences. <http://oeis.org>, 2011. [Online; accessed 31-April-2016].

BIBLIOGRAPHY

- K. A. Olive et al. Review of Particle Physics. *Chin. Phys.*, C38:090001, 2014. doi: 10.1088/1674-1137/38/9/090001.
- J. C. Osborn, K. Splittorff, and J. J. M. Verbaarschot. Statistical QCD with non-positive measure. In *Continous advances in QCD. Proceedings, 8th Workshop, CAQCD-08, Minneapolis, USA, May 15-18, 2008*, pages 135–147, 2008.
- G. Parisi and Y. Wu. Perturbation Theory Without Gauge Fixing. *Sci. Sin.*, 24:483, 1981.
- R.K. Pathria and P.D. Beale. *Statistical Mechanics*. Elsevier Science, 3 edition, 2011. ISBN 9780123821898.
- M. E. Peskin and D. V. Schroeder. *An Introduction To Quantum Field Theory*. Frontiers in physics. Westview Press, 1995. ISBN 9780813345437.
- O. Philipsen. Lattice QCD at non-zero temperature and baryon density. In *Modern perspectives in lattice QCD: Quantum field theory and high performance computing. Proceedings, International School, 93rd Session, Les Houches, France, August 3-28, 2009*, pages 273–330, 2010.
- O. Philipsen and C. Pinke. The $N_f = 2$ QCD chiral phase transition with Wilson fermions at zero and imaginary chemical potential. *Phys. Rev.*, D93(11):114507, 2016. doi: 10.1103/PhysRevD.93.114507.
- A. Pordt and T. Reisz. Linked cluster expansions beyond nearest neighbor interactions: Convergence and graph classes. *Int. J. Mod. Phys.*, A12:3739–3758, 1997. doi: 10.1142/S0217751X97001924.
- K. Rajagopal and F. Wilczek. *The Condensed matter physics of QCD*. 2000.
- T. Reisz. Advanced linked cluster expansion. Scalar fields at finite temperature. *Nucl. Phys.*, B450:569–602, 1995. doi: 10.1016/0550-3213(95)00370-8.
- T. Rindlisbacher and P. de Forcrand. Two-flavor lattice QCD with a finite density of heavy quarks: heavy-dense limit and “particle-hole” symmetry. *JHEP*, 02:051, 2016. doi: 10.1007/JHEP02(2016)051.
- D. H. Rischke. The Quark gluon plasma in equilibrium. *Prog. Part. Nucl. Phys.*, 52:197–296, 2004. doi: 10.1016/j.pnpnp.2003.09.002.
- A. Roberge and N. Weiss. Gauge Theories With Imaginary Chemical Potential and the Phases of QCD. *Nucl. Phys.*, B275:734–745, 1986. doi: 10.1016/0550-3213(86)90582-1.
- G. S. Rushbrooke, P. J. Wood, and G. A. Baker. Heisenberg Model. In C. Domb and M. S. Green, editors, *Phase Transitions and Critical Phenomena*, volume 3, pages 245–356. London, England: Academic Press 694p, 1974.
- P. Scior and L. von Smekal. Baryonic Matter Onset in Two-Color QCD with Heavy Quarks. *Phys. Rev.*, D92(9):094504, 2015. doi: 10.1103/PhysRevD.92.094504.

- P. Scior and L. von Smekal. Effective Polyakov loop models for QCD-like theories at finite chemical potential. In *Proceedings, 33rd International Symposium on Lattice Field Theory (Lattice 2015)*, 2016. URL <http://inspirehep.net/record/1421653/files/arXiv:1602.04614.pdf>.
- E. Seiler, D. Sexty, and I. O. Stamatescu. Gauge cooling in complex Langevin for QCD with heavy quarks. *Phys. Lett.*, B723:213–216, 2013. doi: 10.1016/j.physletb.2013.04.062.
- J. Smit. *Introduction to Quantum Fields on a Lattice*. Cambridge Lecture Notes in Physics. Cambridge University Press, 2002. ISBN 9780521890519.
- R. Sommer. A New way to set the energy scale in lattice gauge theories and its applications to the static force and alpha-s in SU(2) Yang-Mills theory. *Nucl. Phys.*, B411: 839–854, 1994. doi: 10.1016/0550-3213(94)90473-1.
- M. A. Stephanov. Random matrix model of QCD at finite density and the nature of the quenched limit. *Phys. Rev. Lett.*, 76:4472–4475, 1996. doi: 10.1103/PhysRevLett.76.4472.
- G. 't Hooft. A Planar Diagram Theory for Strong Interactions. *Nucl. Phys.*, B72:461, 1974. doi: 10.1016/0550-3213(74)90154-0.
- G. 't Hooft. Symmetry Breaking Through Bell-Jackiw Anomalies. *Phys. Rev. Lett.*, 37: 8–11, 1976. doi: 10.1103/PhysRevLett.37.8.
- G. 't Hooft. The Conceptual Basis of Quantum Field Theory. *Submitted to: Phys. Phil. A:661-729*, 2002.
- T. E. Tilma and G. Sudarshan. Generalized Euler angle parametrization for U(N) with applications to SU(N) coset volume measures. *J. Geom. Phys.*, 52:263–283, 2004. doi: 10.1016/j.geomphys.2004.03.003.
- M. Troyer and U.-J. Wiese. Computational complexity and fundamental limitations to fermionic quantum Monte Carlo simulations. *Phys. Rev. Lett.*, 94:170201, 2005. doi: 10.1103/PhysRevLett.94.170201.
- W. Unger. Combinatorics of Lattice QCD at Strong Coupling. *PoS, LATTICE2014:192*, 2014.
- H. Weyl. Gravitation and electricity. *Sitzungsber. Preuss. Akad. Wiss. Berlin (Math. Phys.)*, 1918:465, 1918.
- E. Witten. Baryons in the 1/N Expansion. *Nucl. Phys.*, B160:57–115, 1979. doi: 10.1016/0550-3213(79)90232-3.
- M. Wortis. Linked Cluster Expansion. In C. Domb and M. S. Green, editors, *Phase Transitions and Critical Phenomena*, volume 3, pages 113–180. London, England: Academic Press 694p, 1974.
- C. Wozar, T. Kaestner, A. Wipf, and T. Heinzl. Inverse Monte-Carlo determination of effective lattice models for SU(3) Yang-Mills theory at finite temperature. *Phys. Rev.*, D76:085004, 2007. doi: 10.1103/PhysRevD.76.085004.

BIBLIOGRAPHY

- L.-K. Wu and X.-F. Meng. Nature of the Roberge-Weiss transition end points in two-flavor lattice QCD with Wilson quarks. *Phys. Rev.*, D87(9):094508, 2013. doi: 10.1103/PhysRevD.87.094508.
- T. T. Wu and C. N. Yang. Concept of Nonintegrable Phase Factors and Global Formulation of Gauge Fields. *Phys. Rev.*, D12:3845–3857, 1975. doi: 10.1103/PhysRevD.12.3845.
- C. N. Yang and T. D. Lee. Statistical theory of equations of state and phase transitions. 2. Lattice gas and Ising model. *Phys. Rev.*, 87:410–419, 1952a. doi: 10.1103/PhysRev.87.410.
- C. N. Yang and T. D. Lee. Statistical theory of equations of state and phase transitions. 1. Theory of condensation. *Phys. Rev.*, 87:404–409, 1952b. doi: 10.1103/PhysRev.87.404.